

Photophysics of Bio-Inspired Solar Energy Conversion

by

Robert Schmitz

A Dissertation Presented in Partial Fulfillment
of the Requirements for the Degree
Doctor of Philosophy

Approved April 2014 by the
Graduate Supervisory Committee:

Devens Gust, Chair
Daniel Buttry
Anne Jones

ARIZONA STATE UNIVERSITY

May 2014

ABSTRACT

Increased global demand for energy has led to prolific use of fossil fuels, which produce and release greenhouse gases, such as carbon dioxide. This increase in atmospheric carbon dioxide affects the global weather system and has been cited as a cause for global warming. For humans to continue to meet demands for energy while reducing greenhouse emission, a sustainable, carbon-neutral energy source must be developed. In natural photosynthesis, organisms use chlorophyll as a chromophore to absorb the sun's energy. Bio-inspired systems use close analogues like porphyrins and phthalocyanines. In this dissertation, a soluble, semiconducting porphyrin polymer is reported. The polymer was synthesized via a Buchwald-Hartwig style coupling of porphyrin monomers which produced a polyaniline-like chain with porphyrins incorporated into the backbone. Spectroscopic and electrochemical studies were performed, which show evidence of excited state intrachromophore charge transfer and a first oxidation potential of 0.58 V (vs SCE). These properties suggest that the polymer could be involved in excited state electron donation to fullerenes and other electron acceptors, which could be beneficial in organic photovoltaics, sensors, and other applications. Molecular dyads and triads capable of charge separation have been studied for decades, and the spectroscopic properties of two novel systems are reported in this dissertation. A peripherally-connected zinc-phthalocyanine-C60 dyad was studied, and showed excited state electron transfer from the phthalocyanine excited state to the C60, with a long-lived charge separated state. An axially-linked carotene-Si-phthalocyanine-C60 triad was studied. It showed excited state electron transfer to the phthalocyanine from the carotene, but fast recombination before electron transfer can occur to the fullerene. Analogues of the electron transport mechanisms used in many biological systems use iron-sulfur clusters to shuttle electrons from donors to acceptors. In this dissertation, the spectroscopic properties of a de novo protein were studied. Nanosecond transient absorption was used to characterize the electron and energy transfer from an excited porphyrin to the oxidized [FeS] clusters incorporated in the protein. The triplet state of the porphyrin was strongly quenched by the holo-protein without formation of a porphyrin cation, suggesting that only Dexter-type energy transfer occurs between the sensitized porphyrin and the [FeS] clusters.

DEDICATION

To my parents Scott and Michelle, whose nurturing of my curiosity has led to a life of wonder and fulfillment.

To my family, whose love and support has always been amazing.

ACKNOWLEDGMENTS

First of all I would like to thank my advisor Professor Devens Gust for his guidance and support throughout my years at Arizona State University. His willingness to allow me to learn a completely new type of chemistry and his patience while I learned have been greatly appreciated. I would also like to thank Professors Ana and Thomas Moore for their guidance and support.

I would also like to thank Dr. Gerdenis Kodis for all of his help and wisdom teaching me the theory and practice of transient spectroscopy. I would not have been nearly as successful without his determined help and willingness to spend late nights in the laser lab cajoling data out of the samples with me.

Without the brilliant synthetic work of Dr. Paul Liddell and Jaro Arero, there would have been no systems for me to study, and therefore, no dissertation. They gave me their painstakingly crafted molecules and I destroyed them, time after time. I would also like to thank other collaborators I worked with: Dayn Sommer, for the protein maquette system; Chelsea Brown, for her help in purifying porphyrins for study; and Michael Kenney and Nolan Oster for their help as research assistants.

Not mentioned in this thesis were collaborations with Professor Peter Hore, Professor Jason Gillmore, and Professor Ernesto Rivera. I am grateful to all of these collaborators and look forward to continuing work with them in the future.

I sincerely appreciate all of the help from my labmates, current and past. Everyone in the lab has contributed to how I practice and conceptualize chemistry and science in general. The amount of knowledge sharing and kindness in the Gust, Moore, Moore labs has been spectacular and will be the model and expectation for all of my scientific endeavors in the future.

I would also like to acknowledge all of the unbelievable friends I have made in Arizona who have been instrumental in my understanding and communication of chemistry. Whether through long lunch breaks, long coffee breaks, or long weekends, I couldn't have done it without them.

TABLE OF CONTENTS

	Page
LIST OF FIGURES	v
CHAPTER	
1 INTRODUCTION	1
1.1 Significance.....	1
1.2 Bio-Inspired Chromophores	3
1.3 Bio-Inspired Charge Separation.....	6
1.4 Bio-Inspired Electron Transport	8
1.5 Summary.....	10
2 METHODOLOGY	12
2.1 Transient Absorption	14
2.1.1 Femtosecond Transient Absorption Apparatus.....	17
2.1.2 Nanosecond Flash Photolysis Apparatus.....	18
2.2 Transient Fluorescence.....	19
2.2.1 Time Correlated Single Photon Counting Apparatus	20
2.3 Data Analysis.....	21
2.4 Summary.....	23
3 SYNTHESIS AND SPECTROSCOPIC PROPERTIES OF A SOLUBLE SEMICONDUCTING PORPHYRIN POLYMER	24
3.1 Author Contribution.....	24
3.2 Manuscript	24
4 SYNTHESIS AND PHOTOPHYSICAL STUDIES OF A CAROTENOID-SI-PC-C60 TRIAD	61
4.1 Author Contribution.....	61
4.2 Manuscript	61
5 DE NOVO DESIGN AND SYNTHESIS OF AN ARTIFICIAL SYNTHETIC FERREDOXIN	79
5.1 Author Contribution.....	79
5.2 Manuscript	79

CHAPTER	Page
6 SUMMARY AND PERSPECTIVE	102
7 REFERENCES	104

LIST OF FIGURES

Figure		Page
1.	Atmospheric carbon dioxide recorded at Mauna Low Observatory by year	2
2.	Chromophores used in natural and bio-inspired solar energy conversion	5
3.	Carotenoid-Porphyrin-C ₆₀ molecular triad	7
4.	Structure of Photosystem I from cyanobacteria <i>Synechococcus elongatus</i>	9
5.	Jablonski Diagram of the different photophysical processes	13
6.	Jablonski Diagram of the processes of transient absorption	15
7.	Femtosecond transient absorption apparatus	17
8.	Diagram of the transient fluorescence TCSPC set-up	20
9.	Structure and synthesis of porphyrin polymer P-(PN) _n	27
10.	Structures of model monomeric and dimeric porphyrins	30
11.	Spectra of model compounds in 2-methyltetrahydrofuran	32
12.	Fluorescence emission from a solution of MPN with excitation at 420 nm	34
13.	Decay-associated emission spectra in various solvents of MPN	38
14.	Decay-associated emission spectra with excitation at 520 nm in 2-meTHF	40
15.	Spectra in 2-meTHF	42
16.	Fluorescence anisotropy decays with excitation at 680 nm	45
17.	Cyclic voltammograms for dimer MP-PN and polymer P-(PN) _n	47
18.	Femtosecond pump-probe measurement of C-Pc model	63
19.	Femtosecond transient absorption DADS of Pc-C ₆₀ model dyad	65
20.	Femtosecond pump-probe DADS of C-Pc-C ₆₀ triad	67
21.	Scheme 1	69
22.	Scheme 2	70
23.	Absorption spectrum of all compounds	72
24.	Absorption spectra of all compounds normalised at 480 nm	73
25.	Structure of [FeFe] hydrogenase from <i>Desulfovibrio desulfuricans</i>	81
26.	Design Strategy for DSD-Fdm	86

Figure		Page
27.	Gel filtration data of Apo and Holo DSD-Fdm	88
28.	UV-Vis spectra of holo DSD-Fdm before and after dithionate reduction	89
29.	Guanidine HCl mel of apo and holo DSD-Fdm	91
30.	CW EPR spectra of dithionate reduced holo DSD-Fdm	93
31.	Cyclic voltammogram of DSD-Fdm	95
32.	UV-Vis spectra of DSD-Fdm Cytochrom C assay	97
33.	Nanosecond transient absorption DADS investigating sensitization	98

CHAPTER 1
INTRODUCTION

21.2 **Significance**

Throughout the past century, human demand for energy has increased drastically and the primary energy source utilized to meet this demand has been fossil fuels¹. Combustion of these fuels has increased atmospheric levels of carbon dioxide considerably since the industrial revolution (Figure 1). This heightened level of CO₂ and other greenhouse gases has increased the average global temperature² and will have unknown effects on the world's oceans and weathersphere. Because of these effects, finding carbon neutral energy sources and utilizing sustainable technologies is of utmost importance.

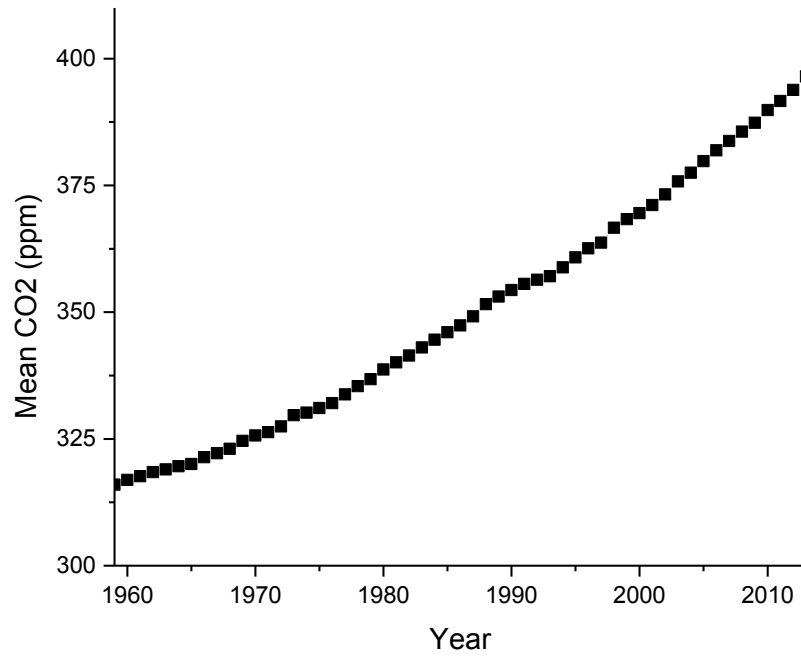


Figure 1. Atmospheric carbon dioxide recorded at Mauna Loa Observatory by year. These data show the increase in atmospheric CO₂ concentration as a function of time since 1959. CO₂ is a greenhouse gas and has been implicated in global warming. The increase in CO₂ is attributed to human consumption of fossil fuels³.

While there are many carbon neutral and sustainable technologies, sunlight is the ultimate source of energy for most of life on earth and any reasonable scheme for replacement of fossil fuels must incorporate solar power. The amount of solar energy hitting the earth's surface far surpasses current human demands⁴ and will continue to do so for the foreseeable future. Humans must learn to harness this energy in an efficient and cost-effective manner if there is to be any hope of quelling the rise of atmospheric carbon dioxide levels.

Humans have recently devised ways to capture solar energy, but nature has been doing so for billions of years via photosynthesis. Photosynthetic organisms convert solar energy into stored chemical energy in the form of sugars. This storage process allows the organism to use the fuel when there is no incident sunlight, which is a major stalling point of artificial solar energy conversion. In Photosystem I (PSI), these organisms use antennas made primarily of chlorophylls to absorb the sun's light⁵. The excitons in these molecules can undergo charge separation, facilitated by nearby electron acceptors. The electrons can go on to be stored in new chemical bonds in the fuel. The oxidized chromophore will then be reduced by an electron transport chain which starts from water, which is oxidized at the oxygen evolving complex in Photosystem II⁶.

For humans to efficiently harvest solar energy, there are many places in this pathway where they can draw inspiration. In this thesis, I will address bio-inspired light harvesting chromophores, molecules for efficient charge separation, and a *de novo* protein containing [FeS] clusters that draw inspiration from many biological systems, including PSI.

Key in the understanding of any application of solar energy is deciphering the movement of electrons through the system of interest. The relationship between the absorption of photons and how those electrons move can be understood utilizing steady-state and transient spectroscopies, which will be the focus of this dissertation.

1.2 Bio-Inspired Chromophores

Photosynthetic organisms use chlorophyll as their primary chromophore to absorb solar energy. Chlorophyll is a cofactor in Photosystem I, an enzyme contained in the thylakoid membranes of

plants, algae, and cyanobacteria⁶. The absorption spectrum of the chromophore must have strong overlap with the solar irradiation spectrum, because the absorption of light drives all the reactions that occur within the cell. When these chromophores are excited, a high energy electron is created, which has the potential to facilitate chemistry around the enzyme. The chromophores are arranged in Photosystem II so that facile electron transfer can occur to other cofactors to reduce plastoquinone and from oxidized water in the oxygen evolving complex.⁵

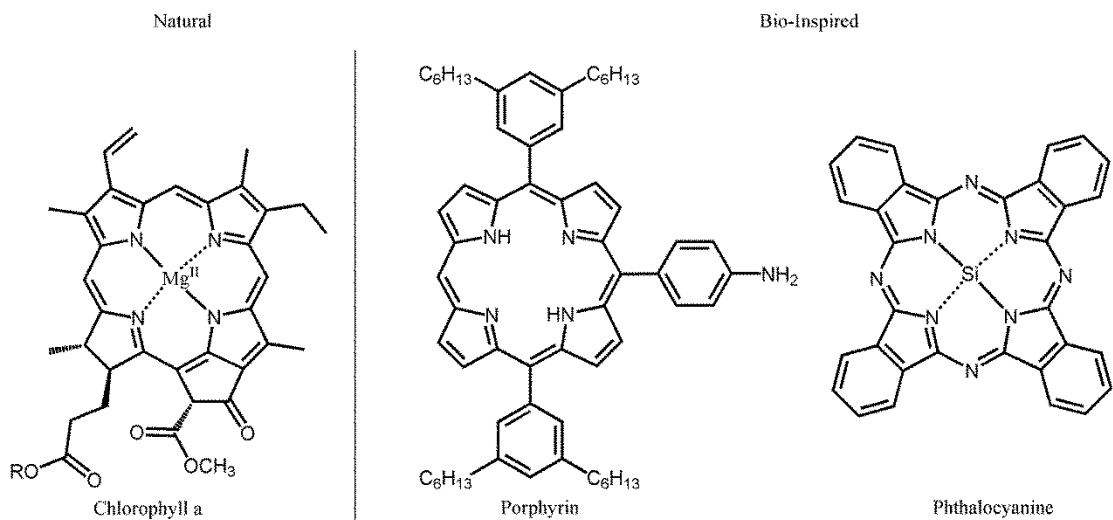


Figure 2. Chromophores used in natural and bio-inspired solar energy conversion. Organisms use chlorophyll a (left) in natural photosynthesis and porphyrins (middle) and phthalocyanines (right) are used in bio-inspired solar energy conversion. Each chromophore absorbs a different region of the visible spectrum and can be used for different applications.

Chlorophyll is difficult to synthesize in the laboratory because of its asymmetry, so structural analogues must be used if these bio-inspired systems will be utilized in a meaningful way. Chlorophyll is in a class of macrocyclic chromophores along with porphyrins and phthalocyanines (Figure 2), which have relatively facile syntheses. These two types of chromophores have different absorption spectra than chlorophyll, porphyrin absorbing strongly in the purple region and phthalocyanine in the red. They have very high extinction coefficients (ϵ), which allow them to absorb a large amount of light relative to their concentration I , per Beer's Law

$$A = \epsilon bc \quad (1)$$

where absorption (A) is also defined by the path length (b) of the light. These chromophores can be used as units of polymers, parts of dyadic and triadic systems, and as sensitizers in electron transfer systems, among many other things.

1.3 Bio-Inspired Charge Separation

Photosynthetic organisms utilize photoinduced charge separation (PICS) in Photosystem I and II to oxidize water and reduce NADP^+ . PICS occurs when a chromophore is excited and there is a nearby molecule that can overcome the coulombic energy in the exciton and accept the electron. In natural photosynthesis, an electron in chlorophyll a (ChlA) is excited, and pheophytin accepts the excited electron. Pheophytin then reduces a tightly bound quinone, which reduces a loosely bound quinone, which finally reduces a plastoquinone, which is free to shuttle to Photosystem I where it will eventually complete the reduction of NADP^+ .⁷

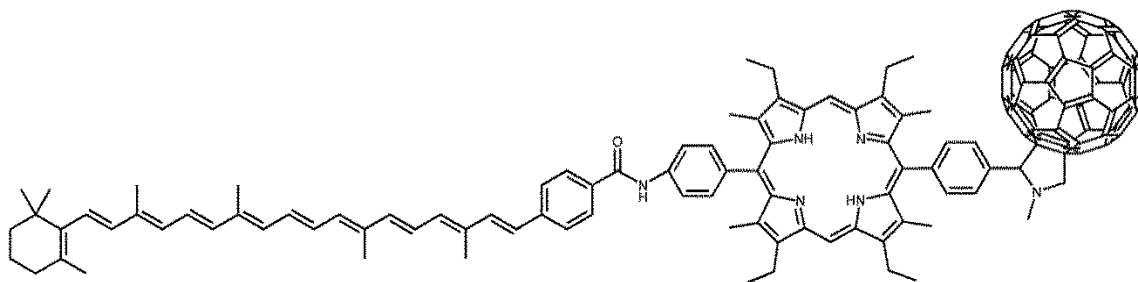


Figure 3. Carotenoid-Porphyrin-C₆₀ molecular triad. Upon excitation of the porphyrin, this molecular triad undergoes photoinduced charge separation, with the final charge-separated state C⁺-P-C₆₀⁻.

Systems that undergo intramolecular photoinduced charge separation have been studied for decades. One such system is the Carotene-Porphyrin- C_{60} (C-P- C_{60}) triad (Figure 3) which, upon excitation of the porphyrin (C-P^{*}- C_{60}) undergoes PICS to the C_{60} (C-P⁺- C_{60}^{-}) and then rapid electron transfer occurs from the carotene to the porphyrin (C⁺-P- C_{60}^{-}).⁸ This system has been the inspiration for many systems over the years and two such systems were studied in this dissertation.

1.4 Bio-Inspired Electron Transport

Organisms use iron-sulfur [FeS] clusters to shuttle electrons through proteins⁷. Active sites are often buried in the hydrophobic inner protein, inaccessible to redox mediators in solution. To work around this limitation, proteins have [FeS] clusters spaced between solvent accessible areas and active sites. These clusters have evolved to be placed between electron donors and acceptors. This distance maximizes electronic coupling between the clusters which increases the electron transfer rate between donor and acceptor⁷. This electron shuttling mechanism is employed across a vast array of proteins, but this dissertation will focus on the [FeS] clusters in photosystem I (Figure 4).

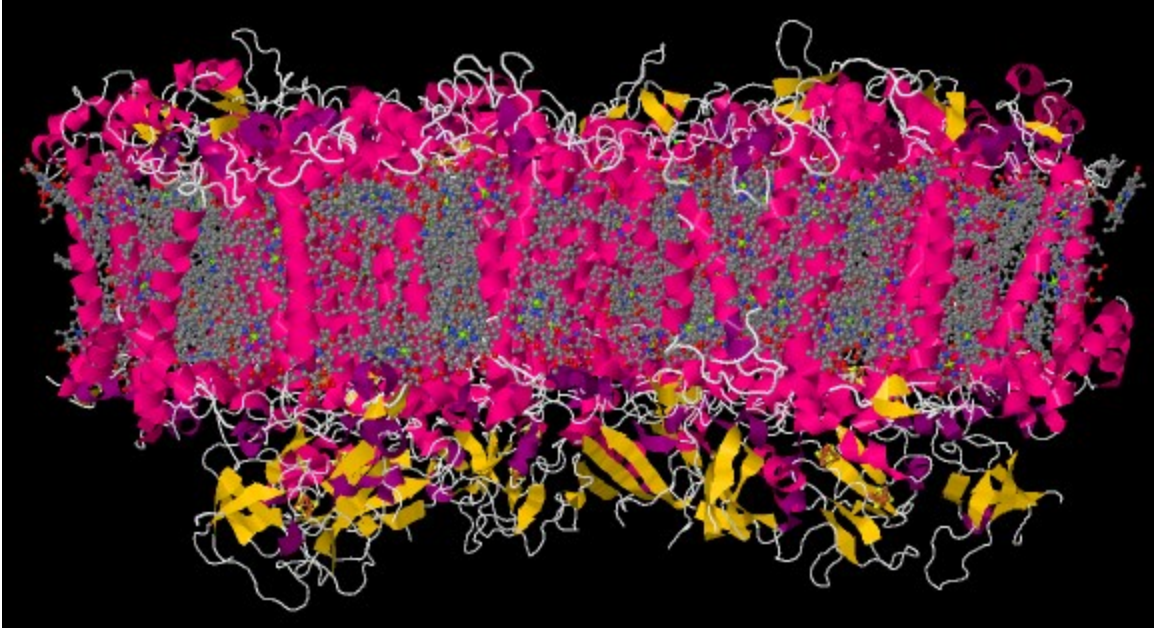


Figure 4. Structure of Photosystem I from cyanobacteria *Synechococcus ysteyne9*. All of the systems in this dissertation draw inspiration from photosynthesis. Electrons from Photosystem II shuttle over to photosystem I via reduced plastquinone where three [FeS] clusters eventually reduce ferredoxin. Image generated from PDB.org code 1JB0⁹.

In Photosystem II, chlorophyll a is excited, and those excited electrons are used to reduce plastoquinone¹⁰. Plastoquinone then shuttles over to b₆f, where it reduces multiple [FeS] clusters to eventually reduce ferredoxin. To reduce the chromophore, electrons are transported from water via the oxygen evolving complex (OEC). The very beginnings of a system inspired by these elegant enzymes are being designed and tested by collaborators in this dissertation.

1.5 Summary

Through the study of biological photosynthesis, researchers have built an expansive body of work. As the need for alternative energy sources increases, scientists continue to tap into this body of work to incorporate the elegant designs of nature into technological solutions. The utilization of chromophores that are analogous to natural chlorophyll a allows efficient capture of solar radiation and is a robust field in itself. The design of systems that undergo photoinduced charge separation combats recombination of charge in solar cells. The new use of multiple [FeS] clusters in a *de novo* protein shows great promise for future incorporation in novel proteins. Transient spectroscopy is a great tool to study the photophysics of these bio-inspired systems. The following chapters will describe this technique, as well as research performed on bio-inspired systems.

References

1. Conti, J. *et al.* International Energy Outlook 2013. DOE/IEA-0484 (2013).
2. Stocker, T. F. *et al.* IPCC 2013: *Climate Change 2013: The Physical Science Basis. Contribution of Working Group I to the Fifth Assessment Report of the Intergovernmental Panel on Climate Change.* (2013).
3. ftp://aftp.cmdl.noaa.gov/products/trends/co2/co2_anmmean_mlo.txt.
4. Sherman, B. D. *et al.* Evolution of reaction center mimics to systems capable of generating solar fuel. *Photosynthesis Research* 120, 50 (2014).
5. Duffy, C. D. P., Valkunas, L. & Ruban, A. V. Light-harvesting processes in the dynamic photosynthetic antenna. *Physical Chemistry Chemical Physics* 15, 18752 (2013).
6. Berg, J. M., Tymoczko, J. L. & Stryer, L. in *Biochemistry* (W.H. Freeman & Company, New York City, 2012).

7. Bertini, I., Gray, H. B., Stiefel, E. I. & Valentine, J. S. *Biological Inorganic Chemistry Structure and Reactivity*. (2007).
8. Moore, T. A. *et al.* Photodriven charge separation in a carotenoporphyrinquinone triad. *Nature* 307, 630 (1984).
9. Jordan, P. *et al.* Three-dimensional structure of cyanobacterial photosystem I at 2.5 Å resolution *Nature* 414, 909 (2001).
10. Umena, Y., Kawakami, K., Shen, J. & Kamiya, N. Crystal structure of oxygen-evolving photosystemII at a resolution of 1.9 Å. *Nature* 473, 55 (2011).

CHAPTER 2

METHODOLOGY

Time-resolved spectroscopy is a powerful tool to directly measure chromophore system photophysics (Figure 5). The combination of transient fluorescence, which monitors emissive electronic transitions, and transient absorption, which monitors all electronic transitions, gives great insight into how the system behaves. The time resolution of these methods is determined by duration of the laser pulses employed in the studies and the time resolution of the detection system. Very stable amplified laser pulses with duration less than 10 femtoseconds ($1 \text{ fs} = 10^{-15} \text{ s}$) are produced, enabling studies of transient systems with extremely high time resolution. Transient spectroscopy theory, technique, and data analysis are briefly described below.

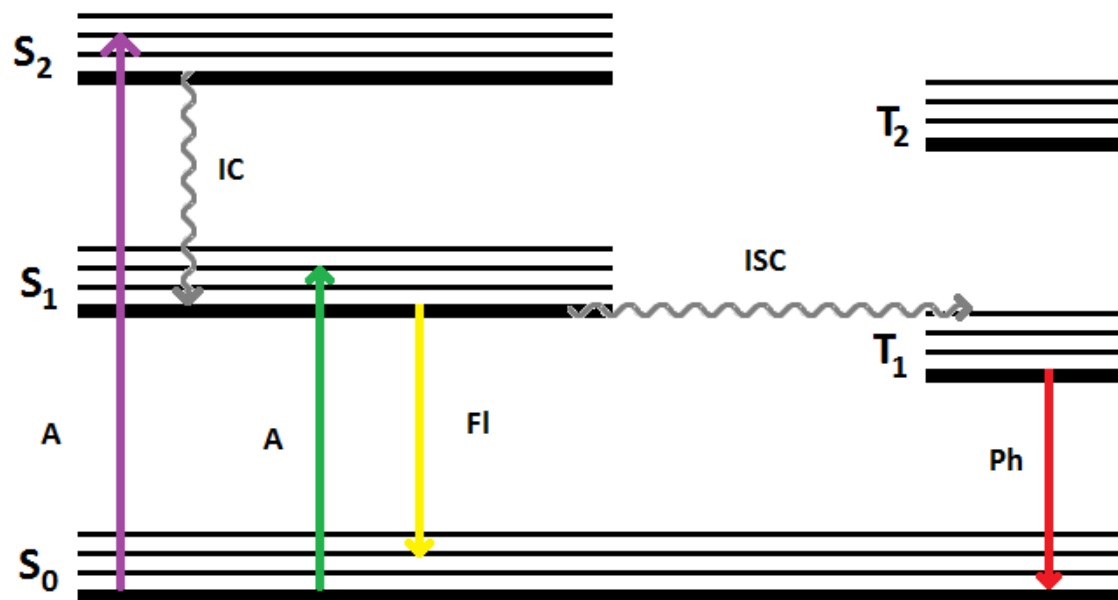


Figure 5. Jablonski diagram of the different photophysical processes. Absorption (A) happens from the singlet ground state (S_0) to a higher singlet electronic (thick lines) state (S_n). Absorption typically happens to a higher vibrational (thin lines) state of an electronic state, which then vibrationally relaxes down to the ground vibrational state of that electronic state. That state can undergo internal conversion (IC) to a lower electronic state, which can then fluoresce (Fl), which emits a photon, to the singlet ground electronic state. Another path can be intersystem crossing (ISC), where the electron flips spin to create a triplet excited state. After vibrational relaxation, this state can phosphoresce (Ph), which emits a photon, to the singlet ground electronic state.

2.1 Transient Absorption

Each of these studies uses highly-colored chromophores and one way of investigating their properties is to measure their absorption of light. The absorbance, or optical density (OD), of any material that contains chromophores is defined by:

$$OD(\lambda) = -\log \frac{I(\lambda)}{I_0(\lambda)} \quad (2)$$

Where $I_0(\lambda)$, the intensity of the incident light, and $I(\lambda)$, the intensity of the light transmitted by the material are the parameters of interest. Optical density is recorded as a function of wavelength λ , resulting in an absorption spectrum of the material¹.

Part of this dissertation deals with transient absorption experiments, which record the time-dependence of the absorption of a material after it has been excited. To be able to measure its time-dependent changes, the absorption change needs to be recorded at several distinct moments in time, rather than as a time-average, as in steady-state measurements. To capture effects that occur on ultrafast timescales the measurement of the absorption is performed with ultrashort laser-pulses. The use of a broad-band “white light” laser probe pulse facilitates the instantaneous recording of the absorption spectrum at a certain moment in time.

The work in this dissertation hinges on pump probe spectroscopy. In a pump probe experiment, an intense laser pulse (pump), resonant with an electronic transition of the chromophore, is administered to the chromophore at some time before applying the probe pulse, and the difference in absorption ΔOD , induced by the pump pulse is recorded as a function of pump probe delay, t :

$$\Delta OD(\lambda, t) = OD(\lambda, t)_{on} - OD(\lambda)_{off} = \log \frac{I(\lambda)_{off}}{I(\lambda, t)_{on}} \quad (3)$$

Where $OD(\lambda, t)_{on}$, $I(\lambda, t)_{on}$ and $OD(\lambda)_{off}$, $I(\lambda)_{off}$ denote the OD measured respectively with and without applying the pump pulse².

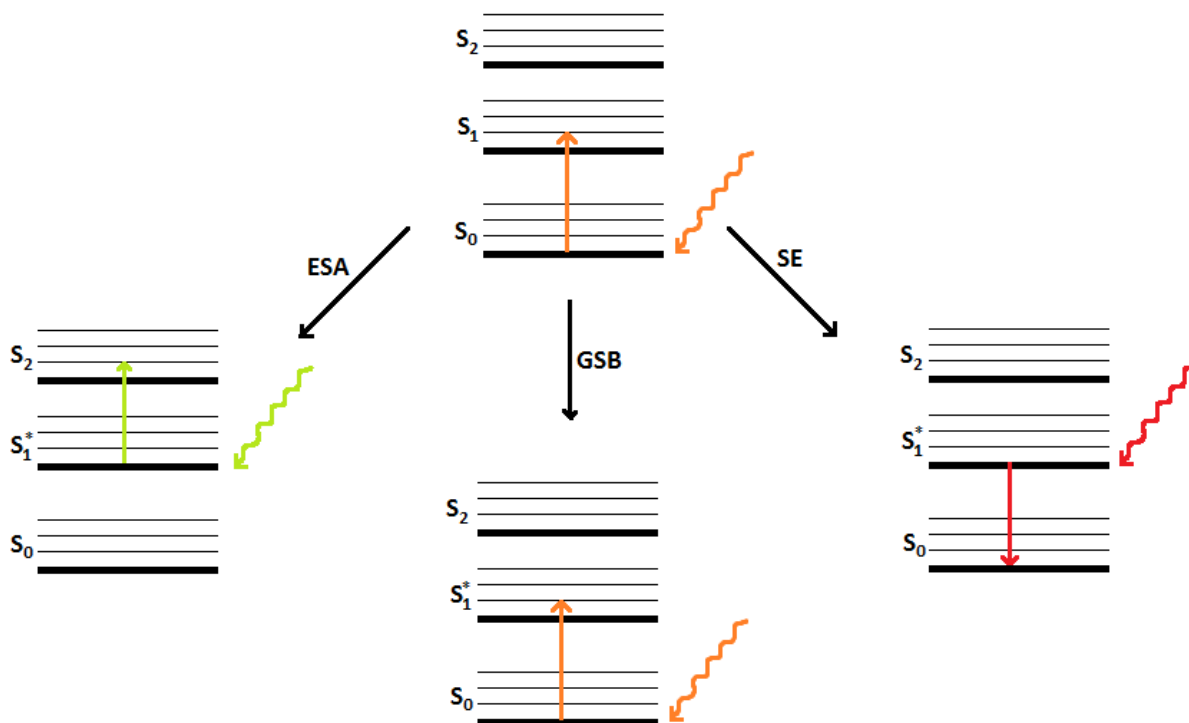


Figure 6. Jablonski diagrams of the processes of transient absorption. The system is first excited by a pumping laser beam, exciting an electron from S_0 to S_1 . Excited state absorption (ESA) arises when a wavelength of light is resonant with a transition from S_1 to $S_{n>1}$. ΔA is positive for this process. Ground state bleaching (GSB) occurs when a fraction of the population is excited and the probe light excites more molecules into their excited states. The absorption of the excited sample is less than that of the nonexcited sample so the ΔA is negative. In stimulated emission (SE), the probe pulse induces emission of a photon from an excited molecule, which relaxes to its ground state. Because of the increase in light intensity, ΔA is negative for this process. The asterisk denotes the location of the electron in the excited state.

In pump-probe experiments, the excited state absorbance at a given wavelength is measured as the difference between the absorbance with and without the first exciting laser pulse. The absorbance is proportional to the population of the different states and thus, both negative and positive signals can occur. Probing at a wavelength that matches the energy difference between excited states gives a positive signal (induced absorption), while probing at a wavelength where the ground state absorbs results in a negative signal. This is known as ground state bleaching and is a consequence of the absorption of the ground state being larger without the exciting pulse. The final type of signal is stimulated emission, which arises from the probe pulse matching the energy of the fluorescence spectrum of the molecule and inducing emission from the first excited state² (Figure 6). Predicting where these processes will occur by studying the steady state spectrum is important. These phenomena often overlap, making eye inspection of the plotted data difficult.

2.1.1 Femtosecond Pump-Probe Apparatus

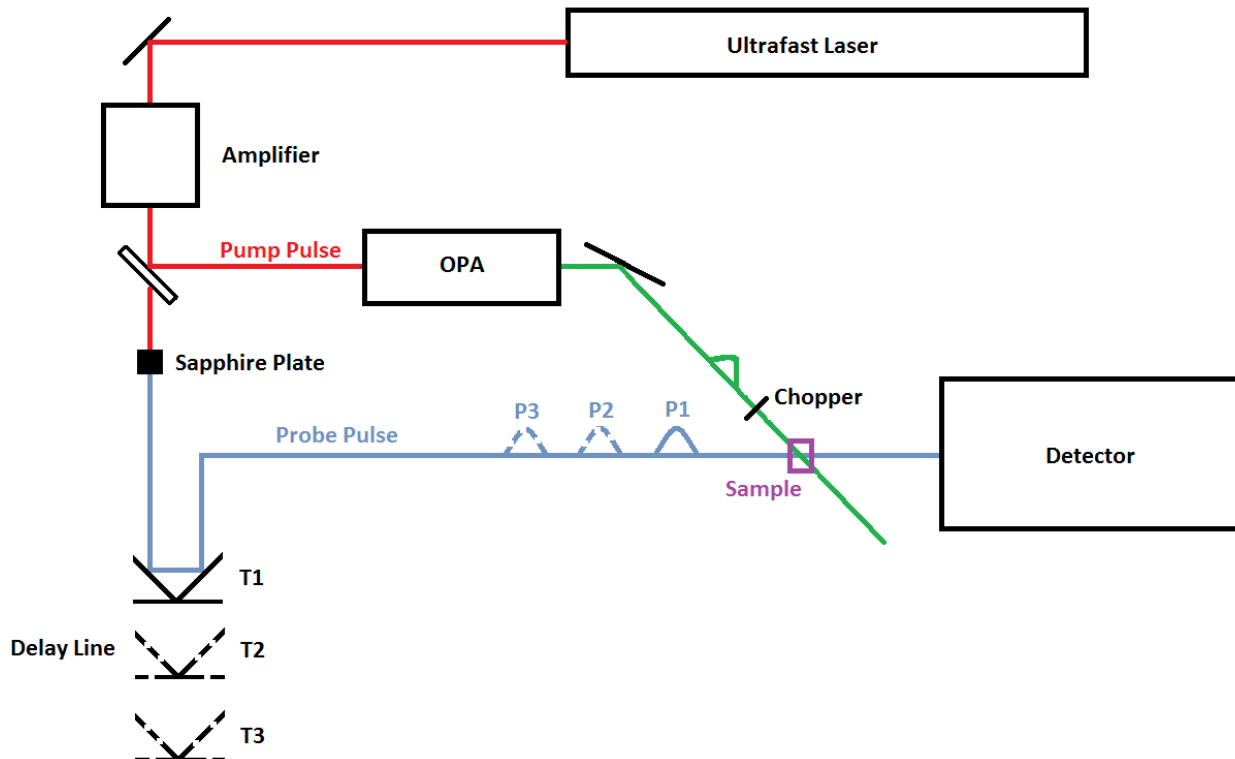


Figure 7. Femtosecond transient absorption apparatus. Femtosecond pulses are derived from an Ti:S oscillator laser that is amplified by a regenerative amplifier. This 780 nm pulse is used to drive the optical parametric amplifier (OPA) which can be tuned throughout the visible spectrum. A smaller part of the fundamental is focused on a sapphire plate for generation of a supercontinuum probe. The spectra are collected as a function of probe delay, which is shown as T1, T2, and T3. The corresponding pulses probe the sample at different times after excitation, leading to a plot of T vs ΔA .

The femtosecond transient absorption apparatus consisted of a pulsed laser source and a pump-probe optical set-up. Femtosecond pulses were obtained from a Titanium:Sapphire (Ti:S) oscillator (Tsunami, Spectra-Physics) pumped by 5 W output of a frequency-doubled, diode-pumped Nd:YVO₄ laser (Millenia VS, Spectra-Physics). These pulses are further amplified by a regenerative Ti:S amplifier (Spitfire, Spectra-Physics) pumped by a Nd:YLF laser (Evolution, Coherent) producing 100 fs pulses at 800 nm. The pulses are split and part of the pulse is focused on a 3 mm sapphire plate to generate a white light continuum for the probe beam and then sent down a delay line. The other part is used to drive an optical parametric amplifier (OPA) (800-C, Spectra-Physics) for generation of excitation pulses, which were selected using a mechanical chopper (Figure 7). After traversing the delay line, the white light probe is compressed by prism pairs before being focused on the sample. After probing, the white light is dispersed by a 300 line grating spectrograph onto a charge-coupled device camera (DU420, Andor Tech). All data were analyzed using in house software (ASUFIT).

2.1.2 Nanosecond Flash Photolysis Apparatus

To measure formation of charge separated states, lifetimes of triplet and long-lived singlet excited states nanosecond pump probe spectroscopy was employed. A Nd:YAG laser and a 150 W Xenon arc lamp were used for excitation and probe light sources, respectively. Excitation was provided from an optical parametric oscillator (OPO) pumped by the third harmonic (355 nm) of a Q-switched Nd:YAG laser (Ekspla NT 342B). The pulse width was 4-5 ns, and the repetition rate was 10 Hz.

Q-switching provides laser pulses with relatively low repetition rates, high energy, and longer pulse durations relative to other pulsing methods, which is suitable for detection of triplet states³. The third harmonic was generated by first doubling the pump wave (1064 nm) in a lithium triborate crystal (LBO) and then mixing the pump and generated second harmonic (532 nm) in a barium borate crystal (BBO). Excitation wavelength is tuned in the OPO by generation of signal and idler waves generated from the third harmonic⁴.

The probe signal was detected by a Proteus spectrophotometer (Ultrafast Systems). Before excitation, the baseline voltage of the probe signal was detected. To measure the decay of the

states, the voltage of the probe signal is measured as a function of time while passing through the excited sample. The difference between these voltages is correlated to a change in optical density, which can later be locally or globally fit with respect to wavelength.

2.2 Transient Fluorescence

Time-resolved fluorescence is a very useful technique when used in conjunction with transient absorption measurements. In the fluorescence measurements only the signals from emitting states are recorded, therefore fewer spectral contributions from different states are observed as compared to transient absorption techniques, resulting in simpler overall picture. In the work presented in this thesis, time-correlated single photon counting (TCSPC) was employed.

2.2.1 Time Correlated Single Photon Counting Apparatus

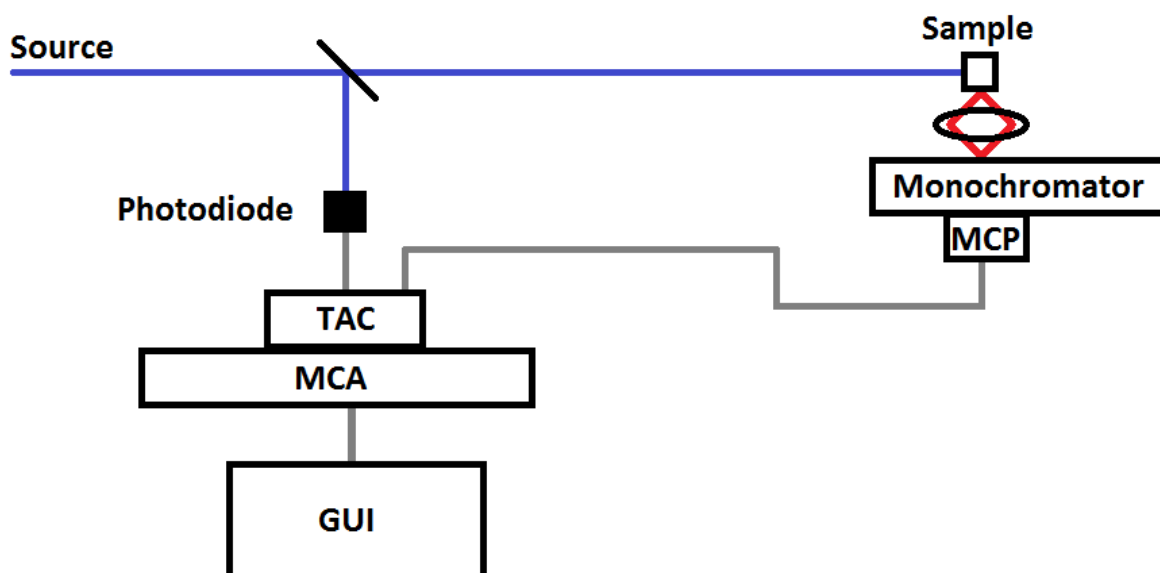


Figure 8. Diagram of the transient fluorescence time-correlated single photon counting set-up. An ultrafast pulse of photons from the laser source is split with one fraction hitting a photodiode, which starts the time-amplitude converter (TAC) voltage ramp. The other fraction of the pulse excites the sample, which emits photons, some of which are refracted by a lens and focused to the monochromator, which passes the selected wavelength to the microchannel plate photomultiplier tube (MCP). The MCP amplifies the signal, which is transmitted to the TAC, where it stops the voltage ramp, which can be correlated with a specific time in the multichannel analyzer (MCA). This data is then used to build a histogram on the graphical user interface (GUI), which corresponds to the decay of the excited state of the sample.

Excitation pulses were obtained using a Fianium Whitelase SC-400-2 supercontinuum fiber laser. The broadband laser is tuned by an acousto-optic tunable filter to select the desired wavelength. Since the tuning of the wavelength is still broad, interference filters must be used to narrow the spectral breadth before excitation of the sample. Fluorescence is collected at 90° to excitation and is detected at the magic angle (54.7°) to polarization of the excitation beam. Fluorescence is detected using a double grating monochromator (Jobin-Yohn, Gemini 180) and a microchannel plate photomultiplier tube (Hamamatsu R3809U-50). After signal amplification, a single photon counting card (Becker-Hickl SPC-830) was used for data acquisition. The instrument response function FWHM was typically ~ 50 ps. Data analysis was carried out using in house software (ASUFIT) to be described below.

2.3 Data Analysis

During time resolved experiments vast amounts of data are collected; a typical pump-probe dataset consists of tens of thousands of individual data points. To fit the decays, global analysis, a highly sophisticated method of analyzing data, is utilized. Global analysis analyzes the whole spectrum at once. Parameters are linked throughout the dataset across each decay, which reduces the total number of parameters. The whole mathematical formulation is beyond the scope of this dissertation, so only a qualitative outline of global analysis will be given.

All systems in this dissertation contain chromophores with excited states with transitions resonant with visible light. These states interact with each other through excitation transfer and each state exhibits its specific decay dynamics. To estimate the parameters that govern these processes a model is proposed, which involves a kinetic scheme and is capable of capturing all the available information. The kinetic scheme is made up of distinct compartments for different decays, which are linked by transition pathways. The suitability of a proposed model is judged by comparison to the spectra it estimates. The model can subsequently be modified and tested. Using such an iterative procedure one may eventually end up with a model that is both physically sound and describes the experimental data properly. Transient absorption datasets consist of numerous spectra measured by the white light probe at several delay points. The signal at any time t and

wavelength λ is modeled with contribution from the n different compartments of the system; if ϵ_λ is the spectrum of the l -th compartment and c_l its contribution, then the signal ($\Psi(\lambda, t)$) is

$$\Psi(\lambda, t) = \sum_{l=1}^n c_l(t) \epsilon_l(\lambda) \quad (4)$$

Since the excitation and probe pulses have a finite width, $c_l(t)$ should account for the instrument response function (IRF) of the experimental setup⁵. This IRF can either be determined directly by performing a separate measurement in a material which has an instantaneous response to the excitation or that can be parameterized and integrated in the global analysis. This procedure will not be further elaborated here.

The first step towards analyzing a data set is to fit the kinetic behavior of the system, using a model with a number of parallel, non-interacting compartments. This model yields a mathematically correct description of the data, in terms of a number of exponential decays and their corresponding concentrations, but generally does not relate directly to the photophysics of the system. The number of compartments is increased iteratively the introduction of an additional compartment does not lead to a significant improvement of the quality of the fit, which is judged on by inspection of structure present in the fit residuals and the chi-squared value. The parallel model yields estimates of the decay-associated difference spectra (DADS) which essentially represent the amplitude of each exponential component at every wavelength at time zero. The model also yields the rate constants, k_i , for each component⁵:

$$c_l(t) = e^{-k_l t} \quad (5)$$

After the number of exponential decays is ascertained, a different model is used to fit the kinetic behavior of the system. Evolution Associated Difference Spectra (EADS) can be fit, using the previously arrive upon decays, and assuming they convert into each other. EADS will more realistically model the system, as it assumes that the shorter components decay into the longer components⁵. This model can also be evaluated iteratively, honing the lifetimes until they best fit the experimental data. This model allows for a better overlap of the decay fits and transition theory. This level of analysis is as deep as this dissertation goes, but there are many more ways to globally fit transient data.

2.4 Summary

Transient spectroscopy is an incredibly powerful technique. Combining transient fluorescence measurements with femto- and nanosecond transient absorption gives a complete picture of how the electronic states of a system change over time when perturbed by visible light. This dissertation only focuses on the electronic transitions in the visible electromagnetic spectrum, but these techniques extend into the UV and IR as well. Data analysis can be carried out very simply, with specialized software and high powered computing, but understanding how the data is fit allows for a holistic understanding of the system. This dissertation is built on steady-state and transient spectroscopy, and that foundation has allowed the study of many very different and interesting systems.

References

1. Turro, N. J., Ramamurthy, V. & Scaiano, J. C. in *Principles of Molecular Photochemistry: An Introduction* (University Science Books, 2009).
2. Cho, M. Coherent Two-Dimensional Optical Spectroscopy. *Chemical Reviews* **108**, 1331 (2008).
3. Piper, J. A. & Pask, H. M. Crystalline Raman Lasers. *IEEE Journal of Selected Topics in Quantum Electronics* **13**, 692 (2007).
4. Henry, M. EKSPLA User's Manual. (2007).
5. van Stokkum, I., Larsen, D. S. & van Grondelle, R. Global and target analysis of time-resolved spectra. *Biochimica et Biophysica Acta*, 82 (2004).

CHAPTER 3
SYNTHESIS AND SPECTROSCOPIC PROPERTIES OF A SOLUBLE SEMICONDUCTING
PORPHYRIN POLYMER

3.1 Author Contribution

In this work, the author contributed all transient photophysical measurements, excluding anisotropy, as well as the electrochemistry. The author wrote the experimental sections for all photophysical and electrochemical studies.

3.2 Manuscript

Robert A. Schmitz, Paul Liddell, Gerdenis Kodis, Michael J. Kenney, Bradley J. Brennan, Nolan Oster, Thomas A. Moore,* Ana L. Moore,* and Devens Gust*

A semiconducting porphyrin polymer that is solution processable and soluble in organic solvents has been synthesized, and its spectroscopic and electrochemical properties have been investigated. The polymer consists of diarylporphyrin units that are linked at *meso*-positions by aminophenyl groups, thus making the porphyrin rings an integral part of the polymer backbone. Hexyl chains on two of the aryl groups impart solubility. The porphyrin units interact only weakly in the ground electronic state. Excitation produces a local excited state that rapidly evolves into a state with charge-transfer character (CT) involving the amino nitrogen and the porphyrin macrocycle. Singlet excitation energy is transferred between porphyrin units in the chain with a time constant of ca. 210 ps. The final CT state has a lifetime of several nanoseconds, and the first oxidation of the polymer occurs at ca. 0.58 V vs SCE. These properties make the polymer a suitable potential excited state electron donor to a variety of fullerenes or other acceptor species, suggesting that the polymer may find use in organic photovoltaics, sensors, and similar applications.

Introduction

Porphyrins and their tetrapyrrolic relatives are important compounds because of their various roles in biology as light absorbers, redox centers and binding sites for small molecules, and because of their applications (real and potential) in artificial photosynthesis, molecule-based (opto)electronics and data processing, sensing, medical imaging and treatment, and related areas. Many of these applications use both the light-absorbing and redox properties of porphyrins to convert light energy into electrochemical potential. For actual device applications, the incorporation of porphyrins into conducting or semiconducting media is especially convenient because it allows photoinduced charge separation involving a porphyrin followed by charge migration to an electrode and thence into an electronic circuit. However, given the plethora of literature on porphyrin chemistry, relatively few conducting or semiconducting porphyrin polymers have been reported. The majority of the research on conducting porphyrin polymers has been carried out by electropolymerization of porphyrin monomers to give semiconducting films on electrodes,¹⁻¹⁶ although a few examples of chemical polymerization have been reported.¹⁷⁻²² We have reported the electrochemical preparation and properties of polyporphyrins^{23,24} and polyporphyrin-fullerene dyads²⁵ based on monomers featuring both a free *meso*-position and a *meso*-aminophenyl group. Electropolymerization generates semiconducting polymers in which porphyrin macrocycles are joined by aminophenyl linkers reminiscent of polyaniline. Although these and other electropolymerized porphyrins are interesting and potentially useful materials, both their study and their applications are limited by the fact that they are bound as thin films to electrodes from which they cannot be removed, and are essentially insoluble in liquids.

We now report the synthesis and spectroscopic properties of a structurally closely related porphyrin polymer which is prepared by chemical reaction in solution, soluble in a variety of organic solvents, and solution processable via spin coating, drop casting or other methods. This polymer (**P-(PN)_n**, Fig. 1) has the same polymeric backbone as the

electropolymers reported earlier, and features 3,5-dihexyl substituted phenyl groups at two *meso*-positions. These hexyl chains greatly increase the solubility of the polymer relative to the electrochemically produced polymers, which had mesityl groups at these two *meso*-positions.

Results and Discussion

Synthesis and Characterization

Zinc monomer **PBr** was synthesized from readily available precursors by a series of reactions (see Experimental Section), and the polymer **P-(PN)_n** was prepared by palladium-catalyzed coupling of **PBr** (Fig. 9). The catalyst was prepared *in situ* in tetrahydrofuran by mixing palladium(II) acetate and bis[(2-diphenylphosphino)phenyl] ether, and then adding an excess of cesium carbonate. Polymerization ensued, leading to the zinc form of the polymer. Treatment with trifluoroacetic acid in dichloromethane removed the zinc to yield free base **P-(PN)_n**. Column chromatography was used to remove impurities and any remaining monomer. Subsequently, chromatography was used to separate the polymer into three fractions, **A**, **B**, and **C**. Details of a typical preparation of the polymer are given in the Experimental Section.

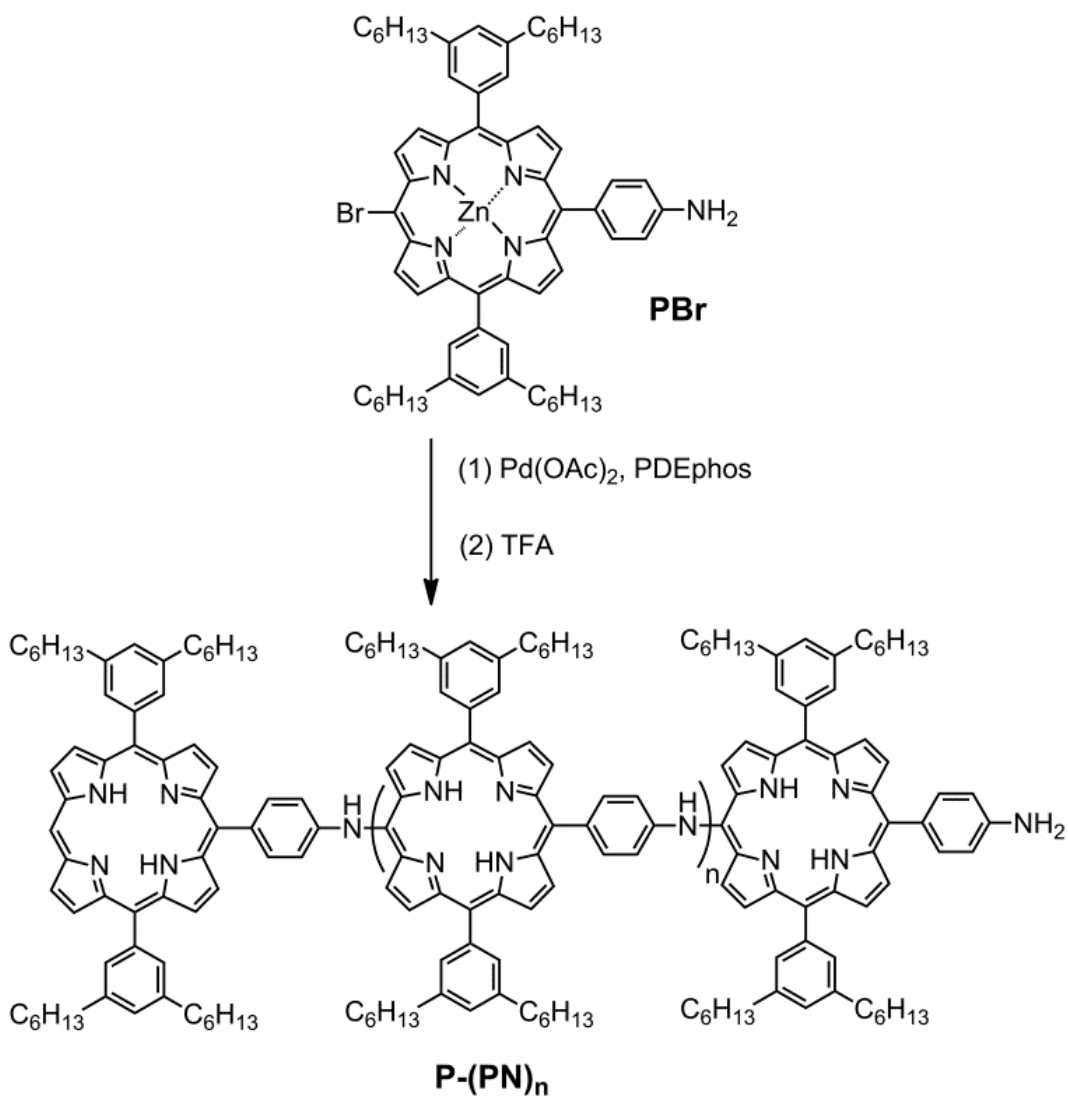


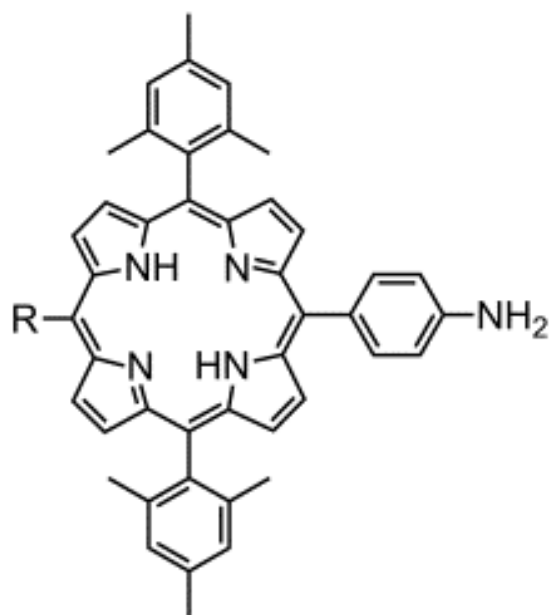
Figure 9. Structure and synthesis of porphyrin polymer **P-(PN)_n**. Synthetic details are given in the text.

Based on the order of elution in column chromatography, fractions **A**, **B**, and **C** were postulated to contain **P-(PN)_n** of increasing average molecular weight, respectively. Inductively coupled plasma elemental analysis showed that there was no detectable palladium in any of these fractions. Mass spectrometry was consistent with this assumption. Analysis was performed using MALDI-TOF instrumentation and a diphenylbutadiene matrix. This technique was not quantitative because the higher oligomers did not volatilize readily in the mass spectrometer. Thus, the ratios of peak heights does not correspond to the relative abundances of the various chains, but the technique verified the presence of the expected polymeric material and allowed some conclusions about average chain length to be drawn. All three fractions showed that no monomer was present, and chain lengths up to at least 13 units could be detected unambiguously. Longer chains were present in these samples, but their low volatility coupled with a tendency of the material to associate with itself in the mass spectrometer prevented their observation. The mass spectrum of fraction **A** showed large contributions of chains with 2-7 units plus longer chains. Fraction **B** was less easily volatilized in the mass spectrometer than **A**, and showed smaller signals for chains with 2, 3, 4 and 6 porphyrins, but significant peaks for 5-unit and longer chains. Fraction **C** was dominated by high molecular weight polymer that did not volatilize, and the signal to noise obtained was therefore low. Chain lengths up to 13 were observed, but most of the material likely consists of longer chains.

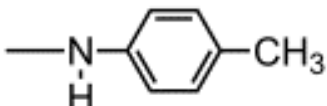
The polymer was also investigated by ¹H-NMR spectroscopy. Solutions of the polymer in deuterated chloroform were studied at 400 MHz. The spectra obtained were characterized by very broad resonances due to the long chain lengths and possible aggregation of the chains. The broadness of the resonances also accentuated resonances from minor impurities with sharp resonances, and this complicated analysis. However, for samples of all three types, resonances expected for the postulated structure were observed, thus confirming the structure. An attempt was made to estimate chain lengths by comparison of the integrals of unique protons at the ends of the polymer chains (i.e. the

meso- and *beta*-protons of the terminal porphyrin which lacks a *meso*-amino group, and the aryl and amino protons of the terminal porphyrin at the other end of the chain) with those of the aliphatic protons of the hexyl side chains of the internal porphyrins. This method was only approximate, as overlapping resonances and large differences in relaxation times are present, but suggested that fraction **A** contained significant amounts of chains with an average length of about 6 porphyrin units, whereas fractions **B** and **C** had average chain lengths of at least 20 units.

Several model compounds were prepared, including a model²³ **MP** for the porphyrin **P** at the end of the chain, a model **MPN** for the porphyrin at the amino end of the polymer chain, and a dimer **MP-PN** model for a two-porphyrin section of the polymer. These are shown in Fig. 10, and details of their preparation are reported in the Experimental Section.



MP: R = H

MPN: R = 

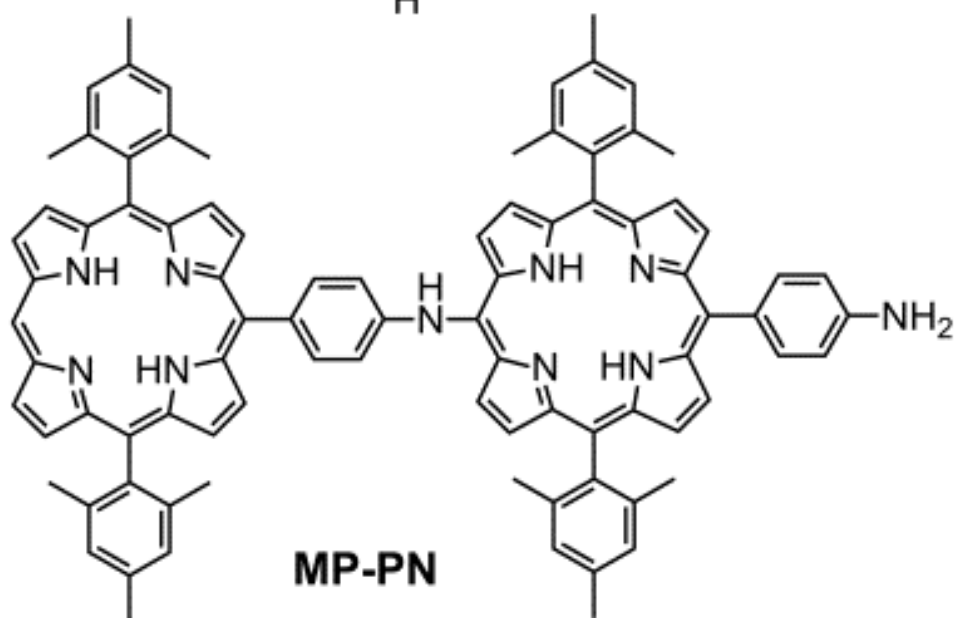


Figure 10. Structures of model monomeric and dimeric porphyrins.

Spectroscopic Properties

Monomers. The spectroscopic properties of model compounds were investigated in order to aid in the elucidation of the spectroscopic properties of the polymer. The absorption spectra in 2-methyltetrahydrofuran solution of model porphyrin **MP**, which has only hydrogen at *meso*-position 15, and model **MPN**, which has an aminotolyl group at the corresponding position, are shown in Fig. 11. The spectrum of **MP** is typical of free base porphyrins with a sharp Soret band at 413 nm and four Q-band maxima at 509, 544, 588 and 642 nm. The spectrum of **MPN**, on the other hand, has a broad Soret band at 428 nm and broad Q-band absorption, with maxima at 521, ca. 570, ca. 590, and 675 nm. Thus, the presence of the *meso*-amino group in **MPN** leads to significant distortion of the spectrum, relative to those of other free base tri- or tetra-arylporphyrins. Differences are also seen in the fluorescence emission spectra (Fig. 11). The spectrum of **MP** is similar to that of other triarylporphyrins, with maxima at 649 and 713 nm. Molecule **MPN**, on other hand, shows an emission peak at 714 nm, with a shoulder at ca. 775 nm.

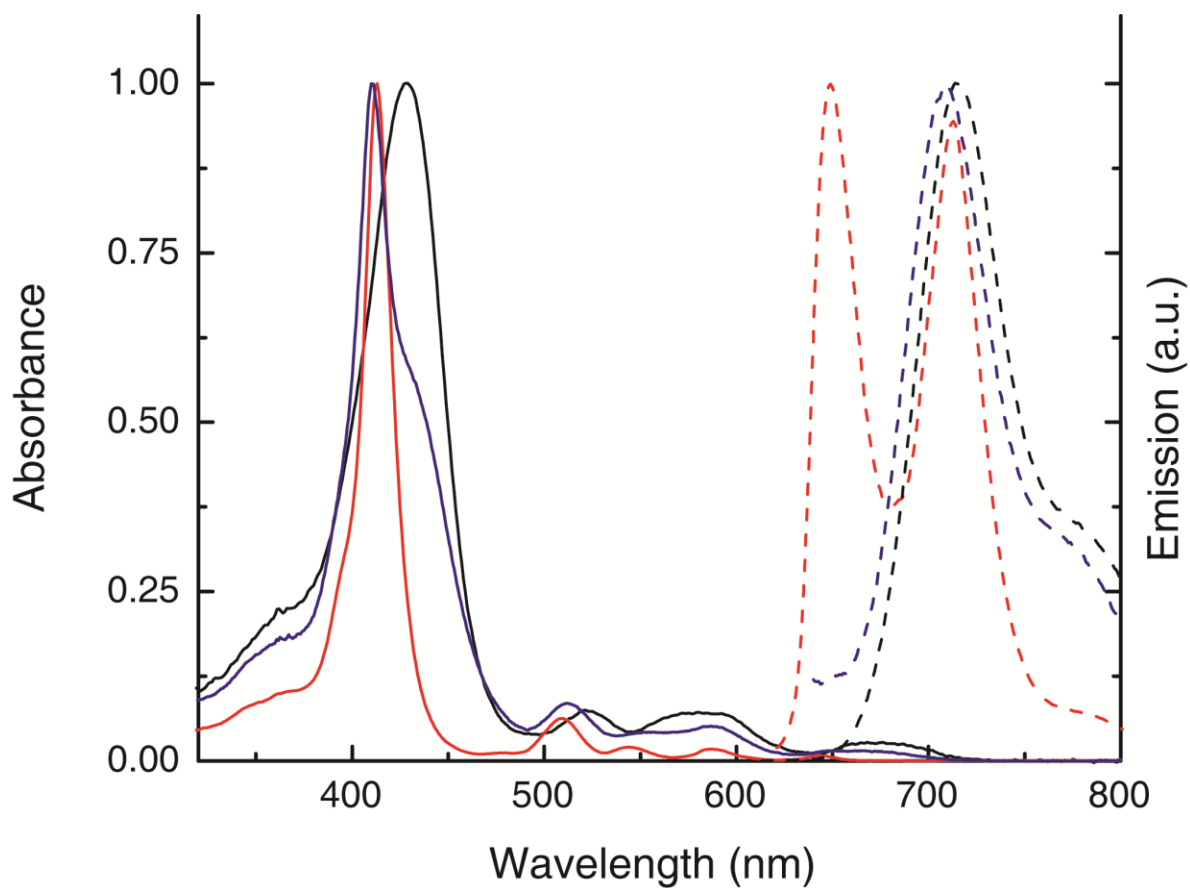


Figure 11. Spectra of model compounds in 2-methyltetrahydrofuran. Absorption spectra of **MP** (red), **MPN** (black), and **MP-PN** (blue) and corrected emission spectra of **MP** (red dash), **MPN** (black dash) and **MP-PN** (blue dash). All spectra have been normalized for ease in comparison.

These results suggest that the excited state of **MPN** is significantly perturbed from that of other porphyrins due to the presence of the *meso*-amino group. We investigated the solvent dependence of the spectra in order to get more information about this perturbation. Five solvents were investigated: acetonitrile ($\epsilon = 37.5$), 1-decanol ($\epsilon = 8.1$), 2-methyltetrahydrofuran ($\epsilon = 7.0$), toluene ($\epsilon = 2.4$) and cyclohexane ($\epsilon = 2.0$). The absorption spectra of **MP** and **MPN** showed relatively small solvent effects over this range of solvents. Porphyrin **MP** also showed only small shifts in emission. The shortest-wavelength emission band of **MP** is found at 647 nm in both cyclohexane and acetonitrile. On the other hand, larger solvent effects were observed for **MPN** in emission (Fig. 12). The main emission band appears at 696 nm in cyclohexane and 720 nm in acetonitrile.

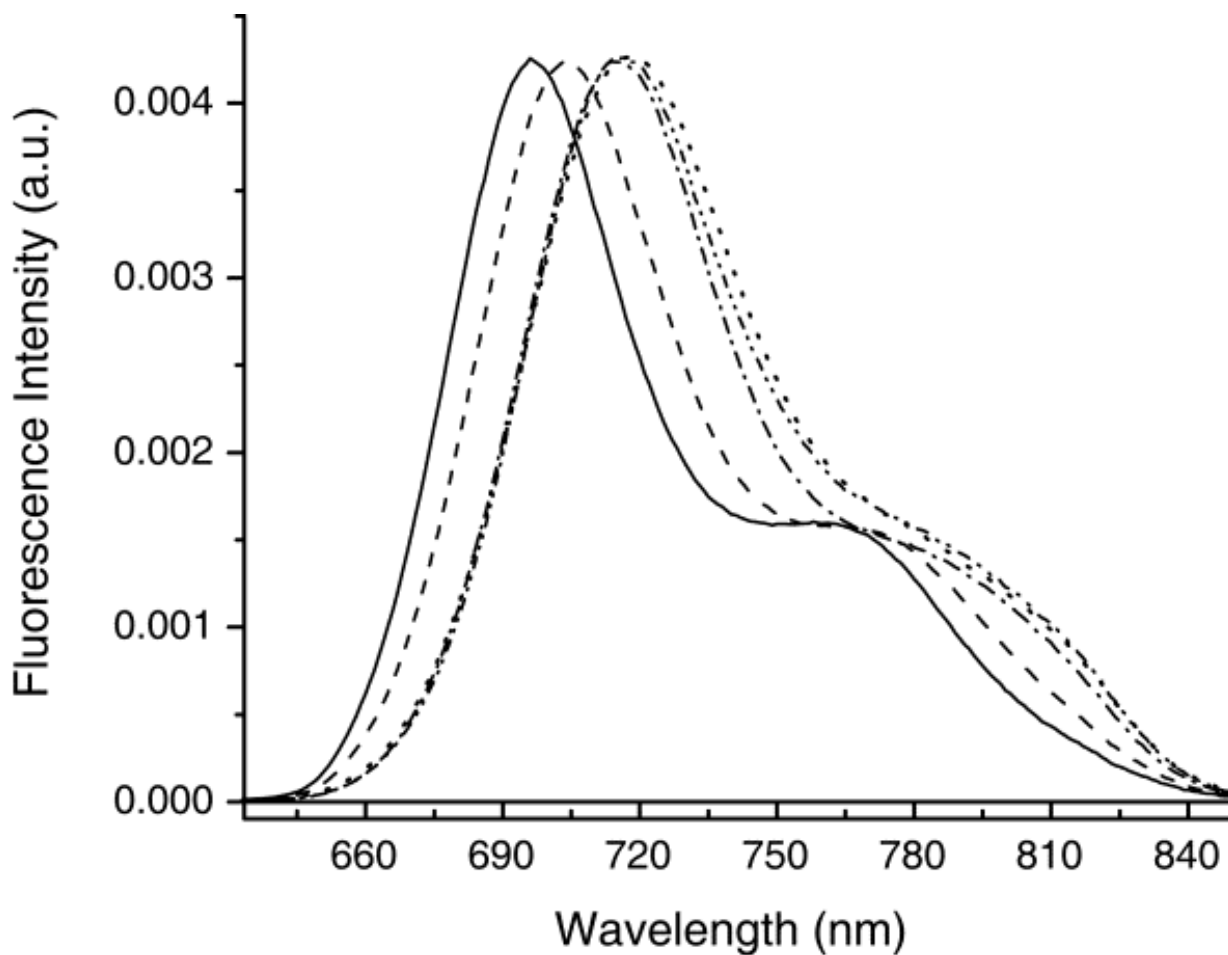


Figure 12. Fluorescence emission from a solution of **MPN** with excitation at 420 nm. The spectra are normalized at the emission maximum. Solvents were cyclohexane (solid), toluene (dashed), 2-methyltetrahydrofuran (dash-dot), 1-decanol (dash-dot-dot), and acetonitrile (dot).

It is clear from these studies that the energy of the relaxed first excited singlet state of **MPN** has a significant dependence on solvent polarity, as illustrated by the emission results, whereas that of **MP** shows only small effects. Upon increasing the dielectric constant of the solvent from 2.0 to 37.5, the shortest wavelength emission band of **MPN** shifts by 24 nm to longer wavelengths, whereas there is no observed shift in the corresponding emission of **MP**. The Stokes shift for **MPN** in 2-methyltetrahydrofuran is 38 nm, whereas that for **MP** is only 7 nm. Clearly, more polar solvents stabilize the excited state of **MPN** relative to the ground state. These data suggest that the excited state of **MPN** has significant charge-transfer (CT) character, and the more polar solvents stabilize the charge-transfer state. Presumably this state arises from increased electron donation from the amino group to the porphyrin macrocycle in the excited state, giving the amino group more positive character.

Because the excited state ³⁵ysteine³⁵ observed in **MP** and **MPN** is also expected to play a role in the photochemistry of the polymer, we investigated the emission of the model compounds as a function of time after excitation. Fluorescence decays were measured using the single photon timing technique. The emission spectrum of **MP** in 2-methyltetrahydrofuran was measured at 8 wavelengths in the 620-760 nm region, and the spectra were fitted globally to derive decay-associated spectra (DAS). The data were fitted well as a single exponential decay ($\chi^2 = 1.06$) with a time constant of 9.53 ns. Such an excited state lifetime is typical for porphyrins of this general type.

The decay-associated spectra from time-resolved fluorescence experiments on **MPN** are shown in Fig. 13. The decays were multiexponential in all of the solvents investigated. Two components were observed in cyclohexane, 2-methyltetrahydrofuran and acetonitrile, and four components were seen in 1-decanol. In all solvents, a relatively long-lived component was observed. The shape of this component is similar to that of the emission spectra shown in Fig. 12: this is expected, as this component is mainly responsible for the steady-state emission spectrum. The lifetime ranges from 7.2 ns in cyclohexane, the least

polar solvent, to 4.9 ns in acetonitrile, the most polar solvent. We ascribe this emission to the charge-transfer excited state discussed above.

The shorter-lived components are assigned to local excited (LE) states of **MPN** that evolve into the final charge-transfer state with the indicated time constants. Consistent with this assignment is the fact that the emission maxima of these states are all found at slightly shorter wavelengths than those of the CT states, indicating that these LE states are of higher energy than the CT state. The results in decanol most clearly show that the decays of the emissions of these shorter-lived states (positive amplitudes in Fig. 13d) have the same time constants as a rise of emission amplitude in the region of CT emission (negative amplitudes in Fig. 13). This indicates that the LE states decay to give the CT state. Decanol is a viscous solvent that may retard intramolecular motions that accompany relaxation of the LE states to the CT state, and permit observation of relaxations that are too fast to measure in the other solvents. It is also possible that different hydrogen bonding interactions between decanol and the *meso*-amino group of **MPN** play a role.

Dimer. We now turn to dimer **MP-PN**, which features a porphyrin bearing a *meso*-amino group linked via this moiety to a porphyrin with only a hydrogen atom at one *meso* position. Thus, it is a model for **P-(PN)₁**. The absorption spectrum of **MP-PN** (Fig. 11) features a Soret maximum at 410 nm with a strong shoulder at ca. 425 nm. The Q-band region is broad, with absorption maxima discernable at 512, ca. 550, 587, and ca. 670 nm. The spectrum is essentially a linear combination of the spectra of **MP** and **MPN**, with very minimal changes due to interactions between the chromophores. The fluorescence emission spectrum of **MP-PN** with excitation at 520 nm is very similar to that of **MPN** (Fig. 11). There is only minimal emission around 650 nm, where **MP** emits. Both porphyrins have some absorbance at 520 nm, yet emission from **PN** dominates the spectrum. This indicates that singlet excitation energy is rapidly transferred from the excited singlet state of **MP** to **PN**. This is expected because the linkage between the two chromophores is short, and the emission of **MP** overlaps well with the absorption of the longest-wavelength

Q-band of **PN**. These conditions 37ystei rapid singlet-singlet energy transfer by the Förster-type (dipole-dipole) mechanism.^{26,27} Thus, in dimer **MP-PN**, the two chromophores appear to not interact strongly in the ground state, and to exhibit efficient energy transfer in the excited state.

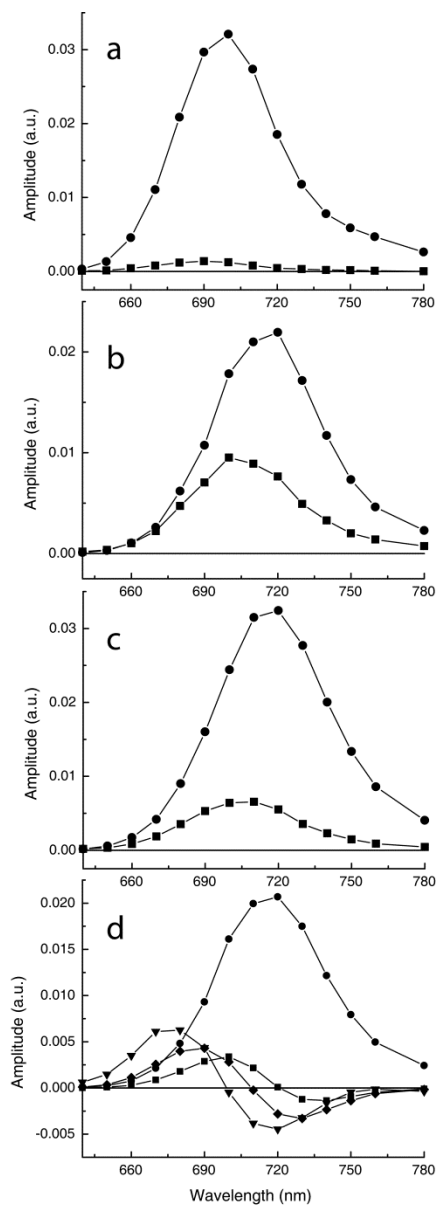


Figure 13. Decay-associated emission spectra in various solvents of **MPN** with excitation at 520 nm. (a) Cyclohexane: 7.2 ns (circles), 190 ps (squares); (b) 2-methyltetrahydrofuran: 5.7 ns (circles), 100 ps (squares); (c) acetonitrile: 4.9 ns (circles), 120 ps (squares); (d) 1-decanol: 5.4 ns (circles), 1.96 ns (squares), 380 ps (diamonds), 63 ps (triangles).

Additional information concerning **MP-PN** comes from time-resolved fluorescence studies. Fig. 14a shows the DAS for **MP-PN** in 2-methyltetrahydrofuran with excitation at 520 nm. The DAS features a long-lived component (6.0 ns) with a shape similar to that of the CT emission from **MPN** which is assigned to decay of the **MP-¹PN** charge-transfer state. Additional decay components of 540 ps and 36 ps have maxima at slightly shorter wavelengths than does the CT state, and the shapes of the DAS prove that these shorter components decay to form the final CT state. We ascribe these components to LE states similar to those noted above for **MPN** alone. It is tempting to ascribe one of these components instead to energy transfer from **¹MP-PN**. However, this could not be verified unambiguously. As mentioned earlier, **MPN** alone shows similar short components, especially in 1-decanol. In addition, a cyclic pentamer, **PN₅**, has been prepared (to be described elsewhere), and its DAS in various solvents show similar components. Energy transfer from a porphyrin having only a hydrogen atom on a *meso*-position is impossible in this pentamer due to the absence of such a porphyrin. Thus, energy transfer from **¹MP-PN** to yield **MP-¹PN** definitely occurs in **MP-PN**, but its time scale cannot be unambiguously deduced from our measurements. Ideally, excitation of **MP** only with observation of emission from **¹PN** could allow determination of such transfer, but as seen in Fig. 11, there is no suitable wavelength for such an experiment.

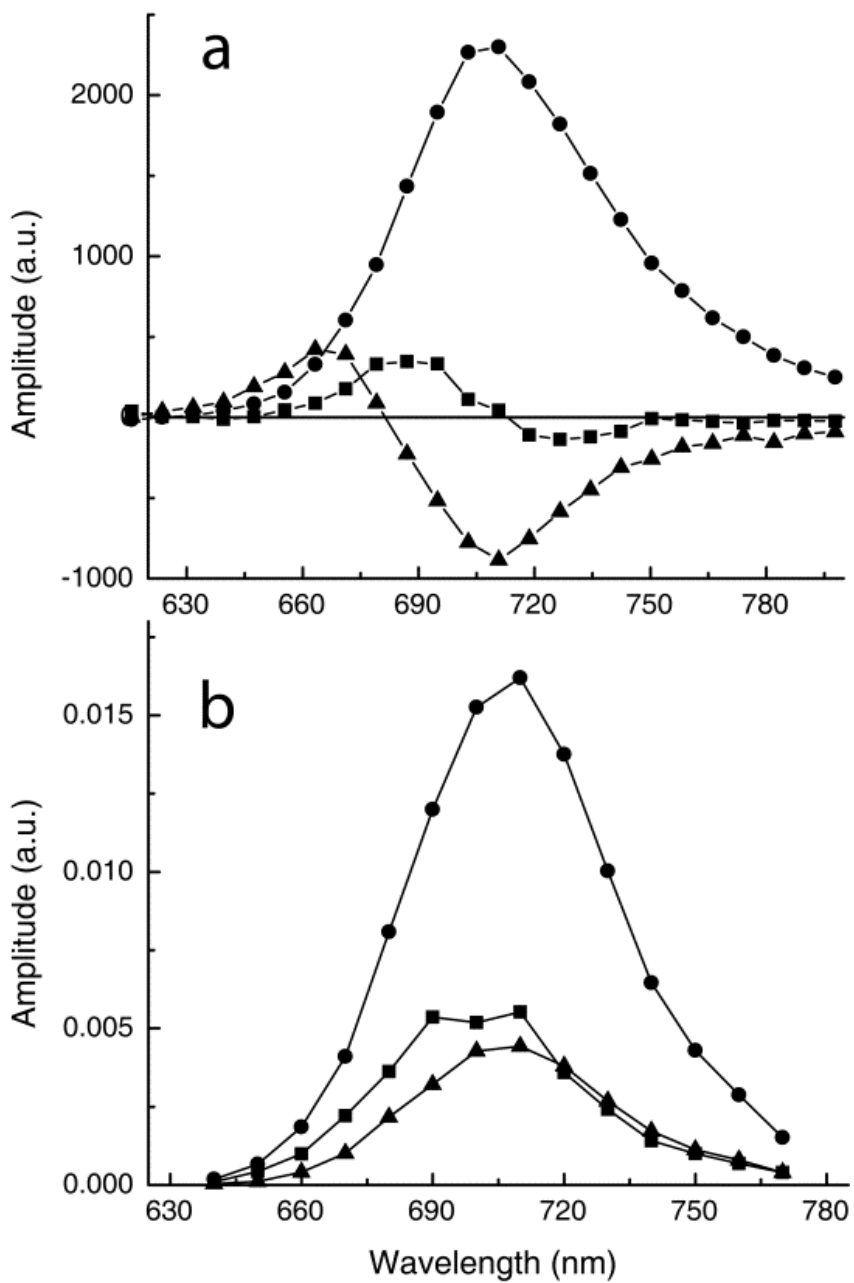


Figure 14. Decay-associated emission spectra with excitation at 520 nm in 2-methyltetrahydrofuran solution. (a) **MP-PN**, 6.0 ns (circles), 540 ps (squares), 36 ps (triangles) (b) **P-(PN)_n**, 5.4 ns (circles), 1.1 ns (triangles), 200 ps squares).

Polymer. With the results for model compounds in hand, we now examine the spectroscopic properties of the polymer **P-(PN)_n**. Experiments were performed on fraction **B** from the synthesis discussed above. The absorption spectrum in 2-methyltetrahydrofuran of the polymer, which consists of a range of chain lengths, is shown in Fig. 15, along with that of dimer **MP-PN** for comparison. The Soret band appears at 415 nm in the polymer (vs. 410 for **MP-PN**), and is very broad, with no sharp peak the region where **MP** absorbs. This is due to the higher ratio of **PN** to **P** in the oligomeric material. Absorption in the Q-band region is broad, with maxima at 520, 575, and 664. In fact, the Q-band region appears very similar to the corresponding region for **MPN** (Fig. 11). Thus, the spectrum indicates limited ground-state interaction between the porphyrin units.

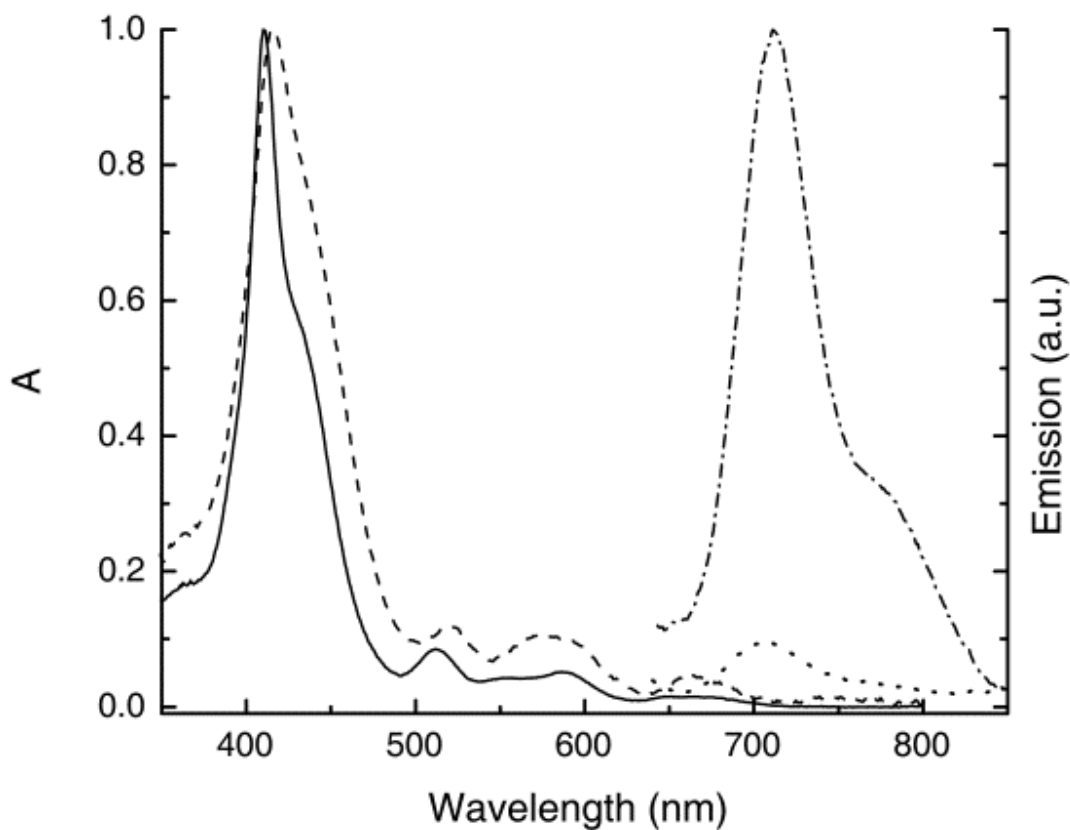


Figure 15. Spectra in 2-methyltetrahydrofuran: Absorption of **MP-PN** (solid) and **P-(PN)_n** (dash) and emission with excitation at 520 nm of **MP-PN** (dash-dot) and **P-(PN)_n** (dot). The absorption spectra have been normalized at the Soret maximum. The emission spectra show emission intensity ratios with excitation of solutions of equal absorbance at 520 nm.

Excitation of a solution of **P-(PN)_n** in 2-methyltetrahydrofuran at 520 nm yielded the emission spectrum shown in Fig. 15. The shape of the emission is similar to that of the emission of **MP-PN** as well as that of **MPN** (Fig. 11), indicating that emission arises entirely from the **PN** subunits. With identical absorbance at the excitation wavelength, the emission of **P-(PN)_n** is about 10 times weaker than that from **MP-PN**.

A time-resolved study of the emission of **P-(PN)_n** was performed in 2-methyltetrahydrofuran, with excitation at 520 nm. As shown in Fig. 6b, the main emission component has a decay time constant of 5.4 ns, which is only slightly shorter than that for **MP-PN**. Additional decay components were observed, as was the case with the dimer and **MPN** monomer. These had values of 200 ps and 1.1 ns. We assign these short components to LE states that decay to give the longer-lived CT state, as occurs in the monomer and dimer. We assume that the shorter-lived transient states in **P-(PN)_n** and **MP-PN** decay into the longest-lived emitting states, as was seen in **MP-PN**. Without knowing the yields of the conversion of the LE states into the CT state for each molecule, we cannot determine whether a portion of the 10-fold quenching in emission intensity in the polymer relative to **MP-PN** may be due to differences in the rates of processes that occur in both compounds, or to processes not present in the model dimer.

Fluorescence anisotropy and energy transfer. In principle, singlet-singlet energy transfer between porphyrin units in the polymer is possible. We isolated, by careful and repeated chromatography, a fraction of polymer containing essentially pure **P-(PN)₃** in order to investigate this phenomenon. Fluorescence anisotropy decay measurements were carried out on **MP-PN** and **P-(PN)₃** in 2-methyltetrahydrofuran solution at ambient temperatures (Fig. 16). The molecules were excited at 680 nm where the porphyrins bearing *meso*-amino substituents absorb and the fluorescence anisotropy was measured at 780 nm, where emission is also from the PN components. Fluorescence anisotropy will decay with time constants related to overall tumbling of the molecule in solution and also energy transfer between porphyrins, which results, in effect, in reorientation of the transition dipole. The anisotropy decay for dimer **MP-PN** was well fitted by a single

exponential time constant of 635 ps. This is ascribed to rotational tumbling of the molecule in solution. The decay for tetramer **P-(PN)₃** required two exponential components with time constants of 105 ps (49% of the decay) and 1.49 ns (51% of the decay). The 1.49 ns component is due to overall tumbling of the molecule, and is longer than the corresponding component in **MP-PN** because of the larger size of the molecule. The 105 ps component is assigned to energy transfer between adjacent *meso*-aminoporphyrins, and corresponds to an approximate time constant for singlet-singlet energy transfer of 210 ps. Although two adjacent porphyrin moieties are relatively close together spatially their excited states are isoenergetic, which results in a relatively small spectral overlap integral in the Förster equation²⁷ for singlet-singlet energy transfer and relatively slow energy transfer compared to systems in which the spectral overlap integral is large (e.g., energy transfer from zinc porphyrins to free base porphyrins).

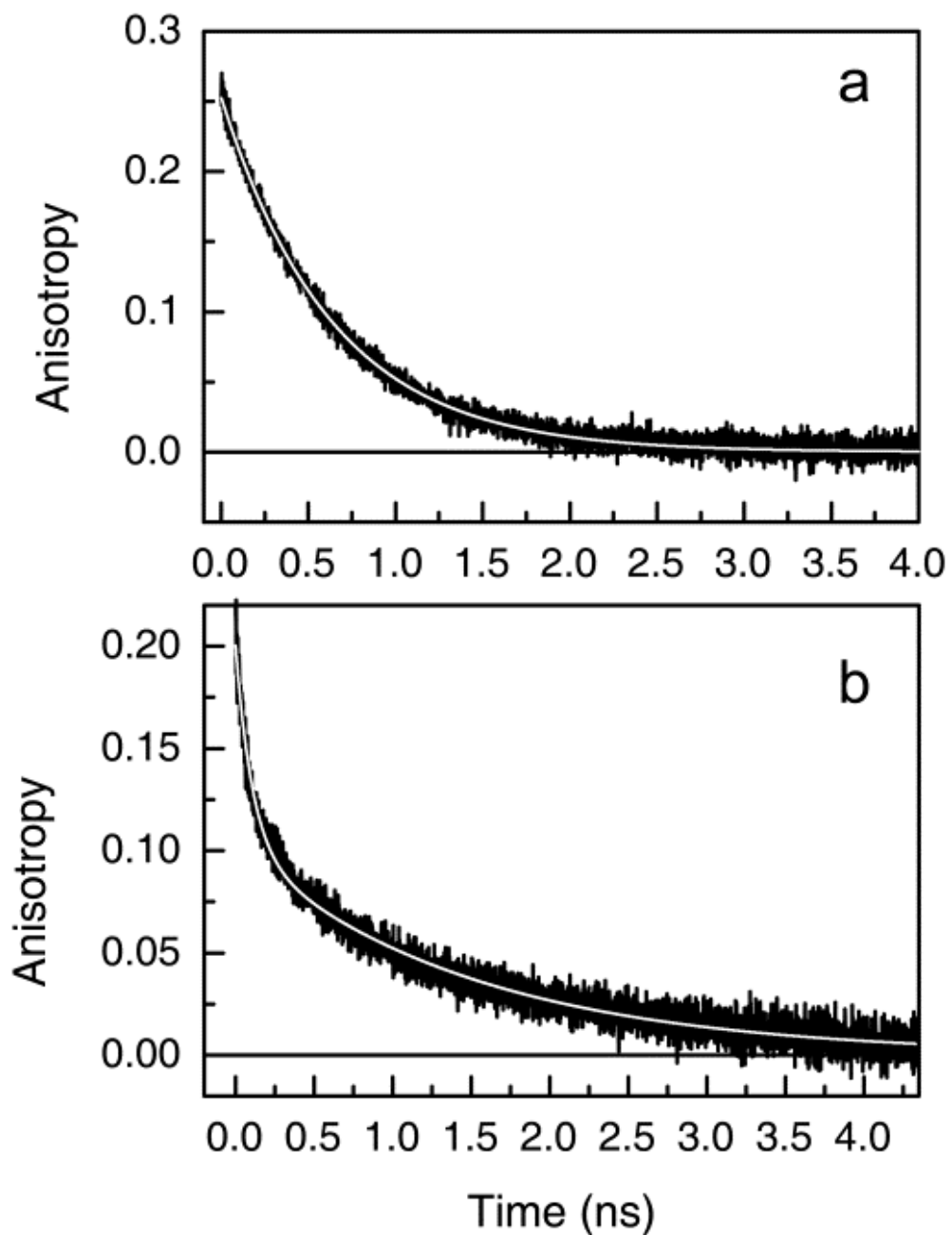


Figure 16. Fluorescence anisotropy decays with excitation at 680 nm and detection at 780 nm. (a) Dimer **MP-PN**. The white line is a best exponential fit to the data with a time constant of 635 ps. (b) Tetramer **P-(PN)₃**. The white line is a best exponential fit to the data with a time constants of 105 ps and 1.49 ns.

Electrochemical Properties

The cyclic voltammograms of the polymer and model compounds were obtained in benzonitrile solution with tetra-*n*-butylammonium hexafluorophosphate as supporting electrolyte. As reported previously,²³ monomer **MP** shows two irreversible overlapping oxidation peaks in the region 0.9 – 1.1 V vs SCE and a third irreversible peak around 1.3 V. These potentials are similar to the first and second oxidation potentials of 5,10,15,20-tetraphenylporphyrin in benzonitrile (1.08 and 1.25 V)²⁸ and the redox potential of aniline in acetonitrile (0.90 V).²⁹ The lack of reversibility is consistent with formation of an electropolymerized film on the platinum electrode. Fig. 9a shows cyclic voltammograms for dimer **MP-PN** in benzonitrile. The solubility of the dimer and the polymer were low in this solvent, which resulted in a large capacitive current contribution to the voltammogram. The first potential sweep shows oxidations at 0.58 V and 1.04 V that are essentially irreversible. The peak at 1.04 V is assigned to the first oxidation of the porphyrin with the free *meso*-position by analogy to monomer **MP** and the second oxidation of **PN**. The peak at 0.58 V is assigned to the first oxidation of porphyrin **PN**, which bears both a *meso*-amino functionality and an aniline ring. This value is consistent with redox potentials for other porphyrins with *meso*-amino substituents.³⁰ As can be seen in Fig. 17a, the second and subsequent voltage scans of **MP-PN** show irreversible 46ysteine46 under these conditions, and each sweep results in less current than the previous scan. This is consistent with formation of a film of some sort on the electrode, although **MP-PN** cannot form polymer chains, as does **MP**.

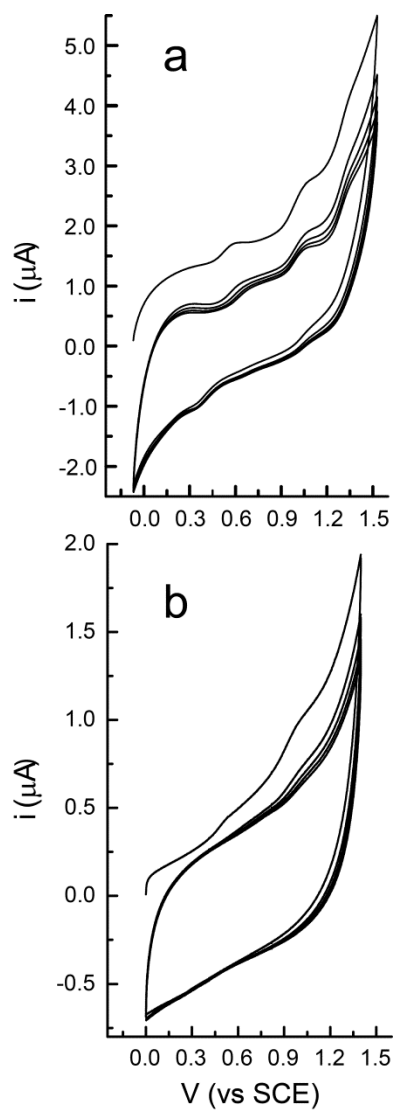


Figure 17. Cyclic voltammograms for (a) dimer **MP-PN** and polymer **P-(PN)_n** in deaerated benzonitrile containing tetra-*n*-butylammonium hexafluoro-phosphate. Voltage was swept at 100 mV s^{-1} .

Turning now to polymer **P-(PN)_n**, the voltammograms in Fig. 17b, it is clear that the 48ysteine48 is generally similar to that observed for the dimer **MP-PN**, although the peaks are not well resolved due to lack of solubility, the irreversible 48ysteine48 and deposition of a film on the electrode. Oxidation waves at ca. 0.6 and 1.0 V vs SCE are observed. The 0.6 V wave is ascribed to oxidation of porphyrin molecules within the polymer chain, and the 1.0 V wave is due to the second oxidation of these porphyrins and any contributions from the terminal porphyrins.

Experimental Section

Synthesis. The preparation of **MP** was reported previously.²³ The ¹H NMR spectra were recorded on a Varian Inova 400 or a Varian Inova 500 spectrometer. Mass spectra were obtained on a matrix-assisted laser desorption/ionization time-of-flight spectrometer (MALDI-TOF). Ultraviolet-visible ground state absorption spectra were measured on a Shimadzu UV2100U spectrometer.

3,5-Dihexylbenzaldehyde (1) To a flask containing 4.0 g (13 mmol) of methyl-3,5-dihexylbenzoate³¹ and 80 mL of tetrahydrofuran (THF) was added 0.50 g (13 mmol) of lithium 48ysteine48 hydride (LAH) in small quantities until the ester had been reduced to the corresponding alcohol. The progress of the reaction was followed by thin layer chromatography (THC) (hexanes/10% ethyl acetate). The reaction mixture was cooled in ice water and small lumps of ice were added to the reaction flask to quench excess LAH. The resulting suspension was filtered through celite and the residue was washed with dichloromethane/10% methanol. The filtrate was evaporated to dryness, and the residue was redissolved in dichloromethane (100 mL) and then washed with aqueous citric acid followed by aqueous sodium bicarbonate. The organic layer was dried over anhydrous sodium 48ysteine and concentrated to a viscous oil by evaporation of the solvent at reduced pressure. This material was dissolved in dichloromethane (100 mL) and to the stirred solution was added portions of activated manganese dioxide such that the alcohol was converted to the corresponding aldehyde. The progress of the reaction was followed

by TLC (hexanes/10% ethyl acetate). Once the reaction was complete, the suspension was filtered through Celite and the residue was washed with dichloromethane/20% methanol solution (100 mL). The filtrate was evaporated to dryness and the residue was chromatographed on silica gel (hexanes/5% ethyl acetate) to give **1** as a viscous oil (2.92 g, 81% yield). ¹H NMR (400 MHz) δ 0.88(6H,t,J=6 Hz,-CH₃), 1.31-1.38 (12H,m,-CH₂-), 1.59-1.67(4H,m,-CH₂-), 2.65(4H,t,J=8 Hz,-CH₂-), 7.26(1H,s,Ar-H partially obscured by CDCl₃), 7.51(2H,s,Ar-H), 9.97(1H,s,-CHO); MALDI-TOF-MS m/z calcd. For C₁₉H₃₀O₁ 274.2, obsd 273.8.

5,15-Bis-(3,5-dihexylphenyl)porphyrin (2). To a flask containing 3.30 g (22.6 mmol) of 2,2'-dipyrrromethane, 6.20 g (22.7 mmol) of 3,5-dihexylbenzaldehyde (**1**) and 2.3 L of chloroform was added 1.72 mL of boron trifluoride diethyl etherate. Stirring under an argon atmosphere was carried out in the dark for 30 min. A 5.14 g portion of 2,3-dichloro-5,6-dicyanobenzoquinone (DDQ) was added to the reaction mixture and stirring was continued for 1 h. The dark solution was reduced in volume to approximately 1 L by distillation of the solvent at reduced pressure and then gently shaken with aqueous sodium bicarbonate (1 L). Once the two layers had separated the organic phase was washed a further three times with fresh bicarbonate solution. The organic layer was then concentrated to a viscous oil by distillation of the solvent at reduced pressure and this oil was chromatographed on silica gel (hexanes/dichloromethane, 5:1 to 3:1). The appropriate fractions were combined, the solvent was evaporated and the residue was recrystallized from dichloromethane/methanol to give 3.56 g of **2** (40% yield). ¹H NMR (400 MHz) δ 0.92-0.95 (12H, t, J=7 Hz, -CH₃), 1.37-1.45 (16H, m, -CH₂-), 1.50-1.58 (8H, m, -CH₂-), 1.92-1.85 (8H, m, -CH₂-), 2.92 (8H, t, J=8 Hz,-CH₂-), 7.43 (2H, s, Ar-H), 7.91 (4H, s, Ar-H), 9.12 (4H, d, J=5 Hz, β-H), 9.38 (4H, d, J=5 Hz, β-H), 10.30 (2H, s, *meso*-H); MALDI-TOF-MS m/z calcd. For C₅₆H₇₀N₄ 798.6, obsd. 798.5; UV/vis (CH₂Cl₂) 408, 503, 537, 576, 631 (nm).

5-Bromo-10,20-bis-(3,5-dihexylphenyl)porphyrin (3). To a flask containing 1.00 g (1.25 mmol) of **2** and 200 mL of chloroform was added 223 mg (1.25 mmol) of N-

bromosuccinimide. After stirring the reaction mixture for 15 min, TLC (hexanes/dichloromethane, 2:1) indicated that the product was present together with lesser amounts of the starting material and the dibrominated porphyrin. The reaction mixture was concentrated to a viscous oil by evaporation of the solvent at reduced pressure and this oil was chromatographed on silica gel (hexanes/dichloromethane, 4:1 to 3:1) to give 1.17 g of **3** (68% yield). ^1H NMR (400 MHz) δ -2.97 (2H, s, -NH), 0.93 (12H, t, $J=7$ Hz, -CH₃), 1.36-1.44 (16H, m, -CH₂-), 1.48-1.56 (8H, m, -CH₂-), 1.83-1.91 (8H, m, -CH₂-), 2.89 (8H, t, $J=8$ Hz, -CH₂-), 7.43 (2H, s, Ar-H), 7.85 (4H, s, Ar-H), 8.99 (2H, d, $J=4$ Hz, β -H), 9.00 (2H, d, $J=4$ Hz, β -H), 9.28 (2H, d, $J=4$ Hz, β -H), 9.73 (2H, d, $J=5$ Hz, β -H), 10.16 (1H, s, *meso*-H); MALDI-TOF-MS m/z calcd. For C₅₆H₆₉N₄Br 876.5, obsd. 876.4; UV/vis (CH₂Cl₂) 416, 512, 547, 588, 645 (nm).

5-(4-*t*-Butylphenylcarbamate)-10,20-bis-(3,5-dihexylphenyl)porphyrin (4). To a heavy walled glass tube was added 1.00 g (1.14 mmol) of **3**, 3.64 g (11.4 mmol) of 4-(boc-amino)benzeneboronic acid pinacol, 4.83 g (22.8 mmol) of tribasic potassium phosphate and 20 mL of THF. The suspension was flushed with a stream of argon gas for 10 min, 132 mg (0.11 mmol) of tetrakis-(triphenylphosphine)palladium(0) was added and the argon flushing procedure was continued for an additional 10 min. The tube was sealed with a Teflon™ screw plug and warmed to 67 °C. After 17 h, the tube was cooled and TLC (hexanes/dichloromethane, 1:1) of the contents indicated that all the starting material had been consumed. The reaction mixture was filtered through Celite and the filtrate was concentrated to dryness by evaporation of the solvent. The residue was chromatographed on silica gel (hexanes/dichloromethane, 2:1 to 1:1) to give 985 mg (87% yield) of **4**. ^1H NMR (400 MHz) δ -2.98 (2H, s, -NH), 0.92 (12H, t, $J=7$ Hz, -CH₃), 1.32-1.42 (16H, m, -CH₂-), 1.46-1.56 (8H, m, -CH₂-), 1.64 (9H, s, -CH₃), 1.82-1.88 (8H, m, -CH₂-), 2.88 (8H, t, $J=8$ Hz, -CH₂-), 6.83 (1H, s, -NH), 7.41 (2H, s, Ar-H), 7.75 (2H, d, $J=8$ Hz, Ar-H), 7.82 (4H, s, Ar-H), 8.13 (2H, d, $J=8$ Hz, Ar-H), 8.89 (2H, d, $J=4$ Hz, β -H), 8.93 (2H, d, $J=4$ Hz, β -H), 9.04 (2H, d, $J=4$ Hz, β -H), 9.32 (2H, d, $J=4$ Hz, β -H), 10.19 (1H, s, *meso*-H); MALDI-TOF-

MS m/z calcd. For $C_{67}H_{83}N_5O_2$ 989.6, obsd. 989.6; UV/vis (CH_2Cl_2) 414, 510, 545, 584, 639 (nm).

5-Bromo-15-(4-tert-butylphenylcarbamate)-10,20-bis-(3,5-dihexylphenyl)porphyrin (5). To a 1 L flask containing 2.90 g (2.93 mmol) of **4** and 400 mL of chloroform was added 547 mg (3.07 mmol) of N-bromosuccinimide. The solution was stirred for 20 min, after which time TLC (hexanes/dichloromethane, 1:1) indicated that the reaction was complete. The reaction mixture was washed with aqueous sodium bicarbonate, dried over anhydrous sodium 51ysteine, and concentrated to dryness by distillation of the solvent under reduced pressure. The resulting material was chromatographed on silica gel (hexanes/dichloromethane, 5:2 to 3:2) to give 2.81 g (90% yield) of **5**. 1H NMR (400 MHz) δ -2.74 (2H, s, -NH), 0.91 (12H, t, $J=7$ Hz, $-CH_3$), 1.34-1.41 (16H, m, $-CH_2-$), 1.46-1.52 (8H, m, $-CH_2-$), 1.64 (9H, s, $-CH_3$), 1.81-1.88 (8H, m, $-CH_2-$), 2.87 (8H, t, $J=8$ Hz, $-CH_2-$), 6.82 (1H, s, -NH), 7.41 (2H, s, Ar-H), 7.75 (2H, d, $J=8$ Hz, Ar-H), 7.82 (4H, s, Ar-H), 8.10 (2H, d, $J=8$ Hz, Ar-H), 8.82 (4H, s, β -H), 8.92 (2H, d, $J=4$ Hz, β -H), 9.65 (2H, d, $J=5$ Hz, β -H); MALDI-TOF-MS m/z calcd. For $C_{67}H_{82}N_5O_2Br$ 1067.6, obsd. 1067.5; UV/vis (CH_2Cl_2) 422, 520, 556, 597, 654 (nm).

5-Bromo-15-(4-aminophenyl)- 10,20-bis-(3,5-dihexyl-phenyl)porphyrin (6). To a flask containing a solution of 1.5 g (1.40 mmol) of **5** dissolved in 40 mL of dichloromethane was added 60 mL of trifluoroacetic acid. The green solution was stirred under an argon atmosphere for 20 min, whereupon TLC (hexanes/dichloromethane, 1:1) indicated that the reaction was complete. The reaction mixture was diluted with 200 mL of dichloromethane and washed with water (200 mL) several times. The organic layer was then washed with aqueous sodium bicarbonate, dried over anhydrous sodium 51ysteine and then concentrated to dryness by evaporation of the solvent. The residue was chromatographed on silica gel (dichloromethane/hexanes, 3:4 to 1:1) to give 1.24 g (91% yield) of **6**. 1H NMR (400 MHz) δ -2.71 (2H, s, -NH), 0.91 (12H, t, $J=7$ Hz, $-CH_3$), 1.34-1.42 (16H, m, $-CH_2-$), 1.46-1.52 (8H, m, $-CH_2-$), 1.81-1.88 (8H, m, $-CH_2-$), 2.86 (8H, t, $J=8$ Hz, $-CH_2-$), 3.98 (2H, s, -NH), 7.02 (2H, d, $J=8$ Hz, Ar-H), 7.40 (2H, s, Ar-H), 7.82 (4H, s, Ar-H), 7.94

(2H, d, $J=8$ Hz, Ar-H), 8.84 (2H, d, $J=5$ Hz, β -H), 8.87 (2H, d, $J=5$ Hz, β -H), 8.92 (2H, d, $J=5$ Hz, β -H), 9.64 (2H, d, $J=5$ Hz, β -H); MALDI-TOF-MS m/z calcd. For $C_{62}H_{74}N_5Br$ 967.5, obsd. 967.5; UV/vis (CH_2Cl_2) 423, 521, 559, 598, 656 (nm).

[5-Bromo-15-(4-aminophenyl)-10,20-bis-(3,5-dihexylphenyl)porphyrino]zinc(II) (PBr). To a flask containing 1.20 g (1.24 mmol) of **6** and 200 mL of dichloromethane was added 50 mL of a saturated solution of zinc acetate 52ysteine52 in methanol. After stirring for 1 h, TLC (hexanes/methylene chloride, 1:1) indicated that all the starting material had been consumed and a single product had formed. The pink reaction mixture was washed with water (200 mL) several times and then with aqueous sodium bicarbonate; it was then dried over anhydrous sodium 52ysteine. The solvent was evaporated at reduced pressure and the remaining solid was dried under high vacuum to give 1.21 g (95% yield) of **PBr**. 1H NMR (400 MHz) δ 0.91 (12H, t, $J=7$ Hz, $-CH_3$), 1.32-1.41 (16H, m, $-CH_2-$), 1.45-1.51 (8H, m, $-CH_2-$), 1.80-1.88 (8H, m, $-CH_2-$), 2.86 (8H, t, $J=7$ Hz, $-CH_2-$), 3.82 (2H, s, $-NH$), 6.93 (2H, d, $J=8$ Hz, Ar-H), 7.38 (2H, s, Ar-H), 7.82 (4H, s, Ar-H), 7.92 (2H, d, $J=8$ Hz, Ar-H), 8.86 (2H, d, $J=4$ Hz, β -H), 8.90 (2H, d, $J=4$ Hz, β -H), 8.96 (2H, d, $J=5$ Hz, β -H), 9.70 (2H, d, $J=5$ Hz, β -H); MALDI-TOF-MS m/z calcd. For $C_{62}H_{72}N_5BrZn$ 1029.4, obsd. 1029.4; UV/vis (CH_2Cl_2) 424, 517(sh), 553, 595 (nm).

Polymer P-(PN)_n. To a 250 mL heavy walled glass flask was added 1.00g (0.97 mmol) of **PBr**, 78 mg (0.15 mmol) of bis[(2-diphenylphosphino)phenyl] ether, 442 mg (1.36 mmol) of cesium carbonate and 200 mL of THF. The suspension was flushed with a stream of argon for 15 min, 21 mg (0.01 mmol) of palladium(II) acetate was added and the argon flushing process was continued for a further 10 min. The flask was sealed with a Teflon™ screw plug and the reaction mixture was stirred at 67°C for 42 h. A TLC on silica gel (dichloromethane/hexanes, 1:1) of the reaction mixture indicated that most if not all of the starting material had been consumed and that many other compounds (polymers of different chain lengths) had formed. The reaction mixture was filtered through Celite and the residual material was thoroughly washed with THF. The combined filtrate was concentrated by distillation of the solvent at reduced pressure and dried under high

vacuum. The residue was dissolved in a mixture of dichloromethane (200 mL) and trifluoroacetic acid (200 mL) and stirred under an argon atmosphere for 1 h. The reaction mixture was then diluted with dichloromethane (200 mL) and washed with water followed by aqueous sodium bicarbonate. The solvent was then evaporated and the residue was chromatographed on silica gel (dichloromethane/2% THF, dichloromethane/20% THF and finally dichloromethane/20% THF/10% methanol) to give three fractions **A**, **B** and **C** the weight of each being, 0.43 g, 0.33 g, and 0.21g. Characterization was performed as discussed in the Results and Discussion section.

5-Bromo-15-(4-*tert*-butylphenylcarbamate)-10,20-bis(2,4,6-trimethylphenyl)porphyrin (7). To a flask containing a solution of 159 mg (0.203 mmol) of 10-(4-*tert*-butylphenylcarbamate)-5,15-bis(2,4,6-trimethylphenyl)porphyrin (**8**)²³ and 50 mL of chloroform was added 38 mg (0.21 mmol) of N-bromosuccinimide. The reaction mixture was stirred for 30 min, at which time the solvent was evaporated at reduced pressure and the residue was chromatographed on silica gel (dichloromethane/hexanes, 1:1) to give 153 mg (92% yield) of **7**. ¹H NMR (300 MHz) δ -2.59 (2H, s, N-H), 1.63 (9H, s, -CH₃), 1.83 (12H, s, Ar-CH₃), 2.63 (6H, s, Ar-CH₃), 6.82 (1H, s, N-H), 7.28 (4H, s, Ar-H), 7.74 (2H, d, *J*=8 Hz, Ar-H), 8.10 (2H, d, *J*=8 Hz, Ar-H), 8.64 (2H, d, *J*=5 Hz, β -H), 8.73 (2H, d, *J*=5 Hz, β -H), 8.78 (2H, d, *J*=4 Hz, β -H), 9.59 (2H, d, *J*=5 Hz, β -H); MALDI-TOF-MS *m/z* calcd. For C₄₉H₄₆N₅O₂Br 815.28, obsd. 815.29; Uv/vis (CH₂Cl₂) 421, 520, 553, 596, 653 (nm).

Carbamate-protected form of MP-PN (9). To a glass tube was added 86 mg (0.14 mmol) of 10-(4-aminophenyl)-5,15-bis(2,4,6-trimethylphenyl)porphyrin,²³ 100 mg (0.122 mmol) of **7**, 56 mg (0.17 mmol) of cesium carbonate, 10 mg (0.018 mmol) of bis[(2-diphenylphosphino)phenyl] ether and 20 mL of THF. The suspension was flushed with argon for 10 min, 3 mg (0.012 mmol) of palladium acetate was added and the flushing procedure was continued for an additional 5 min. The tube was sealed with a Teflon[®] screw plug and the reaction mixture was warmed to 67 °C for 18 h. Once cool, the solvent was evaporated by distillation at reduced pressure and the residue was chromatographed

on silica gel (hexanes/15% ethyl acetate) to give 163 mg of **9** (97% yield). ^1H NMR (300 MHz) δ -2.88 (2H, s, N-H), -2.26 (2H, s, N-H), 1.63 (9H, s, -CH₃), 1.82 (12H, s, Ar-CH₃), 1.89 (12H, s, Ar-CH₃), 2.65 (12H, s, Ar-CH₃), 6.82 (1H, s, N-H), 7.29 (4H, s, Ar-H), 7.30 (4H, s, Ar-H), 7.3 (2H, m, Ar-H partially obscured), 7.73 (2H, d, $J=8$ Hz, Ar-H), 8.02 (2H, d, $J=8$ Hz, Ar-H), 8.05 (1H, s, N-H), 8.11 (2H, d, $J=8$ Hz, Ar-H), 8.65 (2H, d, $J=5$ Hz, β -H), 8.73-8.81 (8H, m, β -H), 9.03 (2H, d, $J=5$ Hz, β -H), 9.23 (2H, d, $J=5$ Hz, β -H), 9.60 (2H, d, $J=5$ Hz, β -H), 10.06 (1H, s, *meso*-H); MALDI-TOF-MS m/z calcd. For C₉₃H₈₄N₁₀O₂ 1372.68, obsd. 1372.68; Uv/vis (CH₂Cl₂) 413, 426 (sh), 514, 551, 587, 647, 668 (nm).

Dyad MP-PN. Compound **9** (150 mg, 0.109 mmol) was added to a flask along with 30 mL of trifluoroacetic acid. The green solution was stirred under a nitrogen atmosphere for 20 min and then diluted with dichloromethane (150 mL). After washing with water and aqueous sodium bicarbonate, the solution was dried over sodium 54ysteine and then concentrated by distillation of the solvent at reduced pressure. The residue was chromatographed on silica gel (dichloromethane/20-5% hexanes) to give 125 mg of **MP-PN** (90% yield). ^1H NMR (300 MHz) δ -2.88 (2H, s, N-H), -2.25 (2H, s, N-H), 1.82 (12H, s, Ar-CH₃), 1.89 (12H, s, Ar-CH₃), 2.64 (12H, s, Ar-CH₃), 3.98 (2H, s, N-H), 7.03 (2H, d, $J=8$ Hz, Ar-H), 7.29 (4H, s, Ar-H), 7.30 (4H, s, Ar-H), 7.3(2H, m, Ar-H partially obscured), 7.96 (2H, d, $J=8$ Hz, Ar-H), 8.02 (2H, d, $J=8$ Hz, Ar-H), 8.02 (1H, s, N-H), 8.65 (2H, d, $J=4$ Hz, β -H), 8.73-8.84 (8H, m, β -H), 9.03 (2H, d, $J=5$ Hz, β -H), 9.22 (2H, d, $J=4$ Hz, β -H), 9.59 (2H, d, $J=5$ Hz, β -H), 10.06 (1H, s, *meso*-H); MALDI-TOF-MS m/z calcd. For C₈₈H₇₆N₁₀ 1272.63, obsd. 1272.62; Uv/vis (CH₂Cl₂) 412, 426 (sh), 514, 554, 587, 649, 662 (nm).

Carbamate Protected Form of MPN (10). To a heavy walled glass tube was added 190 mg (0.23 mmol) of **7**, 75 mg (0.70 mmol) of *p*-toluidine, 106 mg (0.33 mmol) of cesium carbonate, 19 mg (0.04 mmol) of bis[(2-diphenylphosphino)phenyl] ether and 60 mL of THF. The mixture was flushed with argon gas for 15 min, 5.2 mg (0.02 mmol) of palladium acetate was added and the argon gas flushing process was continued for an additional 10 min. The tube was sealed with a Teflon™ screw plug and the reaction mixture was warmed to 67 °C. After 17 h the reaction mixture was cooled and TLC (hexanes/20% ethyl

acetate) indicated that all the starting porphyrin had been consumed. The reaction mixture was filtered through Celite and the residue was washed thoroughly with THF (100 mL). The filtrate was concentrated to dryness by removal of the solvent at reduced pressure and the residue was chromatographed on silica gel (hexanes/5-7.5% ethyl acetate) to give 163 mg of **10** (83% yield). $^1\text{H NMR}$ (400 MHz) δ -2.31 (2H, s, N-H), 1.63 (9H, s, $-\text{CH}_3$), 1.84 (12H, s, Ar- CH_3), 2.26 (3H, s, Ar- CH_3), 2.62 (6H, s, Ar- CH_3), 6.81 (1H, s, N-H), 6.87 (2H, d, $J=8$ Hz, Ar-H), 6.99 (2H, d, $J=8$ Hz, Ar-H), 7.26 (4H, s, Ar-H partially obscured), 7.63 (1H, s, N-H), 7.73 (2H, d, $J=8$ Hz, Ar-H), 8.09 (2H, d, $J=8$ Hz, Ar-H), 8.59 (2H, d, $J=5$ Hz, β -H), 8.60 (2H, d, $J=5$ Hz, β -H), 8.74 (2H, d, $J=5$ Hz, β -H), 9.27 (2H, d, $J=4$ Hz, β -H); MALDI-TOF-MS m/z calcd. For $\text{C}_{56}\text{H}_{54}\text{N}_6\text{O}_2$ 842.4, obsd. 842.4; UV/vis (CH_2Cl_2) 423, 520, 572, 590, 663 (nm).

MPN. To a flask containing 150 mg (0.18 mmol) of **10** and 20 mL of dichloromethane was added 20 mL of trifluoroacetic acid. The green solution was stirred at room temperature under an argon atmosphere for 30 min. A TLC (hexanes/20% ethyl acetate) indicated that the reaction was complete. The reaction mixture was diluted with dichloromethane (100 mL) and washed with water (2×100 mL) and then with aqueous sodium bicarbonate (100 mL). The solution was dried over anhydrous sodium 55ysteine and filtered, and the filtrate was concentrated to a purple solid. This material was chromatographed on silica gel (hexanes/25% ethyl acetate) to give 120 mg of **MPN** (91% yield). $^1\text{H NMR}$ (400 MHz) δ -2.31 (2H, s, N-H), 1.84 (12H, s, Ar- CH_3), 2.26 (3H, s, Ar- CH_3), 2.62 (6H, s, Ar- CH_3), 4.01 (2H, s, N-H), 6.86 (2H, d, $J=8$ Hz, Ar-H), 6.99 (2H, d, $J=8$ Hz, Ar-H), 7.04 (2H, d, $J=8$ Hz, Ar-H), 7.24 (4H, s, Ar-H partially obscured), 7.61 (1H, s, N-H), 7.95 (2H, d, $J=8$ Hz, Ar-H), 8.59 (2H, d, $J=5$ Hz, β -H), 8.61 (2H, d, $J=5$ Hz, β -H), 8.80 (2H, d, $J=5$ Hz, β -H), 9.27 (2H, d, $J=5$ Hz, β -H); MALDI-TOF-MS m/z calcd. For $\text{C}_{51}\text{H}_{46}\text{N}_6$ 742.4, obsd. 742.6; UV/vis (CH_2Cl_2) 427, 521, 570, 590, 665 (nm).

Electrochemical Measurements. The voltammetric characterization of the redox processes for the molecules was performed with a CHI 620 potentiostat (CH Instruments) using a Pt disk working electrode, a Pt wire mesh counter electrode, and a silver wire

quasi-reference electrode in a conventional three-electrode cell. Electrochemical studies were carried out in anhydrous benzonitrile containing 0.10 M tetra-*n*-butylammonium hexafluorophosphate as the supporting electrolyte. The working electrode was cleaned between experiments by polishing with diamond paste slurry, followed by solvent rinses. After each voltammetric experiment, ferrocene was added to the solution, and the potential axis was calibrated against the formal potential of the ferrocenium/ferrocene redox couple (taken as 0.45 V vs SCE in dichloromethane).

Steady-state spectroscopy. Absorption spectra were measured on a Shimadzu UV-3101PC UV-vis-NIR spectrometer. Steady-state fluorescence spectra were measured using a Photon Technology International MP-1 spectrometer and corrected for detection system response. Excitation was provided by a 75 W xenon-arc lamp and single grating monochromator. Fluorescence was detected 90° to the excitation beam via a single grating monochromator and an R928 photomultiplier tube having S-20 spectral response and operating in the single photon counting mode.

Time-resolved fluorescence. Fluorescence decay kinetics were measured using the time-correlated single-photon counting technique. The excitation source was a fiber supercontinuum laser based on a passive modelocked fiber laser and a high-nonlinearity photonic crystal fiber supercontinuum generator (Fianium SC450). The laser provides 6-ps pulses at a repetition rate variable between 0.1 – 40 MHz. The laser output was sent through an Acousto-Optical Tunable Filter (Fianium AOTF) to obtain excitation pulses at the desired wavelength. Fluorescence emission was collected at 90° and detected using a double-grating monochromator (Jobin-Yvon, Gemini-180) and a microchannel plate photomultiplier tube (Hamamatsu R3809U-50). The polarization of the emission was 54.7° relative to that of the excitation. Data acquisition was done using a single photon counting card (Becker-Hickl, SPC-830). The instrument response function had a FWHM of 50 ps, as measured from the scattering of the sample at the excitation wavelength. The data were fitted with a sum of exponentials decay model at a single wavelength.

Conclusions

The palladium 57ysteine57 coupling method described here for preparation of **P-(PN)_n** yields a semiconducting polymer with the porphyrin moieties as part of the polymer backbone that is similar to the polymers previously prepared by electropolymerization.^{23,25} Replacement of the mesityl groups used in the electropolymers with 3,5-dihexylphenyl groups yields a soluble polymer that can be studied easily in solution. It is amenable to spin-coating or other film-forming procedures and should be useful for making polymer phases intimately mixed with fullerene phases for construction of bulk heterojunction organic photoelectrochemical cells. Comparison of the spectroscopic properties of the polymer with those of the model compounds shows that linking the polymer rings via *meso*-aminophenyl groups allows the porphyrin moieties to retain many of the absorption and redox properties of the monomer, rather than generating a highly delocalized chromophoric system. At the same time, the close similarity in structure between **P-(PN)_n** and the electropolymers studied previously^{23,25} suggest that the polymer chains form a semiconducting material through which positive charge is expected to flow readily. The relatively long excited singlet state lifetime observed for the polymer shows that this state is kinetically competent to inject charge into a suitably located electron acceptor. This in turn suggests that polymers of this type could be useful in organic photovoltaics or light emitting diodes, sensors, or other optoelectronic applications.

The spectroscopic studies of the polymer and model compounds suggest that the presence of an amino group at the *meso*-position of a porphyrin leads to formation of initial local excited states that quickly evolve into excited states with charge-transfer character. Presumably, the lone pair electrons of the amino group are somewhat delocalized into the porphyrin macrocycle, leaving a partial positive charge on the amino substituent and a partial negative charge on the macrocycle. The formation of charge transfer states of this general type in molecules with an amino group attached to an aromatic residue with some electron accepting character is widely observed and has been

extensively studied, although the exact nature of the CT state has been greatly debated and is still not completely understood.³²

Energy transfer between porphyrin units along the polymer chain is moderately rapid. The singlet state lifetimes suggest that in a film structure, energy transfer could also occur between adjacent polymer chains. The electrochemical experiments show that the polymer chain is readily oxidized at ca. +0.6 V vs SCE, indicating that the excited states of the porphyrin moieties are thermodynamically competent to inject charge into a wide variety of electron acceptors, including typical fullerenes. Thus, porphyrins of this general type have properties that could prove useful in a variety of optoelectronic, sensing and solar energy conversion applications.

Acknowledgements

We thank Aurelie Marcotte for inductively coupled plasma experiments. This work was supported by a grant from the U. S. Department of Energy (DE-FG02-03ER15393). GK was supported as part of the Center for Bio-Inspired Solar Fuel Production, an Energy Frontier Research Center funded by the U.S. Department of Energy, Office of Science, Office of Basic Energy Sciences under Award Number DE-SC0001016. MJK gratefully acknowledges support from a Goldwater Scholarship.

Notes and references

Department of Chemistry and Biochemistry, Center for Bioenergy and Photosynthesis, Arizona State University, Tempe, AZ 85287-1604, eE-mail: gust@asu.edu, tmoore@asu.edu, amoore@asu.edu

- 1 F. Bedioui, J. Devynck, and C. Bied-Charreton, *Acc. Chem. Res.*, 1995, **28**, 30-36.
- 2 J. R. Fish, E. Kubaszewski, A. Peat, T. Malinski, J. Kaczor, P. Kus, and L. Czuchajowski, *Chem. Mater.*, 1992, **4**, 795-803.

- 3 C. Poriel, Y. Ferrand, P. Le Maux, C. Paul-Roth, G. Simonneaux, and J. Rault-Berthelot, *J. Electroanal. Chem.*, 2005, **583**, 92-103.
- 4 J. Basu and K. K. Rohatgimukherjee, *Solar Energy Mater.*, 1991, **21**, 317-325.
- 5 D.-S. Duanmu, Z.-P. Chen, X.-S. Yu, and X. Zhou, *Chin. J. Chem.*, 2004, **22**, 779-781.
- 6 D. Wöhrle, R. Benters, O. Suvorova, G. Schnurpfeil, N. Trombach, and T. Bogdahn-Rai, *J. Porphyrins Phthalocyanines*, 2000, **4**, 491-497.
- 7 G. Li, S. Bhosale, S. Tao, R. Guo, S. Bhosale, F. Li, T. Zhang, T. Wang, and J.-H. Furhop, *Polymer*, 2005, **46**, 5299-5307.
- 8 C. Y. Lin, Y. C. Hung, C. M. Liu, C. F. Lo, Y. C. Lin, and C. L. Lin, *Dalton Trans.*, 2005, 396-401.
- 9 K. A. Macor, Y. O. Su, L. A. Miller, and T. G. Spiro, *Inorg. Chem.*, 1987, **26**, 2594-2598.
- 10 A. Bettelheim, B. White, S. Raybuck, and R. W. Murray, *Inorg. Chem.*, 1987, **26**, 1009-1017.
- 11 A. Bettelheim, B. A. White, and R. W. Murray, *J. Electroanal. Chem.*, 1987, **217**, 271-286.
- 12 A. Bettelheim, D. Ozer, R. Harth, and R. W. Murray, *J. Electroanal. Chem.*, 1989, **266**, 93-108.
- 13 B. A. White and R. W. Murray, *J. Electroanal. Chem.*, 1985, **189**, 345-352.
- 14 E. M. Bruti, M. Giannetto, G. Mori, and R. Seeber, *Electroanalysis*, 1999, **11**, 565-572.
- 15 S. Griveau, V. Albin, T. Pauporte, J. H. Zagal, and F. Bedioui, *J. Mater. Chem.*, 2002, **12**, 225-232.
- 16 E. Mazzotta and C. Malitesta, *Sensors and Actuators B-Chemical*, 2010, **148**, 186-194.
- 17 J. S. Lindsey and D. F. Bocian, *Acc. Chem. Res.*, 2011, **44**, 638-650.
- 18 H. Zhan, S. Lamare, A. Ng, T. Kenny, H. Guernon, W. K. Chan, A. B. Djuricic, P. D. Harvey, and W. Y. Wong, *Macromolecules*, 2011, **44**, 5155-5167.
- 19 J. Y. Lee, H. J. Song, S. M. Lee, J. H. Lee, and D. K. Moon, *European Polymer Journal*, 2011, **47**, 1686-1693.
- 20 J.-H. Fuhrhop, *Langmuir*, 2014, **30**, 1-12.
- 21 Z. M. Liu, I. Schmidt, P. Thamyongkit, R. S. Loewe, D. Syomin, J. R. Diers, Q. Zhao, V. Misra, J. S. Lindsey, and D. F. Bocian, *Chem. Mater.*, 2005, **17**, 3728-3742.

- 22 S. Lamare, S. M. Aly, D. Fortin, and P. D. Harvey, *Chemical Communications*, 2011, **47**, 10942-10944.
- 23 P. A. Liddell, M. Gervaldo, J. W. Bridgewater, A. E. Keirstead, S. Lin, T. A. Moore, A. L. Moore, and D. Gust, *Chem. Mater.*, 2008, **20**, 135-142.
- 24 B. J. Brennan, P. A. Liddell, T. A. Moore, A. L. Moore, and D. Gust, *J. Phys. Chem. B*, 2013, **117**, 426-432.
- 25 M. Gervaldo, P. A. Liddell, G. Kodis, B. J. Brennan, C. R. Johnson, J. W. Bridgewater, A. L. Moore, T. A. Moore, and D. Gust, *Photochem. Photobiol. Sci.*, 2010, **9**, 890-900.
- 26 T. Förster, *Annalen der Physik*, 1948, **2**, 55-75.
- 27 T. Förster, *Disc. Faraday Soc.*, 1959, **27**, 7-17.
- 28 M. E. Jamin and R. T. Iwamoto, *Inorganica Chimica Acta*, 1978, **27**, 135-143.
- 29 R. L. Hand and R. F. Nelson, *J. Am. Chem. Soc.*, 1974, **96**, 850-860.
- 30 K. Kurotobi, Y. Toude, K. Kawamoto, Y. Fujimori, S. Ito, P. Chabera, V. Sundstrom, and H. Imahori, *Chemistry-A European Journal*, 2013, **19**, 17075-17081.
- 31 H. F. Chow, M. K. Ng, C. W. Leung, and G. X. Wang, *J. Am. Chem. Soc.*, 2004, **126**, 12907-12915.
- 32 Z. R. Grabowski, K. Rotkiewicz, and W. Rettig, *Chem. Rev.*, 2003, **103**, 3899-4031.

CHAPTER 4

SYNTHESIS AND PHOTOPHYSICAL STUDIES OF A CAROTENOID SILICON- PHTHALOCYANINE C60 TRIAD

4.1 Author Contribution

The author contributed all of the photophysics for this paper. The author wrote the experimental section for the photophysics as well as the discussion section

4.2 Manuscript

Jaro Arero, Robert A. Schmitz Gerdenis Kodis, Thomas Moore, Ana Moore, Devens Gust

Introduction

Phthalocyanines (Pcs) are structural analogues of porphyrins which have strong absorption in the visible region and near-infrared. They have been extensively investigated for their promising electrical, optoelectronic, photochemical and catalytic properties.¹ Due to the presence of an 18 π -electron aromatic cloud, most phthalocyanines have cofacial intermolecular π - π interactions even at low concentrations and this causes aggregation which leads to fluorescence quenching and poor solubility.² However, owing to the steric effect of axial substituents, silicon phthalocyanines have been shown to exhibit a non-aggregation characteristics and solubility in common organic solvents.³

Phthalocyanines with two symmetrical fullerene substituents connected axially through a central silicon have been reported in the last few years.⁴⁻⁷ In addition to improving the solubility by diminishing intermolecular interactions fullerenes bring special properties to the phthalocyanine molecule. Fullerenes (C60) are good electron acceptors and have low reorganization energy, λ ⁸. C60-SiPc-C60 triads are good mimics for aspects of the photosynthetic reaction center. However, to develop a better mimic of natural photosynthesis, artificial photosynthesis will require a system with two electron donors and one acceptor where a long-lived charge separation can be achieved via a step-wise electron transfer.⁹

In the present work, the synthesis and photophysical properties of a carotene-silicon phthalocyanine-fullerene (C-SiPc-C60) triad is reported. In natural photosynthesis the roles of carotenoids include transferring excitation energy to the photosynthetic reaction center¹⁰ as well

as photoprotection by quenching chlorophyll triplet states to prevent generation of the cell damaging reactive singlet oxygen species.^{10,11} Under stress conditions of Mn-depleted PSII or low temperature, β -carotene has been observed to be an electron donor to the highly oxidizing P680+.¹²

The development and study of a simple artificial photosynthetic system consisting of a carotene, phthalocyanine and a fullerene acceptor will give an insight into the electron transfer process in natural photosynthesis. Incorporating carotenoids in organic photovoltaic devices will come with the benefit of long-lived charge separated states and photoprotection. Also use of carotene and phthalocyanine together will ensure access to a wider spectral window of solar radiation.

To the best of our knowledge an asymmetrical linkage on a Si phthalocyanine with a potential electron donor on one side and a potential electron acceptor on the other side has not been reported. In the current work, we are presenting synthesis of carotene and fullerene axially connected to phthalocyanine 1 (Scheme 21). Electron transfer and energy transfer processes in the triad were investigated by use of spectroscopic and electrochemical methods.

Results and Discussion

Femtosecond transient absorption measurements were taken of the system and its models. The models were measured in benzonitrile and excited with 695 nm radiation. In the carotene-phthalocyanine model (C-Pc), electron transfer was seen from the carotene to the phthalocyanine to create the C⁺--Pc⁻ charge separated (CS) state in 3.3 ps. This CS state decayed in 13.3 ps. There is also a 940 ps decay of the CS state (Figure 18). There is a long component that decays on a scale longer than the detection limit of the apparatus.

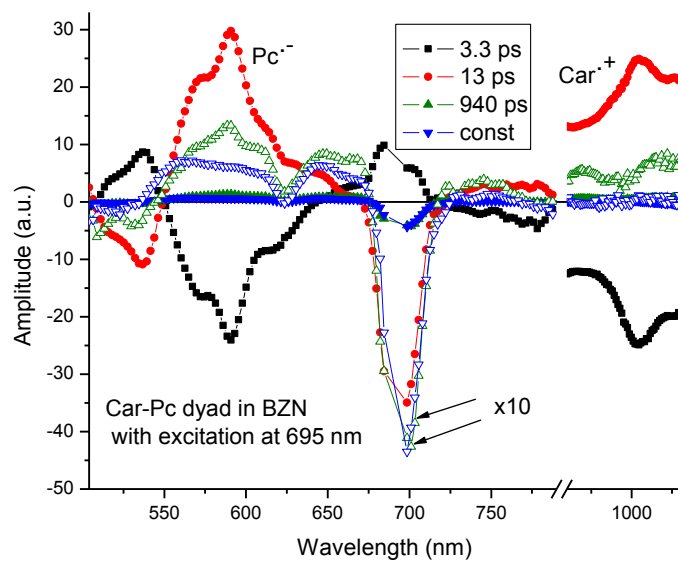


Figure 18. Femtosecond pump-probe measurement of C-Pc model. Charge separated state formation occurs in 3.3 ps (black), CS decay occurs in 13 ps (red), another conformation of the dyad decays in 940 ps (green), there is some phthalocyanine impurity that does not decay on the time scale of the detector (blue).

In the model phthalocyanine-C60 (Pc-C60) energy transfer was seen from the Pc to the C60 in 24 ps. There is formation of the CS state in 540 ps. There is formation of the C60 triplet state that occurs before formation of the CS state, which decays on a time scale longer than the detection limit. The CS state decays in 4.5 ns (Figure 19).

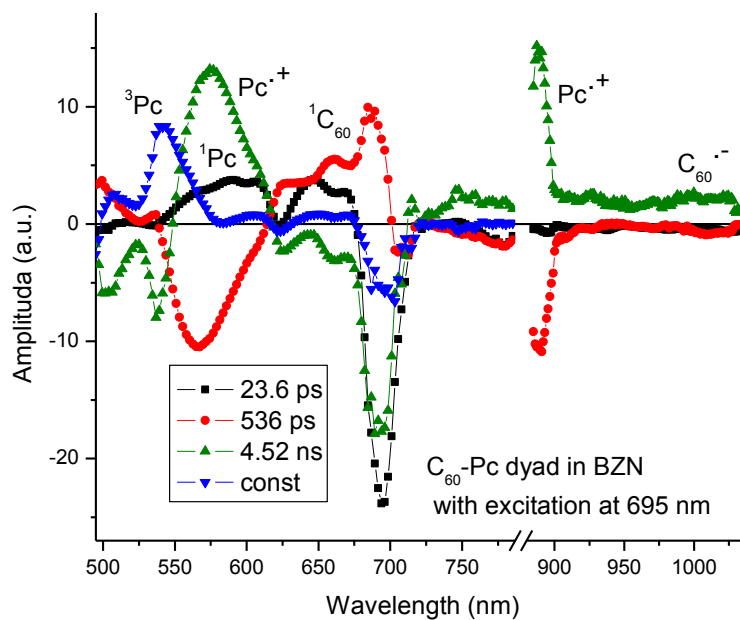


Figure 19. Femtosecond transient absorption DADS of Pc-C60 model dyad. Energy transfer occurs from the excited phthalocyanine to the C60 in 24 ps (black). The CS state forms in 540 ps (red). The C60 triplet excited state is formed and decays on a timescale longer than the detection limit of the apparatus (blue). The CS state decays in 4.5 ns (green).

In the triad (C-Pc-C60), very fast electron transfer is seen in 2.5 ps to form the C⁺-Pc—C60 species. This CS state decays in 17 ps. There is also a CS conformation that decays in 940 ps. There is no evidence of charge transfer to the C60. There is a component that does not decay that is attributed to phthalocyanine monomer in solution (Figure 20).

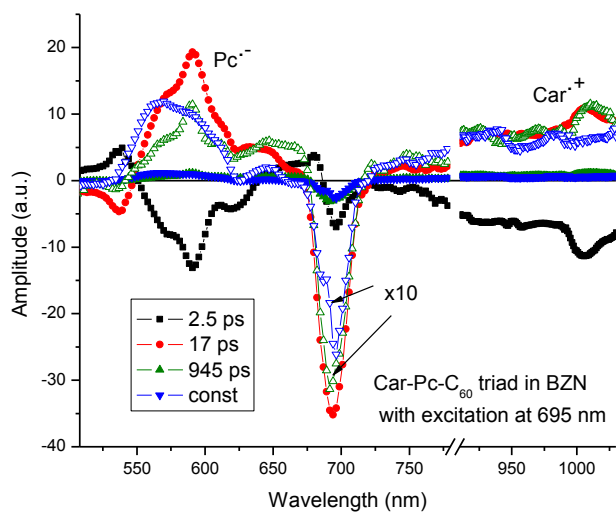


Figure 20. Femtosecond pump-probe DADS spectra of the C-Pc-C₆₀ triad. The C⁺-Pc-C₆₀ CS state occurs in 2.5 ps (black). One conformation of the CS state decays in 17 ps (red) and another in 945 ps (green). There is a decay longer than the detection limit of the apparatus (blue) that is attributed to free phthalocyanine in solution.

Synthesis

Axially substituted phthalocyanine 2 was afforded by a reaction between a commercially available silicon phthalocyanine dihydroxide with 4-iodobenzoate and 4-formylbenzoate (1:1) as shown in Scheme 1. By column purification, phthalocyanine 2 was obtained in 30 % yield. An amination reaction between phthalocyanine 2 and 7'-apo-7'-(4-aminophenyl)- β -carotene¹³ in presence of a commercially obtained mixture of tris(dibenzylidene acetone) dipalladium (0): BINAP: sodium tert-butoxide (1:3:4) at 80°C followed by column purification gave a 31 % yield of silicon phthalocyanine carotene dyad 3. Triad 1 was afforded by a single Prato reaction from (p-7'-apo-7'-(4-aminophenyl)- β -carotenobenzoate)-(p-formylbenzoate)(2,9,16,23-tetra-tert-butylphthalocyaninato)silicon 3 in 62 % yield after purification by silica column chromatography.

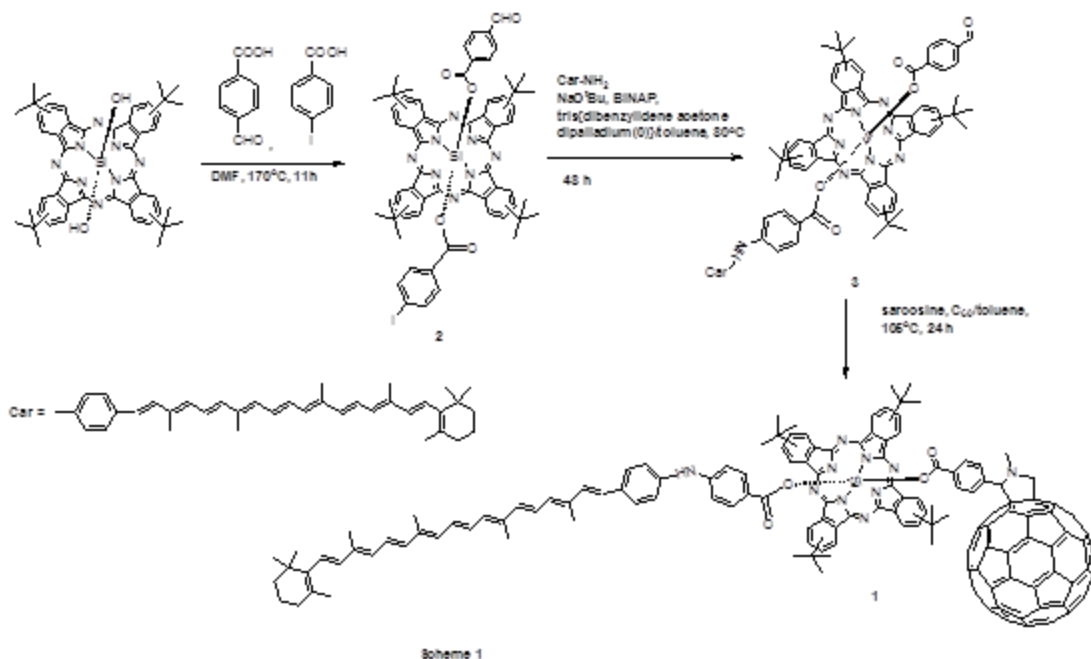
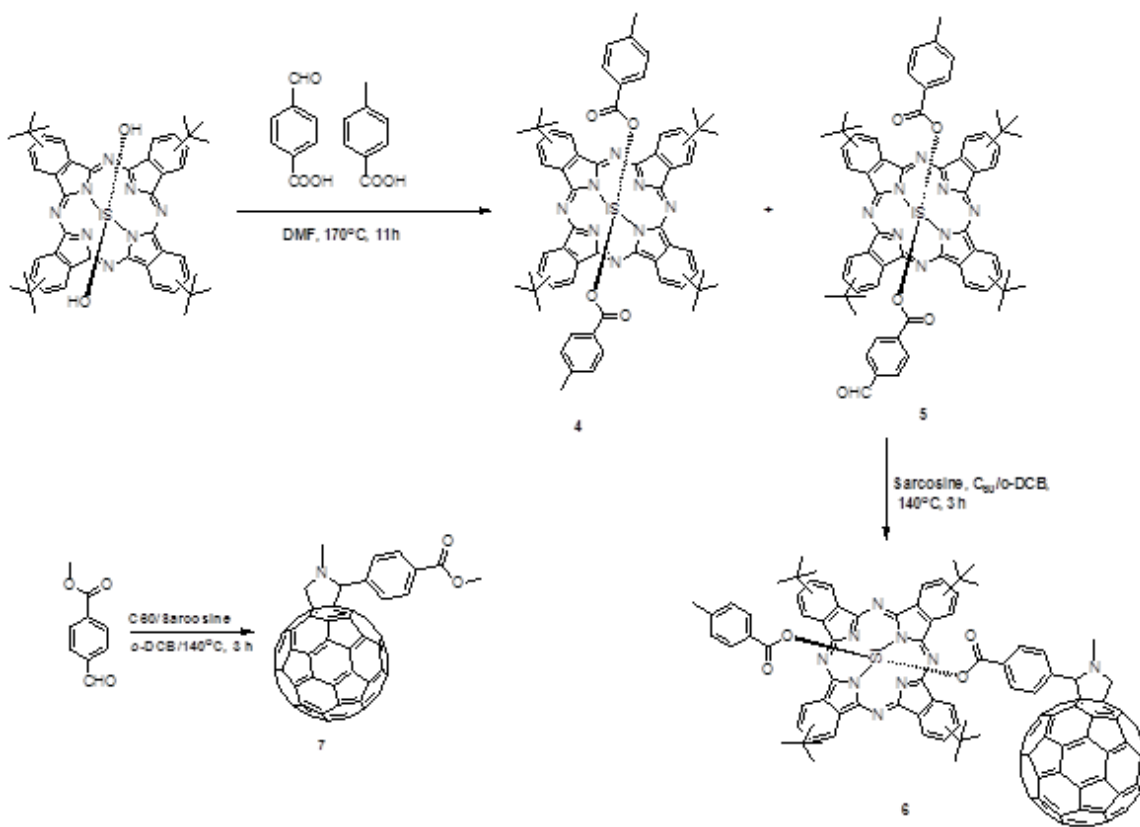


Figure 21. The SiPc 4, SiPc-C60 6 dyad and C60 7 reference compounds were synthesized as shown in Scheme 2. Compound 1-7 were fully characterized by ^1H NMR, UV-Vis, and MALDI-TOF.



Scheme 2

Figure 22. Synthetic scheme of Pc-C60 dyad.

NMR

¹H NMR (CDCl₃) spectrum of phthalocyanine 2 shows an upfield shift of the signals of benzoate protons to the range 6.67-4.83 ppm as opposed to the expected signals at around 8 ppm for benzoate protons. This observation confirms the influence of the shielding effect of the phthalocyanine π cloud. In addition, the presence of four distinct benzoate signals at 6.73, 4.58, 5.26 and 4.83 ppm gives further support to the presence of an asymmetric axial linkage on the phthalocyanine. On the other hand, attachment of the carotene to the phthalocyanine to form dyad 3 had no effect on the resonance signals of either of the components, i.e. phthalocyanine and carotene. The ¹H NMR (CDCl₃) spectrum of carotene-phthalocyanine dyad 3 was a linear combination of the spectra of the two parts. This could be attributed to the presence of the phenyl rings that separates the two components and hence protects the carotene from the shielding effect of the phthalocyanine. In contrast an earlier work by our group showed that when carotene is directly attached to Si phthalocyanine axially there was a very significant shift in the resonance signals of the carotene protons.¹⁴ On attaching the C60 to form the triad 1, the upfield shift of the benzoate protons and pyrrolidine linker between the C60 and the phthalocyanine was similar to the one reported by Martin-Gomis and co-workers.⁵ The signal of the benzoate protons adjacent to C60, pyrrolidine protons and N-CH₃ protons were all shifted upfield when compared to the corresponding protons of the C60 model 7. Benzoate protons were shifted from 7.84 to 5.17, the pyrrolidine protons at 4.97, 4.96, and 4.25 were moved to 4.63, 4.28, and 3.84; and the N-CH₃ protons were shifted from 2.78 to 2.17. This observation suggests that the attached C60 is in the range of the strong aromatic current of the Pc

UV/Vis

The absorption spectrum of the triad 1 shows that the Q-band of the phthalocyanine is unperturbed on formation of the triad (Figure 23), the addition of the carotenoid pigment causes a larger increase in absorption in the middle of the spectrum. Figure 24 shows that the carotenoid moiety at 480 nm in carotene-Si Phthalocyanine dyad 2 is red-shifted compared to model 4-aminophenyl- β -carotene, which has absorbance at 475 nm. The carotene moiety absorption maximum is at 479 nm in triad 1, which is not a significant change from that observed in the

carotene-phthalocyanine 3 dyad. Overall the absorption spectrum of the triad Car-SiPc-C60 triad 1 in dichloromethane is a close superposition of the spectra of the component chromophores making up the triad. This is an indication that there is not much ground state electronic interaction between the individual chromophores, particularly between the phthalocyanine moiety and the C60. In addition the sharp Q-bands are indications of non-aggregation of the axially substituted Si Phthalocyanines.

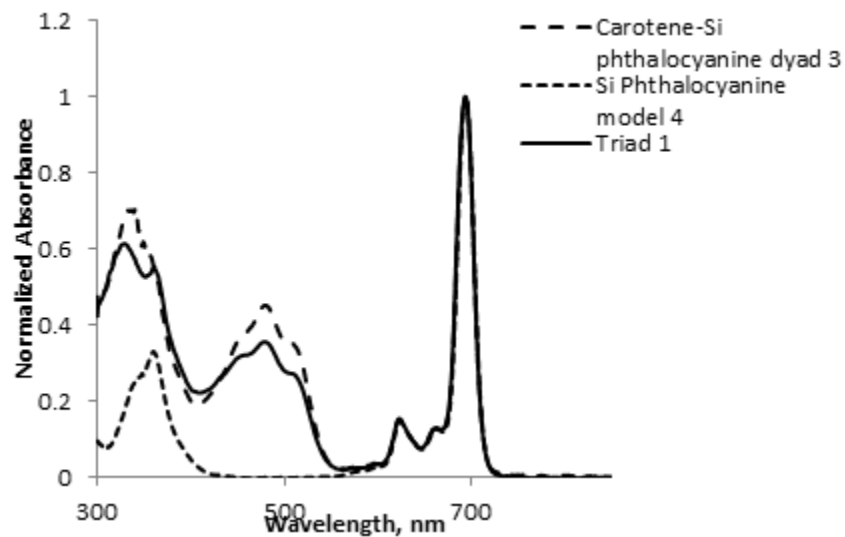


Figure 23. Absorption spectrum of triad 1 with those of reference compounds normalized at $\lambda=694$ nm

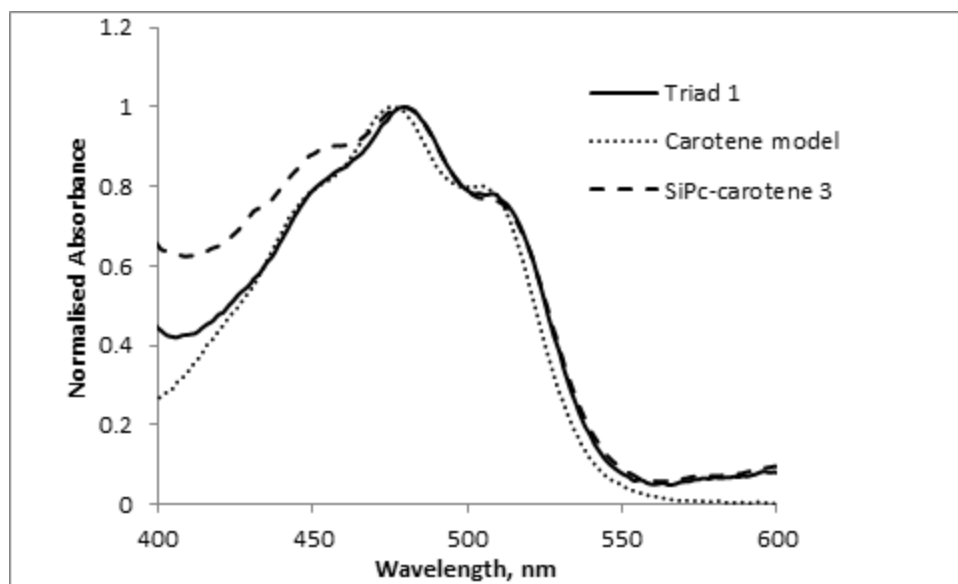


Figure 24. Absorption spectrum of triad 1 with those of reference compounds normalized at $\lambda=480$ nm

Experimental

General analytical: UV–Visible spectroscopy was performed using a Shimadzu UV-3101PC UV–Visible spectrophotometer. Mass spectrometry was performed by the MALDI-TOF method using a Voyager DE STR from Applied Biosystems in reflector mode. ¹H NMR spectra were obtained in deuterated chloroform using a Varian 400 MHz instrument with tetramethylsilane as internal reference.

Materials: All reagents and chemicals were obtained from commercial sources unless noted. All solvents were distilled prior to use. Silica gel chromatography was performed using 230-400 mesh silica gel (Silicycle, Siliflash F60).

Synthesis

(p-iodobenzoate)-(p-formylbenzoate)(2,9,16,23-tetra-tert-butylphthalocyaninato)silicon 2
4-iodobenzoic acid (242 mg, 1.0 mmol), 4-formylbenzoic acid (150 mg, 1.0 mmol) and (tBu)₄SiPc(OH)₂ (92 mg, 0.115 mmol) in 25 mL anhydrous DMF were stirred at 165°C under argon atmosphere for 10 h. The mixture was cooled to room temperature and solvent removed under reduced pressure and the crude purified by flash chromatography (SiO₂, Dichloromethane/Hexane-7:3) to yield 39 mg (30 %) of SiPc 2 as a bluish green solid. ¹H NMR (400 MHz, CDCl₃) δ 9.74-9.56 (8H, m, Pc-Ar-H), 9.37 (1H, s, CHO), 8.45-8.43 (4H, m, Pc-Ar-H), 6.73 (2H, d, J=8 Hz, Ph-Ar-H), 6.58 (2H, d, J=8 Hz, Ph-Ar-H), 5.26 (2H, d, J=8 Hz, Ph-Ar-H), 4.83 (2H, d, J=8 Hz, Ph-Ar-H), 1.80-1.79 (36H, m, 4×(CH₃)₃). UV/Vis (λ_{max}/nm, CH₂Cl₂): 694, 662, 624, 360. MALDI-TOF-MS (Terthiophene matrix) m/z calcd for C₆₃H₅₇IN₈O₅Si 1160.33 obsd 1160.35

Synthesis of (p-7'-apo-7'-(4-aminophenyl)-β-carotenobenzoate)-(p-formylbenzoate)(2,9,16,23-tetra-tert-butylphthalocyaninato)silicon 3
SiPc 2 (53 mg, 0.053 mmol), p-7'-apo-7'-(4-aminophenyl)-β-carotene (31 mg, 0.0608 mmol) and 41 mg of a commercially obtained mixture of tris(dibenzylidene acetone) dipalladium (0): BINAP: sodium tert-butoxide (1:3:4) were stirred in freshly distilled and degassed toluene (28 mL) at

80°C under argon atmosphere for 48 h until almost all of the starting material have been consumed. The solution was then allowed to cool to room temperature. The solvent was evaporated at reduced pressure and the crude purified by chromatography (SiO₂, Hexane/Dichloromethane/EtOAc-8:1.5:0.5) to obtain 17.6 mg (31 %) of the dyad 3. ¹H NMR (400 MHz, CDCl₃) δ 9.68-9.51 (8H, m, Pc-Ar-H), 9.32 (1H, s, CHO), 8.39-8.37 (4H, m, Pc-Ar-H), 7.01-6.99 (2H, m, Ph-Ar-H), 6.68-6.66 (2H, m, Ph-Ar-H), 6.62-6.44 (8H, m), 6.30-6.25 (2H, m), 6.19-6.08 (6H, m), 5.75 (2H, d, J=8 Hz, Ph-Ar-H), 5.20 (2H, d, J=8 Hz, Ph-Ar-H), 5.13 (1H, br s, NH), 4.98 (2H, d, J=9 Hz, Ph-Ar-H), 1.97-1.87 (m, 14H), 1.74-1.64 (m, 36H), 1.58-1.53 (m, 4H), 1.41-1.38 (m, 3H), 0.97-0.96 (m, 6H). UV/Vis (λ_{max}/nm, CH₂Cl₂): 694, 661, 623, 508 (sh), 480, 450 (sh), 341. MALDI-TOF-MS (Terthiophene matrix) m/z calcd for C₁₀₀H₁₀₃N₉O₅Si 1538.79 obsd 1538.60

Bis(p-methylbenzoate)(2,9,16,23-tetra-tert-butylphthalocyaninato)silicon 4 and (p-formylbenzoate)-(p-methylbenzoate)(2,9,16,23-tetra-tert-butylphthalocyaninato)silicon 5
A portion of 4-toluic acid (136 mg, 1.0 mmol), 4-formylbenzoic acid (150 mg, 1.0 mmol) and (tBu)₄SiPc(OH)₂ (92 mg, 0.115 mmol) in 25 ml anhydrous DMF were stirred at 170°C under argon atmosphere for 10 h. The mixture was cooled to room temperature and solvent removed under reduced pressure and the crude purified by flash chromatography (SiO₂, Dichloromethane/Hexane-8:2). The symmetrical SiPc 4 was eluted first, yielding 20.5 mg (17%), followed by asymmetrical SiPc 5 32.7 mg (27 %).

SiPc 4 ¹H NMR (400 MHz, CDCl₃) δ 9.75-9.48 (8H, m, Pc-Ar-H), 8.35-8.33 (4H, m, Pc-Ar-H), 5.95 (4H, d, J= 8 Hz, Ph-Ar-H), 4.96 (4H, d, J= 8 Hz, Ph-Ar-H), 1.73-1.72 (36H, m, 4× (CH₃)₃), 1.60 (3H, s, 2×CH₃). UV/Vis (λ_{max}/nm, CH₂Cl₂): 693, 662, 623, 361. MALDI-TOF-MS (Terthiophene) m/z calcd for C₆₄H₆₂N₈O₄Si 1034.47 obsd 1034.45.

SiPc 5 ¹H NMR (400 MHz, CDCl₃) δ 9.69-9.50 (8H, m, Pc-Ar-H), 9.30 (1H, s, CHO), 8.37-8.35 (4H, m, Pc-Ar-H), 6.67 (2H, d, J= 8 Hz, Ph-Ar-H), 5.95 (2H, d, J= 8 Hz, Ph-Ar-H), 5.20 (2H, d, J= 8 Hz, Ph-Ar-H), 4.97 (2H, d, J= 8 Hz, Ph-Ar-H), 1.73-1.72 (36H, m, 4×(CH₃)₃), 1.60 (3H, s, CH₃)

. UV/Vis ($\lambda_{\text{max}}/\text{nm}$, CH_2Cl_2): 693, 662, 623, 361. MALDI-TOF-MS (Terthiophene) m/z calcd for $\text{C}_{64}\text{H}_{60}\text{N}_8\text{O}_5\text{Si}$ 1048.45 obsd 1048.46

(*p*-methylbenzoate)-[*p*-(*N*-methyl-3',4'-fulleropyrrodin-2'-yl)benzoate](2,9,16,23-tetra-*tert*-butylphthalocyaninato)silicon 6

SiPc 5 (32 mg, 0.0305 mmol), C60 (55 mg, 0.0764 mmol), sarcosine (30 mg, 0.337 mmol) in *o*-dichlorobenzene (12 mL) were stirred at 140°C under argon atmosphere for 2 h. The mixture was cooled and solvent removed under reduced pressure. The crude was purified on silica gel (toluene) yielding 52 mg (94 %) of SiPc-C60 dyad 7 as green solid. ^1H NMR (400 MHz, CDCl_3) δ 9.73-9.55 (8H, m, Pc-Ar-H), 8.42-8.40 (4H, m, Pc-Ar-H), 6.68 (2H, br s, Ph-Ar-H), 6.01 (2H, d, $J=8$ Hz, Ph-Ar-H), 5.23 (2H, br s, Ph-Ar-H), 4.59 (2H, d, $J=8$ Hz, Ph-Ar-H), 4.59 (1H, d, $J=8$ Hz, CHHN), 4.25 (1H, s, CHN), 3.83 (1H, d, $J=8$ Hz, CHHN), 2.17 (3H, s, N-CH₃), 1.79-1.78 (36H, m, 4×(CH₃)₃), 1.66 (3H, s, CH₃). ($\lambda_{\text{max}}/\text{nm}$, CH_2Cl_2): 694, 663, 623, 360, 331. MALDI-TOF-MS (Terthiophene) m/z calcd for $\text{C}_{126}\text{H}_{65}\text{N}_9\text{O}_4\text{Si}$ 1795.49 obsd 1795.35

N-Methyl-2-(*p*-methylbenzoate)-3, 4-fulleropyrrolidine 7

A mixture of C60 (50 mg, 0.0694 mmol), methyl-4-formylbenzoate (30 mg, 0.183 mmol) and sarcosine (28 mg, 0.314 mmol) in toluene (10 mL) were heated to reflux under argon atmosphere for 3 hrs. The mixture was then cooled to room temperature and solvent removed and crude purified by flash chromatography (silica, toluene:/EtOAc-19:1) yielding 9 mg (14 %) of 8 as a brown solid. ^1H NMR (400 MHz, $\text{CDCl}_3/\text{CS}_2$ 1:1) δ 8.03 (2H, d, $J=8$ Hz, Ar-H), 7.83 (2H, br s, Ar-H), 4.96-4.94 (2H, m, CHHN & CHN), 4.25 (1H, d, $J=9.6$ Hz, CHHN), 3.84 (3H, s, N-CH₃), 2.77 (3H, s, CH₃). ($\lambda_{\text{max}}/\text{nm}$, toluene): 703, 432. MALDI-TOF-MS (Terthiophene) m/z calcd for $\text{C}_{71}\text{H}_{13}\text{NO}_2$ 911.09 obsd 910.61

Synthesis of [*p*-7'-apo-7'-(4-aminophenyl)- β -carotenobenzoate]-[*p*-(*N*-methyl-3',4'-fulleropyrrodin-2'-yl)benzoate](2,9,16,23-tetra-*tert*-butylphthalocyaninato)silicon 1

Dyad 3 (23 mg, 0.015 mmol), C60 (54 mg, 0.07 mmol), sarcosine (42 mg, 0.471 mmol) in anhydrous toluene (20 mL) were stirred at 105°C under argon atmosphere for 24 h. The mixture

was then cooled and the solvent removed under reduced pressure. The crude was purified on silica gel (toluene) yielding 21 mg (62 %) of triad 1.

¹H NMR (400 MHz, CDCl₃) δ 9.68 (m, 8H, Pc-Ar-H), 8.36-8.34 (m, 4H, Pc-Ar-H), 7.00-6.98 (d, 2H, J=8, Ph-Ar-H), 6.72-6.43 (m, 10H, vinyl H, Ph-Ar-H), 6.30-6.03 (m, 8H, vinyl H, Ph-Ar-H), 5.75-5.72 (d, 2H, J=12, Ph-Ar-H), 5.18-5.16 (br, d, 2H, Ph-Ar-H), 4.96-4.94 (d, 2H, J=8, Ph-Ar-H), 4.63-4.62 (d, 1H, J=4, CHHN), 4.28 (br s, 1H, CHN), 3.85-3.83 (d, 1H, J=8, CHHN), 2.17 (s, 3H, N-CH₃), 1.97-1.88 (m, 14H, CH₃-18C, CH₃-20C, CH₃-19'C, CH₃-20'C, CH₂-4C), 1.75-1.65 (m, 36H, 4 × (CH₃)₃), 1.57-1.53 (m, 3H, CH₃-19C), 1.41-1.38 (m, 4H, CH₂-2C, CH₂-3C), 0.97-0.96 (m, 6H, CH₃-16 and CH₃-17C)

UV/Vis (λ_{max}/nm, CH₂Cl₂): 693, 663, 623, 508 (sh), 479, 455 (sh), 360, 329.

MALDI-TOF-MS (Terthiophene) m/z calcd for C₁₆₂H₁₀₈N₁₀O₄Si 2284.83 obsd 2284.50

References

1. McKeown, N. B. Phthalocyanine materials :synthesis, structure, and function; Chemistry of solid state materials; Cambridge University Press: Cambridge, U.K.; New York, 1998; Vol. 6, pp 193.
2. Martín-Gomis, L.; Ohkubo, K.; Fernández-Lázaro, F.; Fukuzumi, S.; Sastre-Santos, A. Adiabatic Photoinduced Electron Transfer and Back Electron Transfer in a Series of Axially Substituted Silicon Phthalocyanine Triads. *J. Phys. Chem. C* 2008, 112, 17694-17701.
3. Cheng, G.; Peng, X.; Hao, G.; Kennedy, V. O.; Ivanov, I. N.; Knappenberger, K.; Hill, T. J.; Rodgers, M. A. J.; Kenney, M. E. Synthesis, Photochemistry, and Electrochemistry of a Series of Phthalocyanines with Graded Steric Hindrance. *J. Phys. Chem. A* 2003, 107, 3503-3514.
4. Kim, K. N.; Choi, C. S.; Kay, K. A novel phthalocyanine with two axial fullerene substituents. *Tetrahedron Lett.* 2005, 46, 6791-6795.
5. Martín-Gomis, L.; Ohkubo, K.; Fernández-Lázaro, F.; Fukuzumi, S.; Sastre-Santos, A. Synthesis and photophysical studies of a new nonaggregated C₆₀-silicon phthalocyanine-C₆₀ triad. *Org. Lett.* 2007, 9, 3441-3444.
6. Martín-Gomis, L.; Ohkubo, K.; Fernández-Lázaro, F.; Fukuzumi, S.; Sastre-Santos, A. Adiabatic Photoinduced Electron Transfer and Back Electron Transfer in a Series of Axially Substituted Silicon Phthalocyanine Triads. *J. Phys. Chem. C* 2008, 112, 17694-17701.
7. El-Khouly, M.; Kim, J.; Kay, K.; Choi, C.; Ito, O.; Fukuzumi, S. Synthesis and Photoinduced Intramolecular Processes of Light-Harvesting Silicon Phthalocyanine-Naphthalenediimide-Fullerene Connected Systems. *Chemistry - A European Journal* 2009, 15, 5301-5310.

8. Guldi, D. M.; Martin, N. Fullerenes :from synthesis to optoelectronic properties; Developments in fullerene science; Kluwer Academic Publishers: Boston, 2002; Vol. 4, pp 440.
9. Moore, T. A.; Gust, D.; Mathis, P.; Mialocq, J.; Chachaty, C.; Bensasson, R. V.; Land, E. J.; Doizi, D.; Liddell, P. A.; Lehman, W. R.; Nemeth, G. A.; Moore, A. L. Photodriven charge separation in a carotenoporphyrin-quinone triad. *Nature* 1984, 307, 630-632.
10. Ritz, T.; Damjanovi—ç, A.; Schulten, K.; Zhang, J.; Koyama, Y. Efficient light harvesting through carotenoids. *Photosynthesis Res.* 2000, 66, 125-144.
11. Gust, D.; Moore, T. A.; Moore, A. L. Mimicking Photosynthetic Solar Energy Transduction. *Acc. Chem. Res.* 2001, 34, 40-48.
12. Tracewell, C. A.; Vrettos, J. S.; Bautista, J. A.; Frank, H. A.; Brudvig, G. W. Carotenoid Photooxidation in Photosystem II. *Arch. Biochem. Biophys.* 2001, 385, 61-69.
13. Gust, D.; Moore, T. A.; Moore, A. L.; Liddell, P. A. In [10] Synthesis of carotenoporphyrin models for photosynthetic energy and electron transfer; *Methods in Enzymology*; Academic Press: Vol. Volume 213, pp 87-100.
14. Kodis, G.; Herrero, C.; Palacios, R.; Mariño-Ochoa, E.; Gould, S.; de, I. G.; van Grondelle, R.; Gust, D.; Moore, T. A.; Moore, A. L.; Kennis, J. T. M. Light Harvesting and Photoprotective Functions of Carotenoids in Compact Artificial Photosynthetic Antenna Designs. *J Phys Chem B* 2004, 108, 414-425.

CHAPTER 5

DE NOVO DESIGN AND SYNTHESIS OF AN ARTIFICIAL SYNTHETIC FERREDOXIN

5.1 Author Contribution

The author performed all photophysical experiments, as well as wrote the photophysical experimental section and contributed to the results and discussion section.

5.2 Manuscript

Anindya Roy, Dayn Joseph Sommer, Robert A. Schmitz, Andrei Astachkine, Chelsea Brown, Giovanna Ghirlanda

Introduction:

In nature, redox proteins often employ chains of various [FeS] clusters to shuttle electrons from electron donors to electron acceptors. Individual metallocenters are optimally spaced from one another to allow electronic coupling between them, increasing the rate of electron transfer between the two. Examples of these multi-cluster proteins are the [FeFe] and [NiFe] hydrogenases, enzymes responsible for reversible proton reduction¹. The active site of these enzymes is deeply buried in protein matrix and electronically coupled to the surface of the protein via series of suitably spaced [4Fe4S] clusters [Fig 25]. Very often, these coupled 2[4Fe-4S] clusters appear to adopt a so-called 'β_αββ_αβ' fold or ferredoxin fold^{2,3} [Figure 26]. In general, for 2[4Fe-4S] clusters, a single polypeptide chain folds into two domains that bind each of the 2[4Fe-4S] clusters. The structure often exhibits a pseudo two-fold symmetry that is indicative of ancient sequence/gene duplication². Despite of their structural similarity, 2[4Fe-4S] clusters differ substantially in their cysteine-chemical properties. This diversity emerges from the difference in primary amino acid sequence of the ferredoxins and the specific stereo-electronic properties of the environment surrounding the clusters. Owing to their perceptible importance in redox and non-redox catalysis, there has been a substantial amount of work in the field of *de novo* design attempting to model clusters into peptide maquettes to mimic the natural cluster environment, with the eventual aim to incorporate these model peptides into engineered redox enzymes⁴⁻¹⁰. However, many of these peptides have been designed to incorporate a single, electronically isolated cluster, limiting their usefulness as electron conduits *in vitro*. To address this problem, we

recently developed a general method to design Bis-[4Fe4S] cluster binding peptide using symmetry parameters. We have shown, as a proof of concept, that multiple [4Fe-4S] clusters can be incorporated inside the hydrophobic core of helical bundle separated by a predetermined distance¹¹. We report here characterization of a variant peptide that moves the two clusters to within 12 Å of one another, a biologically relevant distance for effective electron transfer. This designed system shows proof-of-concept redox activity, implicating its use in engineered redox proteins.

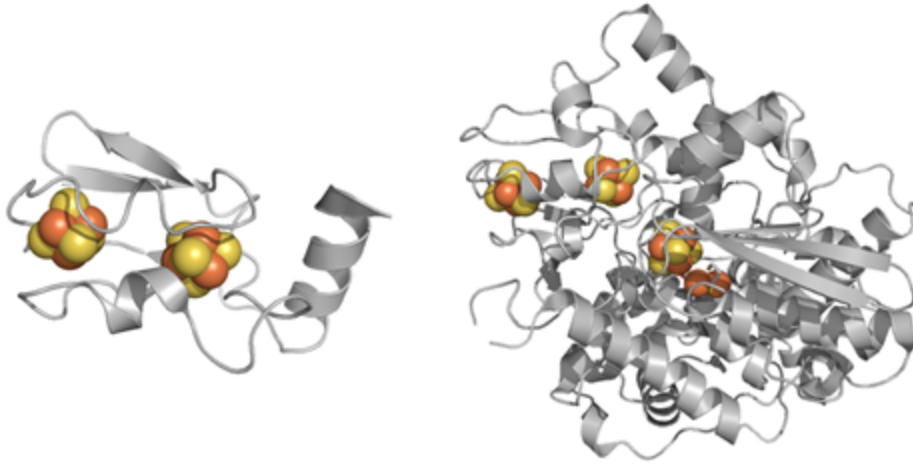


Figure 25. Structure of [FeFe] hydrogenase from *Desulfovibrio desulfuricans* (PDB 1HFE) (adapted from ref.). The ferredoxin-like domain is highlighted on the left. All molecular figures were created with PyMOL (DeLano, W.L. (2002). The PyMOL Molecular Graphics System.

Experimental:

Peptide Synthesis and Purification

Peptide variants were synthesized on a Liberty microwave-assisted solid phase peptide synthesizer (CEM). The synthesis was carried out utilizing standard Fmoc protection procedures. Briefly, Rink Amide resin was doubly deprotected using 20% piperidine, 0.1 M HOBt in DMF. Following deprotection, appropriate amounts of 0.45 M HBTU in DMF, 2M Ethyl-Diisopropylamine (DIEA) in N-Methyl-2-Pyrrolidone, and 0.2 M Fmoc protected amino acid (Novabiochem) were added to the reaction vessel, followed by irradiation with microwaves. Peptides were acetylated on the N-terminus via addition of acetic anhydride in coupling conditions.

Peptides were cleaved from resin utilizing 94% TFA, 2.5% H₂O, 2.5% EDT, and 10% TIS for 3 hours, followed by ether precipitation. Crude, lyophilized peptide was purified utilizing C18 preparatory reverse-phase high performance liquid chromatography (HPLC), with a linear gradient of 99.9% water with 0.1% TFA to 95% Acetonitrile, 4.9% water, and 0.1% TFA, flowing at 10 mL/min. Peptide identity was confirmed by matrix-assisted laser desorption ionization time-of-flight mass spectrometry (MALDI-TOF-MS) and purity by C18 analytical HPLC. Peptide was lyophilized to yield a white powder, >99% purity.

Cluster Incorporation

Iron-sulfur clusters were incorporated into peptide variants following well-established methodologies^{7,11}. All reactions were performed in an anaerobic chamber (Coy Scientific), with a 95% N₂ and 5% H₂ environment. To a solution of 150 μM peptide in 100 mM Tris-HCl, pH 8.5, was added sequentially in 20 minute intervals to a final concentration: 0.8% (v/v) β-mercaptoethanol, 3 mM ferric chloride (FeCl₃), and 3 mM sodium sulfide (Na₂S). Peptide was incubated overnight at 4 °C anaerobically.

The dark brown solution was subjected to desalting utilizing a PD10 G25 column (GE Healthcare) that was equilibrated with 100 mM Tris, pH 7.5. Peptide was characterized immediately or flash frozen and stored at -80 °C.

Gel Filtration

Size exclusion chromatography was performed on a G-25 gel filtration column fit to an Agilent Technologies 1260 Insight FPLC system. To a column pre-equilibrated in 100 mM Tris-HCl, pH 7.5, was injected 200 μ L of 150 μ M apo or holo peptide. Apo peptide was pre-treated with *tris*(2-carboxyethyl)phosphine (TCEP) 30 minutes before injection to eliminate any disulfides formed from air oxidation.

Circular Dichroism Spectroscopy

Spectra were recorded on a JASCO J-815 spectropolarimeter over a range of 260 to 190 nm. Data were recorded every 1 nm and averaged over 3 scans in a 1 mm path length, quartz cuvette. The holo-peptide was sealed in the cuvette to maintain an anaerobic environment. Concentration of apo and holo-peptide was kept at 50 μ M in 100 mM Tris, pH 7.5. Apo-peptide measurements contained an excess amount of TCEP to remove any disulfides formed. Chemical denaturations were performed through iterative additions of an 8M stock of Gu-HCl, followed by mixing and incubation for 5 minutes to allow equilibration.

Electron Paramagnetic Resonance Spectroscopy

Holo-peptide obtained from PD10 desalting was concentrated in a 3000 MWCO centrifuge concentrator to approximately 1 mM peptide concentration. Reduced samples were adjusted to pH 10 by addition of 100 mM sodium dithionite in 1 M glycine buffer, to a final concentration of 10 mM dithionite. EPR samples were prepared by addition of 10% (v/v) glycerol as a cryoprotectant to either oxidized or reduced samples, and placed in quartz EPR tubes. Samples were flash frozen and stored under liquid N₂ until measurement.

Samples were measured on a X-band EPR spectrometer Elexsys E500 (Bruker), utilizing continuous wave methodology (mw frequency, 9.340 GHz; mw power, 2 mW; field modulation amplitude, 0.5 mT). Measurement temperatures ranged from 5-50 K.

Transient Absorption Spectroscopy:

Three buffered solutions of tetra-malonate porphyrin monomers were prepared. The solutions had a Q-band absorption of 0.25 OD at 560 nm. Samples contained: porphyrin, porphyrin and apo-protein (30 μ M), and porphyrin and holo-protein (30 μ M). Samples were excited at 560 nm

with a Nd:YAG laser (EKSLPA) and probed with a 150 W Xenon arc lamp. Probe light was detected by a Proteus system (Ultrafast) and analyzed using in-house fitting software ASUFIT.

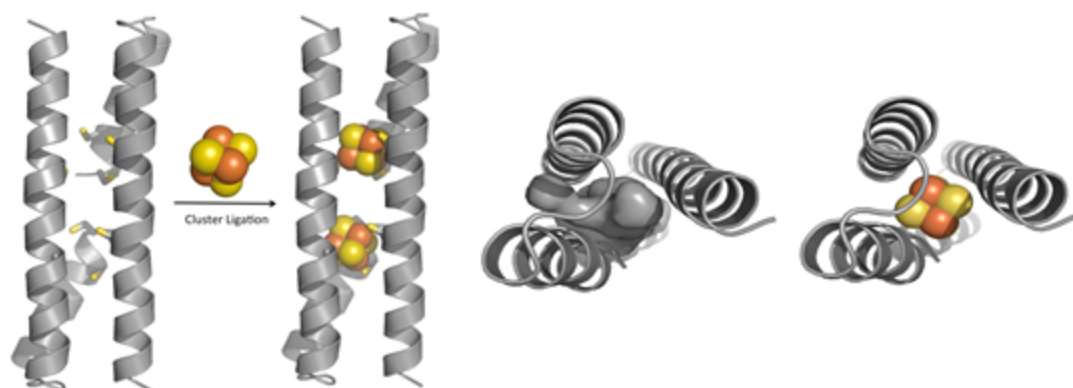
Cytochrome C₅₅₀ Reduction Assay

PD10 fractions of the holo-peptide were reduced via slow addition of dithionite, monitoring the loss of signal at 410 nm. After no more change was seen, and a slight dithionite signal arose at 300 nm, the holo-peptide was subjected to a PD10 column. The first 1.5 mL of the total 3.5 mL elution volume were concentrated to a protein concentration of 300 μ M. To 500 μ L of a solution of Cytochrome C₅₅₀ isolated from *Thermosynechococcus elongates* (7 μ M protein concentration as assayed by absorbance at 550 nm, $\epsilon_{550} = 21000 \text{ M}^{-1} \text{ cm}^{-1}$) was added 1 μ L of reduced holo-peptide. After each addition, UV-Vis spectra were obtained with an Ocean Optics USB4000 detector with a USB-ISS-UV-Vis light source attached. Data were fit to linear regression curves before and after saturation to determine the mole equivalents required to obtain full reduction of the heme.

Protein Design and Synthesis:

DSD-Fdm was designed following a similar protocol as described before {roy:2013vd}. Briefly, We searched for i, i+3 leucine residues inside the hydrophobic core of the helical bundle of DSD¹²(PDB Code 1G6U) that is compatible with ligating a [4Fe-4S] cluster at the N-term of the helix. The first coordination sphere of [4Fe-4S] cluster binding site from *Thermotoga 84ysteine* (PDB ID 2G36)¹³ was then docked manually inside the hydrophobic core of the DSD to find other two positions geometrically compatible to chelate the [4Fe-4S] clusters [Fig 26]. This resulted in translation of the cluster binding site one heptad down, along the axis of the 3-helix bundle as compared to our previous design¹¹. Owing to the inherent two-fold symmetry of the designed protein, DSD-Fdm, incorporates two [4Fe-4S] clusters in the hydrophobic core which is reminiscent of the natural ferredoxin fold. Mutation of eight core leucine to 84ysteine initially causes formation of a polar cavity inside the helical bundle in the apo peptide, while the cavity gets completely occupied by the clusters in Holo Peptide [fig XXXX]. Resulting 49 amino acid residue peptide was synthesized utilizing standard Fmoc chemistry with Microwave-Assisted Solid Phase Peptide Synthesis with high yield and homogeneity. Crude peptide was purified via

reverse-phase HPLC to >95% purity, as assessed by analytical HPLC. Identity of the construct was confirmed with MALDI-TOF Mass Spectrometry.



DSD: **S**L**A**A**L**K**S**E**L**Q**A**L**K**K**E**G**F**S**P**E**E**L**A**A**L**E**S**E**L**Q**A**L**E**K**K****L**A**A**L**K**S**K**L**Q**A**L**G**W**

DSD-Fdm: **S**C**A**A**C**K**S**E**L**Q**A**L**K**K**E**G**F**S**P**E**E**L**A**A**L**E**S**E**C**Q**A**L**E**K**K****C**A**A**L**K**S**K**L**Q**A**L**K**G**

Figure 26. Design Strategy for DSD-Fdm (Left Panel); Polar cavity generated by Leucine to Cystine mutation gets occupied by [4Fe-4S] cluster (Top View, right panel)

Cluster Incorporation, Protein Structure and Stability:

We performed *in situ* cluster incorporation reaction following standard protocol,^{7, 11}. Briefly, β -mercaptoethanol reduced peptide was incubated overnight with 20 molar equivalents of FeCl_3 and Na_2S . This entropically favorable reaction was quenched via desalting on a PD10 column, removing unbound Fe and S equivalents. In agreement with previously characterized peptides, the holo DSD-Fdm shows broad absorbance at 415 and 360 nm, characteristic of [Fe-S] cluster charge transfer bands, which disappear upon reduction [Figure XXX]. This characteristics are typical of a cuboidal [4Fe-4S] cluster^{14, 15} whereas incorporated [4Fe-4S]²⁺ cluster undergo dithionite mediated reduction to [4Fe-4S]¹⁺.

We investigated the oligomeric state for apo and holo DSD-Fdm using a combinatorial analytical centrifugation and gel filtration approach. Apo-DSD-Fdm exists predominantly in dimeric form in solution at $\sim 100\mu\text{M}$ loading concentration (data not shown). When analyzed by gel filtration, both apo and holo DSD-Fdm elutes at comparable volume of elution buffer as shown in Figure 27. For holo peptide, the elution profile contains an additional absorbance at 410 nm, indicating the presence of the [4Fe-4S] cluster.

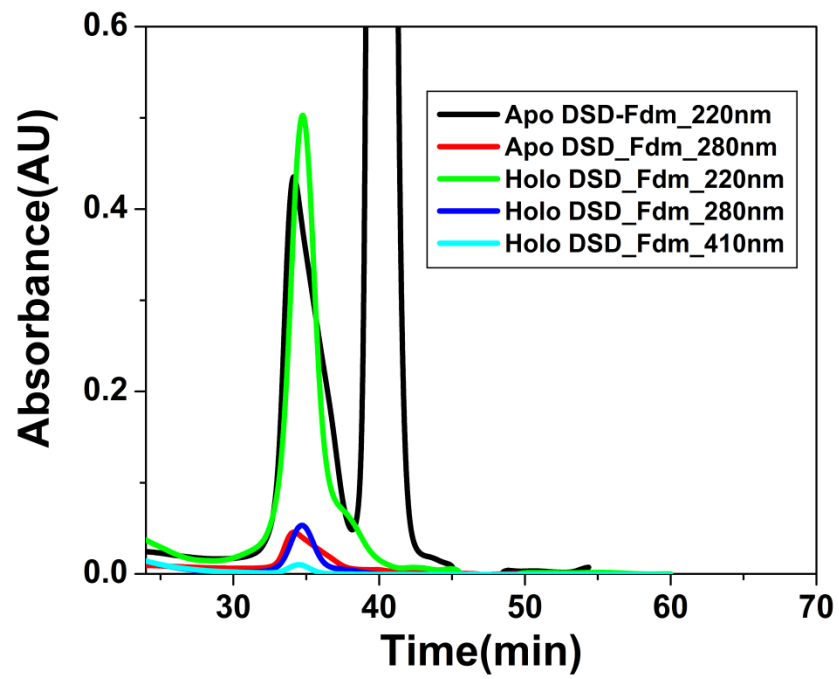


Figure 27. Gel filtration data of Apo and Holo DSD-Fdm. Both Apo and Holo peptide elutes at similar elution volume, confirming same oligomeric state.

The peak centered around 40 min for apo peptide comes from TCEP.HCl used for reduction, which was confirmed from a blank injection of TCEP.HCl by itself (data not shown).

The presence of two clusters was subsequently confirmed through characterization of Fe and protein concentration. Utilizing the same sample, analysis of Fe content via a Ferrozine assay and protein concentration via a Bradford assay, we found that the peptide contains 4.3 ± 0.9 Fe/monomer. Variation in Fe concentration may arise from non-specific binding of Fe^{2+} to the exterior of the DSD-Fdm peptide.

We investigated the secondary structure of both apo and holo DSD-Fdm using far-UV Circular Dichroism (CD) spectroscopy. Both the apo and holo DSD-Fdm shows two minima

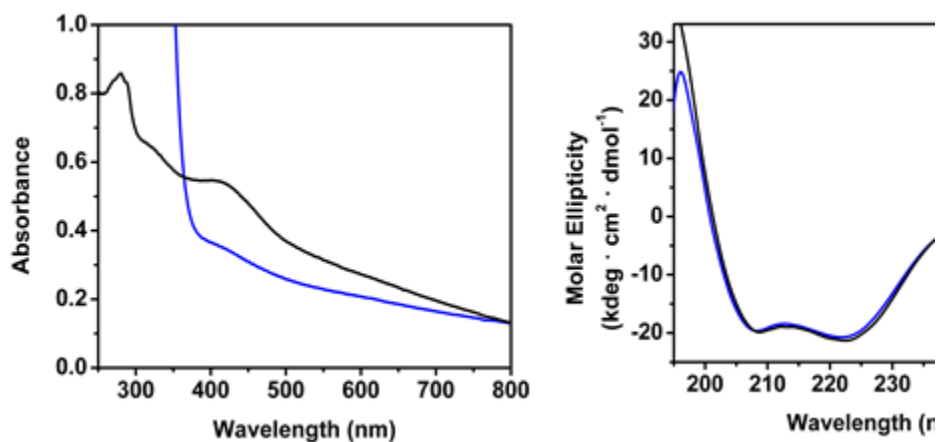


Figure 28. UV-Vis (left panel) spectra of holo DSD-Fdm before and after dithionite reduction. CD Spectra of Apo and Holo DSD-Fdm in the UV range showing two minima around 222nm and 208nm.

Centered around 208nm and 222nm, which is indicative of high helical content of both peptides. Cluster incorporation does not interfere with the folding of the peptide, which is reflected by the similar molar ellipticity value of the holo peptide as compared to the apo peptide.

We also assessed the stability of the Apo and holo peptide towards chemical denaturation procedure in circular dichroism. Briefly, molar ellipticity of apo and holo peptide was monitored

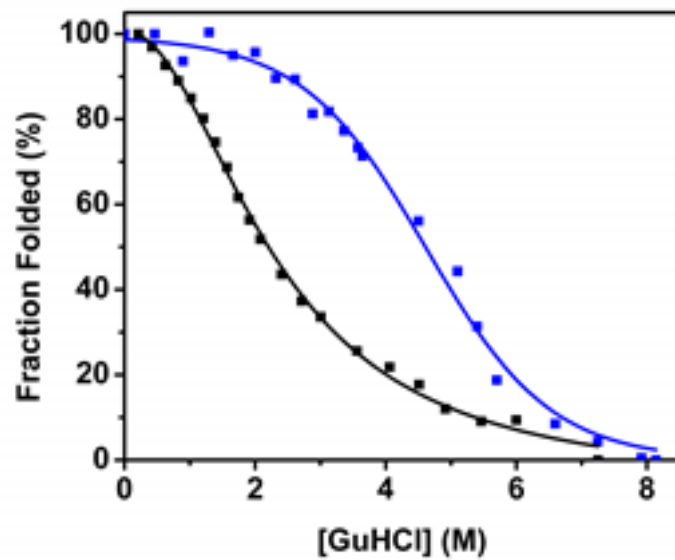


Figure 29. Guanidine.HCl melt of apo and holo DSD-Fdm monitored by CD at 222nm.

At 222nm as a function of chaotropic agent concentration (Guanidine hydrochloride). A remarkable and unambiguous increase in stability towards denaturant was observed from apo to holo DSD-Fdm as shown in Fig 29. Apo peptide denatures at 2.1 (M) Gdn.HCl concentration, while Holo DSD-Fdm denatures at 4.4 (M) Gdn.HCl concentration. This increase in stability can be attributed to cluster incorporation, which results in formation of four 92ysteine-SH to [Fe] bond formation.

EPR Spectroscopy and redox properties of the cluster:

In vitro reconstitution of cuboidal iron sulfur proteins results in formation of $[4\text{Fe-4S}]^{2+}$ clusters, which is EPR silent because of antiferromagnetic coupling of unpaired spins. As reconstituted holo DSD-Fdm shows no EPR signal, whereas upon dithionite reduction a rhombic signal arises confirming incorporation of an intact [4Fe-4S] cluster (Fig 30).

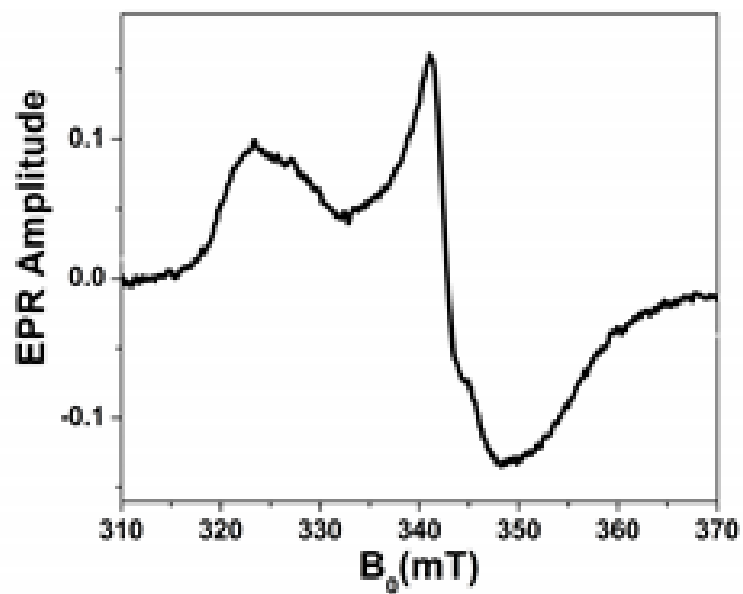


Figure 30. CW EPR spectra of dithionite reduced holo DSD-Fdm, Experimental conditions, Temperature 12K, Microwave Power 2mW.

We also probed the redox properties of DSD-Fdm using cyclic voltammetry. A solution of DSD-Fdm in 100mM Tris, pH 7.5, 100mM NaCl shows no observable redox process by cyclic voltammogram in the range from 0 to -1 (V) vs SHE, presumably because of the absence of interaction between electrode surface and the electroactive species. Neomycin has long been reported to stabilize and enhance interaction of ferredoxin type protein with electrode surface. After addition of 3.5 mM Neomycin, we observed a quasi-reversible process with a cathodic and anodic wave centered around -0.438 and -0.521 V vs SHE respectively, as shown in Figure 31. The estimated redox potential value -0.479 V vs SHE falls in the reported window for low potential [4Fe-4S] clusters in literature confirming presence of a [4Fe-4S]^{2+/1+} cluster.

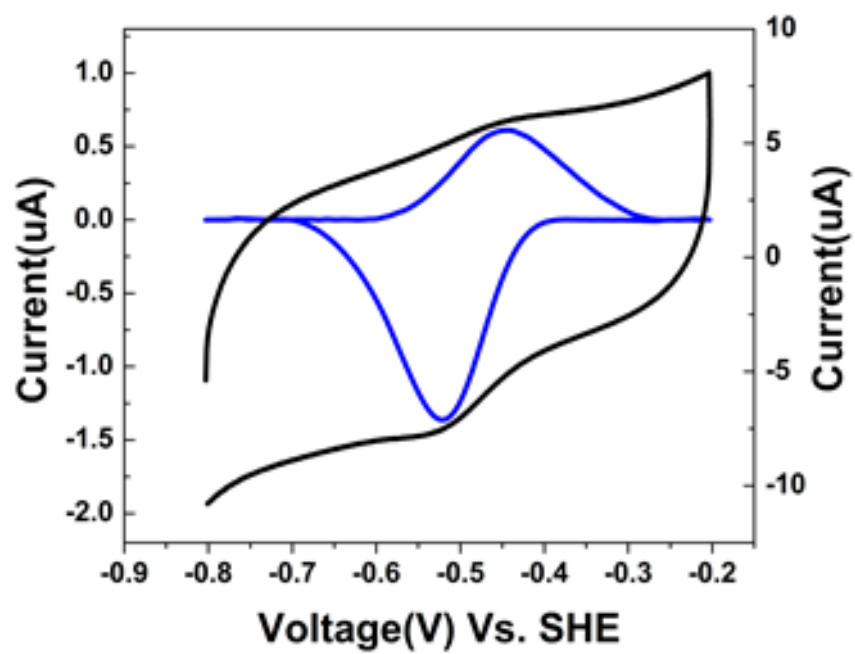


Figure 31. Cyclic voltammogram of holo DSD-Fdm with neomycin.

In nature, Ferredoxin type proteins are involved in numerous electron transfer processes leading up to redox catalysis¹⁷⁻²⁰. Thus, designed systems should also have these capabilities with the ultimate aim of engineering bio-hybrid catalysts that incorporate artificial and natural counterpart, each with fine tunable redox properties. Keeping this in mind, we turned our effort to investigate electron transfer properties of holo DSD-Fdm, with external redox active species. Firstly, to assess the possibility of the holo-DSD-Fdm to function in dye-sensitized solar cells, we characterized the kinetics of electron transfer from a porphyrin photosensitizer to the oxidized cluster utilizing Nanosecond Transient Absorption Spectroscopy. In the presence of the holo-peptide, the triplet state of the utilized porphyrin was quenched 10 times faster relative to the porphyrin in the presence of the apo-protein, indicating interaction with the clusters as shown in Figure 33. Experiments were done to probe the possibility of electron transfer between the $^3P^*$ and the [4Fe4S], but no oxidized porphyrin could be detected. This result points to the possibility of triplet-triplet energy transfer. Because this type of energy transfer is dipole-forbidden, the exchange mechanism must be of the Dexter type, which requires the donor and acceptor to be within 10 Å for sufficient orbital overlap to occur. Enhanced intersystem crossing could also be occurring, meaning that no energy transfer at all is occurring.

Finally, as a proof-of-concept study for the ability of this construct to be incorporated into a *de novo* designed, fully functional redox enzyme, the ability to transfer an electron to oxidized Cytochrome C was assayed. Holo DSD-Fdm was reduced by sequential addition of sodium dithionite, monitoring the loss of absorbance at 410 nm, stopping addition after no more change in signal was seen. Reduced peptide was desalted on a PD10 column to remove possible dithionite excess, and concentrated to an appropriate molarity.

The reduced peptide was then titrated into an air-oxidized Cytochrome C₅₅₀ sample, isolated from *Thermosynechococcus elongates*, while monitoring the UV-Vis spectra. The change in absorbance in the Soret and Q-bands indicate reduction of the protein-bound heme. Fitting the data of the change of absorbance as a function of molar equivalents of holo DSD-Fdm indicated an approximate 1:1 molar ratio of reduction.

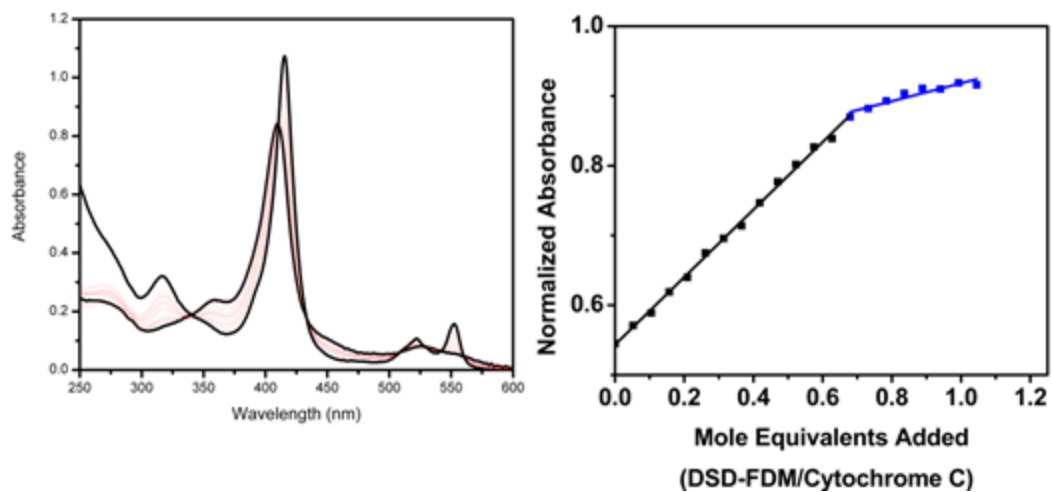


Figure 32. Cytochrome C assay. Decreasing absorbance of the protein bound heme indicate reduction of the heme. Plotting that change versus equivalents of Cytochrome C shows a 1:1 reduction.

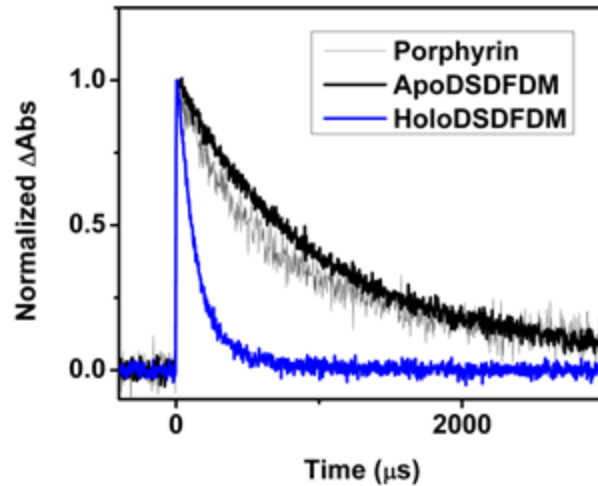


Figure 33. Nanosecond transient absorption DADS investigating energy/electron transfer between sensitized porphyrin monomer and protein. Porphyrin q-band was excited at 560 nm and probed at 450 nm to monitor decay of porphyrin triplet state. Porphyrin monomer triplet state decayed in $\sim 1000 \mu\text{s}$ in the solutions with only porphyrin (grey) and porphyrin + ApoDSDFDM (black). In the solution with porphyrin + HoloDSDFDM (blue), the triplet state decayed in 110 μs . There was no evidence of oxidized porphyrin formation, pointing to energy transfer between excited triplet state and protein.

In conclusion, here we have extended our previous effort¹¹ to design a more realistic artificial model of electron transfer protein assembly where redox active species are separated by a distance biologically relevant for effective electron transfer. Using symmetry property of a *de novo* designed homo-dimeric protein DSD¹², we rationally designed 2[4Fe-4S] cluster binding site in the hydrophobic core the helical bind. Total 8-leucine residues in the core were designed to be replaced by 8-cystine residues that serve as ligands to the [4Fe-4S] clusters. Resulting peptide binds 2[4Fe-4S] cluster with high yield and both apo and holo peptides are highly helical and dimeric in nature. Cofactor binding induces a significant amount of stability towards chemical denaturation, as often seen in designed metalloproteins²¹. Most importantly, for the first time, we show here *de novo* designed Holo DSD-Fdm is able to partake in electron transfer process involving an excited photosensitizer and also soluble, biologically relevant, small electron transfer protein, Cyt-C. This artificial redox proteins opens up new avenue for designing redox catalysts in a modular way, where different component of an engineered redox pathway can be disembodied and fine-tuned as desired for optimization of the whole system.

References

1. Fontecilla-Camps, J. C., Volbeda, A., Cavazza, C. & Nicolet, Y. Structure/Function Relationships of [NiFe]- and [FeFe]- Hydrogenases. *Chemical Reviews* 107, 4273 (2008).
2. Meyer, J. Iron-sulfur protein folds, iron-sulfur chemistry, and evolution. *Journal of Biological Inorganic Chemistry* 13, 157 (2008).
3. Orengo, C. A., Flores, T. P., Taylor, W. R. & Thornton, J. M. Identification and classification of protein folding families. *Protein Engineering Design and Selection* 6, 485 (1993).
4. Scott, M. P. & Biggins, J. Introduction of a [4Fe-4S (S-cys)₄]+1,+2 iron-sulfur center into a four- α helix protein using design parameters from the domain of the Fx cluster in the photosystem I reaction center *Protein Science* 6, 340 (1997).
5. Kennedy, M. C. *et al.* Evidence for the formation of a linear [iron-sulfur] ([3Fe-4S]) cluster in partially unfolded aconitase. *Journal of Biological Chemistry* 259, 14463 (1984).
6. Grzyb, J. *et al.* De novo design of a non-natural fold for an iron-sulfur protein: Alpha-helical coiled-coil with a four-iron four-sulfur cluster binding site in its central core. *Biochimica et Biophysica Acta* 1797, 406 (2010).

7. Antonkine, M. L. *et al.* Chemical rescue of a site-modified ligand to a [4Fe-4S] cluster in PsaC, a bacterial-like dicluster ferredoxin bound to Photosystem I. *Biochimica et Biophysica Acta* 1767, 712 (2007).
8. Antonkine, M. L. *et al.* Synthesis and characterization of de novo designed peptides modelling the binding sites of [4Fe-4S] clusters in photosystem I. *Biochimica et Biophysica Acta* 1787, 995 (2009).
9. Coldren, C. D., Hellinga, H. W. & Caradonna, J. P. The rational design and construction of a cuboidal iron-sulfur protein. *Proceedings of the National Academy of Sciences of the United States of America* 94, 6635 (1997).
10. Gibney, B. R., Mulholland, S. E., Rabanal, F. & Dutton, P. L. Ferredoxin and ferredoxin-heme maquettes *Proceedings of the National Academy of Sciences of the United States of America* 93, 15041 (1996).
11. Roy, A., Sarrou, I., Vaughn, M. D., Astashkine, A. V. & Ghirlanda, G. De Novo Design of an Artificial Bis[4Fe-4S] Binding Protein. *Biochemistry* 52, 7586 (2013).
12. Ogiyama, N. L. *et al.* Design of three-dimensional domain-swapped dimers and fibrous oligomers. *Proceedings of the National Academy of Sciences of the United States of America* 98, 1404 (2001).
13. Han, G. W. *et al.* Structure of a tryptophanyl-tRNA synthetase containing an iron-sulfur cluster. *Acta Crystallographica* 66, 1326 (2010).
14. Jin, Z. *et al.* Biogenesis of iron-sulfur clusters in Photosystem I: holo-NfuA from the cyanobacterium *Synechococcus* sp. PCC 7002 rapidly and efficiently transfers [4Fe-4S] clusters to APO-PsaC in vitro. *Journal of Biological Chemistry* 283, 28426 (2008).
15. Sweeney, W. V. & Rabinowitz, J. C. Proteins containing 4Fe-4S clusters: an overview. 1980 49, 139 (Annual Review of Biochemistry).
16. Koay, M. S., Antonkine, M. L., Gaertner, W. & Lubitz, W. Modelling low-potential [Fe₄S₄] clusters in proteins *Chemistry & Biodiversity* 5, 1571 (2008).
17. Tagawa, K. & Arnon, D. I. Oxidation-reduction potentials and stoichiometry of electron transfer in ferredoxins. *Biochimica et Biophysica Acta* 153, 602 (1968).
18. Mulder, D. W. *et al.* Insights into [FeFe]-hydrogenase structure, mechanism, and maturation. *Structure* 19, 1038 (2011).
19. Kurisu, G. *et al.* Structure of the electron transfer complex between ferredoxin and ferredoxin-NADP⁺ reductase *Nature Structural Biology* 8, 119 (2001).
20. Hanke, G. T., Satomi, Y., Shinmura, K., Takao, T. & Hase, T. A screen for potential ferredoxin electron transfer partners uncovers new, redox dependent interactions. *Biochimica et Biophysica Acta* 1814, 366 (2011).
21. Zastrow, M. L., Peacock, A. F., Stuckey, J. A. & Pecoraro, V. L. Hydrolytic catalysis and structural stabilization in a designed metalloprotein. *Nature Chemistry* 4, 118 (2012).

CHAPTER 6

SUMMARY AND PERSPECTIVE

A soluble, semiconducting porphyrin polymer has been synthesized and characterized. Because the polymer is soluble, it can be incorporated into bulk heterojunction solar cells or any other application that was previously inaccessible because of solubility concerns. The chemical nature of its polymerization means that it can be deposited onto any substrate, and not just electrodes. The semiconducting nature of the polymer will likely allow it to shuttle holes down its backbone, which has broad application, including solar cells. There are many other interesting facets of these polymers that have yet to be studied.

Two separate charge separating molecules have been studied. The first, a peripherally connected zinc-phthalocyanine-C₆₀ dyad has shown charge transfer behavior, according to photophysical data. The second, an axially connected carotene-Si-phthalocyanine-C₆₀ triad has shown limited charge transfer behavior. There is evidence of initial charge transfer from the carotene to the phthalocyanine, but rapid recombination must occur, as there is no signal for a C₆₀ anion. This result is disappointing, as this was the first asymmetrically modified phthalocyanine triad.

A *de novo* protein with iron-sulfur clusters has been studied for its ability to accept charge/energy from an excited porphyrin in solution. Nanosecond flash photolysis showed that the triplet excited state of the porphyrin was quenched by a factor of 10 when in solution with the holo-protein relative to with the apo-protein and compared to the triplet lifetime of the porphyrin. There was no growth of the porphyrin cation signal, which means that there was likely no electron transfer occurring. This leaves energy transfer as an explanation, but since the porphyrin was in its triplet excited state, only the Dexter method of energy transfer is reasonable. This result is disappointing, because definitive electron transfer would have shown that these [FeS] clusters could be readily sensitized and act as electron shuttles. The result does not mean that they are not capable of that, but this experiment did not prove that they are.

This dissertation has described a broad range of bio-inspired systems, ranging from polymer studies to *de novo* protein design, all with respect to their photophysical behavior. Transient spectroscopy is one of the most powerful tools available for looking at the electronic transitions in chromophoric systems and it will continue to be used to elucidate photophysical behavior for many years to come. Future work will likely include synthesis of polymers similar to the one described here, with a different small molecule electropolymer substituted for aniline. Since the porphyrin polymer was made more soluble by the addition of hexyl chains, electropolymerization is a viable option for the monomer used in the study. Incorporating these polymers into bulk heterojunction solar cells will be the next step after their syntheses. There are many other molecular triads that await characterization, and future studies will compare types of linkages (axial or peripheral) between moieties, electron donors, or electron acceptors. The *de novo* protein has incredible potential as an electron shuttle between electron donors and acceptors. Since this is the first of its kind to incorporate two clusters that are electronically coupled, there are myriad possibilities for applications. Mimicking the active sites of many different redox active enzymes can easily be imagined. All of these projects fall under the umbrella of bio-inspired chemistry, and this dissertation has described some of the newest advancements in their respective fields as well as outlined future directions for progress.

CHAPTER 7

REFERENCES

- Conti, J. *et al.* International Energy Outlook 2013. DOE/IEA-0484 (2013).
- Stocker, T. F. *et al.* IPCC 2013: *Climate Change 2013: The Physical Science Basis. Contribution of Working Group I to the Fifth Assessment Report of the Intergovernmental Panel on Climate Change.* (2013).
- ftp://aftp.cmdl.noaa.gov/products/trends/co2/co2_annmean_mlo.txt.
- Sherman, B. D. *et al.* Evolution of reaction center mimics to systems capable of generating solar fuel. *Photosynthesis Research* 120, 50 (2014).
- Duffy, C. D. P., Valkunas, L. & Ruban, A. V. Light-harvesting processes in the dynamic photosynthetic antenna. *Physical Chemistry Chemical Physics* 15, 18752 (2013).
- Berg, J. M., Tymoczko, J. L. & Stryer, L. in *Biochemistry* (W.H. Freeman & Company, New York City, 2012).
- Bertini, I., Gray, H. B., Stiefel, E. I. & Valentine, J. S. *Biological Inorganic Chemistry Structure and Reactivity.* (2007).
- Moore, T. A. *et al.* Photodriven charge separation in a carotenoporphyrinquinone triad. *Nature* 307, 630 (1984).
- Jordan, P. *et al.* Three-dimensional structure of cyanobacterial photosystem I at 2.5 Å resolution *Nature* 114, 909 (2001).
- Umena, Y., Kawakami, K., Shen, J. & Kamiya, N. Crystal structure of oxygen-evolving photosystem II at a resolution of 1.9 Å. *Nature* 473, 55 (2011).
- Turro, N. J., Ramamurthy, V. & Scaiano, J. C. in *Principles of Molecular Photochemistry: An Introduction* (University Science Books, 2009).
- Cho, M. Coherent Two-Dimensional Optical Spectroscopy. *Chemical Reviews* 108, 1331 (2008).
- Piper, J. A. & Pask, H. M. Crystalline Raman Lasers. *IEEE Journal of Selected Topics in Quantum Electronics* 13, 692 (2007).
- Henry, M. EKSPLA User's Manual. (2007).
- van Stokkum, I., Larsen, D. S. & van Grondelle, R. Global and target analysis of time-resolved spectra. *Biochimica et Biophysica Acta*, 82 (2004).
- F. Bedioui, J. Devynck, and C. Bied-Charreton, *Acc. Chem. Res.*, 1995, 28, 30-36.

- J. R. Fish, E. Kubaszewski, A. Peat, T. Malinski, J. Kaczor, P. Kus, and L. Czuchajowski, *Chem. Mater.*, 1992, 4, 795-803.
- C. Poriel, Y. Ferrand, P. Le Maux, C. Paul-Roth, G. Simonneaux, and J. Rault-Berthelot, *J. Electroanal. Chem.*, 2005, 583, 92-103.
- J. Basu and K. K. Rohatgimukherjee, *Solar Energy Mater.*, 1991, 21, 317-325.
- D.-S. Duanmu, Z.-P. Chen, X.-S. Yu, and X. Zhou, *Chin. J. Chem.*, 2004, 22, 779-781.
- D. Wohrle, R. Benters, O. Suvorova, G. Schnurpfeil, N. Trombach, and T. Bogdahn-Rai, *J. Porphyrins Phthalocyanines*, 2000, 4, 491-497.
- G. Li, S. Bhosale, S. Tao, R. Guo, S. Bhosale, F. Li, T. Zhang, T. Wang, and J.-H. Furhop, *Polymer*, 2005, 46, 5299-5307.
- C. Y. Lin, Y. C. Hung, C. M. Liu, C. F. Lo, Y. C. Lin, and C. L. Lin, *Dalton Trans.*, 2005, 396-401.
- K. A. Macor, Y. O. Su, L. A. Miller, and T. G. Spiro, *Inorg. Chem.*, 1987, 26, 2594-2598.
- A. Bettelheim, B. White, S. Raybuck, and R. W. Murray, *Inorg. Chem.*, 1987, 26, 1009-1017.
- A. Bettelheim, B. A. White, and R. W. Murray, *J. Electroanal. Chem.*, 1987, 217, 271-286.
- A. Bettelheim, D. Ozer, R. Harth, and R. W. Murray, *J. Electroanal. Chem.*, 1989, 266, 93-108.
- B. A. White and R. W. Murray, *J. Electroanal. Chem.*, 1985, 189, 345-352.
- E. M. Bruti, M. Giannetto, G. Mori, and R. Seeber, *Electroanalysis*, 1999, 11, 565-572.
- S. Griveau, V. Albin, T. Pauporte, J. H. Zagal, and F. Bedioui, *J. Mater. Chem.*, 2002, 12, 225-232.
- E. Mazzotta and C. Malitesta, *Sensors and Actuators B-Chemical*, 2010, 148, 186-194.
- J. S. Lindsey and D. F. Bocian, *Acc. Chem. Res.*, 2011, 44, 638-650.
- H. Zhan, S. Lamare, A. Ng, T. Kenny, H. Guernon, W. K. Chan, A. B. Djurisic, P. D. Harvey, and W. Y. Wong, *Macromolecules*, 2011, 44, 5155-5167.
- J. Y. Lee, H. J. Song, S. M. Lee, J. H. Lee, and D. K. Moon, *European Polymer Journal*, 2011, 47, 1686-1693.
- J.-H. Fuhrhop, *Langmuir*, 2014, 30, 1-12.
- Z. M. Liu, I. Schmidt, P. Thamyongkit, R. S. Loewe, D. Syomin, J. R. Diers, Q. Zhao, V. Misra, J. S. Lindsey, and D. F. Bocian, *Chem. Mater.*, 2005, 17, 3728-3742.

- S. Lamare, S. M. Aly, D. Fortin, and P. D. Harvey, *Chemical Communications*, 2011, 47, 10942-10944.
- P. A. Liddell, M. Gervaldo, J. W. Bridgewater, A. E. Keirstead, S. Lin, T. A. Moore, A. L. Moore, and D. Gust, *Chem. Mater.*, 2008, 20, 135-142.
- B. J. Brennan, P. A. Liddell, T. A. Moore, A. L. Moore, and D. Gust, *J. Phys. Chem. B*, 2013, 117, 426-432.
- M. Gervaldo, P. A. Liddell, G. Kodis, B. J. Brennan, C. R. Johnson, J. W. Bridgewater, A. L. Moore, T. A. Moore, and D. Gust, *Photochem. Photobiol. Sci.*, 2010, 9, 890-900.
- T. Förster, *Annalen der Physik*, 1948, 2, 55-75.
- T. Förster, *Disc. Faraday Soc.*, 1959, 27, 7-17.
- M. E. Jamin and R. T. Iwamoto, *Inorganica Chimica Acta*, 1978, 27, 135-143.
- R. L. Hand and R. F. Nelson, *J. Am. Chem. Soc.*, 1974, 96, 850-860.
- K. Kurotobi, Y. Toude, K. Kawamoto, Y. Fujimori, S. Ito, P. Chabera, V. Sundstrom, and H. Imahori, *Chemistry-A European Journal*, 2013, 19, 17075-17081.
- H. F. Chow, M. K. Ng, C. W. Leung, and G. X. Wang, *J. Am. Chem. Soc.*, 2004, 126, 12907-12915.
- Z. R. Grabowski, K. Rotkiewicz, and W. Rettig, *Chem. Rev.*, 2003, 103, 3899-4031.
- McKeown, N. B. Phthalocyanine materials :synthesis, structure, and function; Chemistry of solid state materials; Cambridge University Press: Cambridge, U.K.; New York, 1998; Vol. 6, pp 193.
- Marti Fún-Gomis, L.; Ohkubo, K.; Fernandez-Lazaro, F.; Fukuzumi, S.; Sastre-Santos, A. Adiabatic Photoinduced Electron Transfer and Back Electron Transfer in a Series of Axially Substituted Silicon Phthalocyanine Triads. *J. Phys. Chem. C* 2008, 112, 17694-17701.
- Cheng, G.; Peng, X.; Hao, G.; Kennedy, V. O.; Ivanov, I. N.; Knappenberger, K.; Hill, T. J.; Rodgers, M. A. J.; Kenney, M. E. Synthesis, Photochemistry, and Electrochemistry of a Series of Phthalocyanines with Graded Steric Hindrance. *J. Phys. Chem. A* 2003, 107, 3503-3514.
- Kim, K. N.; Choi, C. S.; Kay, K. A novel phthalocyanine with two axial fullerene substituents. *Tetrahedron Lett.* 2005, 46, 6791-6795.
- Martin-Gomis, L.; Ohkubo, K.; Fernandez-Lazaro, F.; Fukuzumi, S.; Sastre-Santos, A. Synthesis and photophysical studies of a new nonaggregated C60-silicon phthalocyanine-C60 triad. *Org. Lett.* 2007, 9, 3441-3444.
- Marti Fún-Gomis, L.; Ohkubo, K.; Fernandez-Lazaro, F.; Fukuzumi, S.; Sastre-Santos, A. Adiabatic Photoinduced Electron Transfer and Back Electron Transfer in a Series of Axially Substituted Silicon Phthalocyanine Triads. *J. Phys. Chem. C* 2008, 112, 17694-17701.

- El-Khouly, M.; Kim, J.; Kay, K.; Choi, C.; Ito, O.; Fukuzumi, S. Synthesis and Photoinduced Intramolecular Processes of Light-Harvesting Silicon Phthalocyanine-Naphthalenediimide-Fullerene Connected Systems. *Chemistry – A European Journal* 2009, 15, 5301-5310.
- Guldi, D. M.; Martin, N. Fullerenes :from synthesis to optoelectronic properties; Developments in fullerene science; Kluwer Academic Publishers: Boston, 2002; Vol. 4, pp 440.
- Moore, T. A.; Gust, D.; Mathis, P.; Mialocq, J.; Chachaty, C.; Bensasson, R. V.; Land, E. J.; Doizi, D.; Liddell, P. A.; Lehman, W. R.; Nemeth, G. A.; Moore, A. L. Photodriven charge separation in a carotenoporphyry-quinone triad. *Nature* 1984, 307, 630-632.
- Ritz, T.; Damjanović, A.; Schulten, K.; Zhang, J.; Koyama, Y. Efficient light harvesting through carotenoids. *Photosynthesis Res.* 2000, 66, 125-144.
- Gust, D.; Moore, T. A.; Moore, A. L. Mimicking Photosynthetic Solar Energy Transduction. *Acc. Chem. Res.* 2001, 34, 40-48.
- Tracewell, C. A.; Vrettos, J. S.; Bautista, J. A.; Frank, H. A.; Brudvig, G. W. Carotenoid Photooxidation in Photosystem II. *Arch. Biochem. Biophys.* 2001, 385, 61-69.
- Gust, D.; Moore, T. A.; Moore, A. L.; Liddell, P. A. In [10] Synthesis of carotenoporphyry models for photosynthetic energy and electron transfer; *Methods in Enzymology*; Academic Press: Vol. Volume 213, pp 87-100.
- Kodis, G.; Herrero, C.; Palacios, R.; Mariño-Ochoa, E.; Gould, S.; de, I. G.; van Grondelle, R.; Gust, D.; Moore, T. A.; Moore, A. L.; Kennis, J. T. M. Light Harvesting and Photoprotective Functions of Carotenoids in Compact Artificial Photosynthetic Antenna Designs. *J Phys Chem B* 2004, 108, 414-425.
- Fontecilla-Camps, J. C., Volbeda, A., Cavazza, C. & Nicolet, Y. Structure/Function Relationships of [NiFe]- and [FeFe]- Hydrogenases. *Chemical Reviews* 107, 4273 (2008).
- Meyer, J. Iron-sulfur protein folds, iron-sulfur chemistry, and evolution. *Journal of Biological Inorganic Chemistry* 13, 157 (2008).
- Orengo, C. A., Flores, T. P., Taylor, W. R. & Thornton, J. M. Identification and classification of protein folding families. *Protein Engineering Design and Selection* 6, 485 (1993).
- Scott, M. P. & Biggins, J. Introduction of a [4Fe-4S (S-cys)₄]^{+1,+2} iron-sulfur center into a four- α helix protein using design parameters from the domain of the Fx cluster in the photosystem I reaction center *Protein Science* 6, 340 (1997).
- Kennedy, M. C. *et al.* Evidence for the formation of a linear [iron-sulfur] ([3Fe-4S]) cluster in partially unfolded aconitase. *Journal of Biological Chemistry* 259, 14463 (1984).
- Grzyb, J. *et al.* De novo design of a non-natural fold for an iron-sulfur protein: Alpha-helical coiled-coil with a four-iron four-sulfur cluster binding site in its central core. *Biochimica et Biophysica Acta* 1797, 406 (2010).

- Antonkine, M. L. *et al.* Chemical rescue of a site-modified ligand to a [4Fe-4S] cluster in PsaC, a bacterial-like dicluster ferredoxin bound to Photosystem I. *Biochimica et Biophysica Acta* 1767, 712 (2007).
- Antonkine, M. L. *et al.* Synthesis and characterization of de novo designed peptides modelling the binding sites of [4Fe-4S] clusters in photosystem I. *Biochimica et Biophysica Acta* 1787, 995 (2009).
- Coldren, C. D., Hellinga, H. W. & Caradonna, J. P. The rational design and construction of a cuboidal iron-sulfur protein. *Proceedings of the National Academy of Sciences of the United States of America* 94, 6635 (1997).
- Gibney, B. R., Mulholland, S. E., Rabanal, F. & Dutton, P. L. Ferredoxin and ferredoxin-heme maquettes *Proceedings of the National Academy of Sciences of the United States of America* 93, 15041 (1996).
- Roy, A., Sarrou, I., Vaughn, M. D., Astashkine, A. V. & Ghirlanda, G. De Novo Design of an Artificial Bis[4Fe-4S] Binding Protein. *Biochemistry* 52, 7586 (2013).
- Ogihara, N. L. *et al.* Design of three-dimensional domain-swapped dimers and fibrous oligomers. *Proceedings of the National Academy of Sciences of the United States of America* 98, 1404 (2001).
- Han, G. W. *et al.* Structure of a tryptophanyl-tRNA synthetase containing an iron-sulfur cluster. *Acta Crystallographica* 66, 1326 (2010).
- Jin, Z. *et al.* Biogenesis of iron-sulfur clusters in Photosystem I: holo-NfuA from the cyanobacterium *Synechococcus* sp. PCC 7002 rapidly and efficiently transfers [4Fe-4S] clusters to APO-PsaC in vitro. *Journal of Biological Chemistry* 283, 28426 (2008).
- Sweeney, W. V. & Rabinowitz, J. C. Proteins containing 4Fe-4S clusters: an overview. 1980 49, 139 (Annual Review of Biochemistry).
- Koay, M. S., Antonkine, M. L., Gaertner, W. & Lubitz, W. Modelling low-potential [Fe₄S₄] clusters in proteins *Chemistry & Biodiversity* 5, 1571 (2008).
- Tagawa, K. & Arnon, D. I. Oxidation-reduction potentials and stoichiometry of electron transfer in ferredoxins. *Biochimica et Biophysica Acta* 153, 602 (1968).
- Mulder, D. W. *et al.* Insights into [FeFe]-hydrogenase structure, mechanism, and maturation. *Structure* 19, 1038 (2011).
- Kurusu, G. *et al.* Structure of the electron transfer complex between ferredoxin and ferredoxin-NADP⁺ reductase *Nature Structural Biology* 8, 119 (2001).
- Hanke, G. T., Satomi, Y., Shinmura, K., Takao, T. & Hase, T. A screen for potential ferredoxin electron transfer partners uncovers new, redox dependent interactions. *Biochimica et Biophysica Acta* 1814, 366 (2011).
- Zastrow, M. L., Peacock, A. F., Stuckey, J. A. & Pecoraro, V. L. Hydrolytic catalysis and structural stabilization in a designed metalloprotein. *Nature Chemistry* 4, 118 (2012).

